

EXPLOITING ACQUIRED RESISTANCE MECHANISMS TO MEK INHIBITION IN RAS-
ACTIVATED NEUROBLASTOMA

Grace Coggins

A DISSERTATION

in

Pharmacology

Presented to the Faculties of the University of Pennsylvania

in

Partial Fulfillment of the Requirements for the

Degree of Doctor of Philosophy

2019

Supervisor of Dissertation

John M. Maris M.D.

Giulio D'Angio Professor of Pediatric Oncology

Graduate Group Chairperson

Julie Blendy, Ph.D.

Professor of Pharmacology

Dissertation Committee

Xianxin Hua, M.D., Ph.D.

Professor of Cancer Biology

Jeffrey Field Ph.D.

Professor of Pharmacology

Margaret Chou, Ph.D.

Associate Professor of Pathology and Laboratory Medicine

Yael Mossé, M.D.

Associate Professor of Pediatrics

EXPLOITING ACQUIRED RESISTANCE MECHANISMS TO MEK INHIBITION IN RAS-
ACTIVATED NEUROBLASTOMA

COPYRIGHT

2019

Grace Elizabeth Coggins

This work is licensed under the
Creative Commons Attribution-
NonCommercial-ShareAlike 3.0
License

To view a copy of this license, visit

<https://creativecommons.org/licenses/by-nc-sa/3.0/us/>

ACKNOWLEDGMENTS

I am enormously grateful for the many people whose support and encouragement were integral to my successful completion of this degree. First, I would like to sincerely thank my thesis advisor, Dr. John M. Maris, for your guidance, unwavering support, and mentorship over the past five years. Your unparalleled passion for your patients has been a continual inspiration and was the guiding force behind this thesis work. Thank you for pushing me to step beyond my comfort zone to develop as an independent scientist and critical thinker throughout this process

I am grateful for the many members of the Maris, Mossé, and Diskin labs for their technical expertise and encouragement. In particular, I would like to extend my sincere gratitude to Dr. Jo Lynne Rokita for your unwavering commitment to mentorship and scientific rigor. In addition to advising on all aspects of RNA seq and molecular biology techniques, your encouragement and advocacy enabled me to learn the skills I needed to succeed during my graduate training. I was also extremely fortunate to work with people who have had a direct impact on this work. Thank you to the amazing Karina Cronkite, for your selfless dedication to pediatric cancer research and training and Dr. Alvin Farrel, for your patience and bioinformatics expertise, as well as Dr. Lori Hart, Dr. Kris Bosse, Nathan Kendersky, Kristen Upton, Greg Sacks, Komal Rathi, Colin Hayes, and Smita Matkar. Thank you to Dr. Laura Scolaro, Minu Samanta, Kate Krytska, Tori Kinek,

and Maura Diamond for operational and administrative support that was essential to the success of this project.

Thank you to the research collaborators that were instrumental to this body of work. To Vivace Therapeutics, particularly Dr. Leonard Post and Dr. Tracy Tang, for providing the TEAD palmitoylation inhibitors and enlightening discussions that have inspired future studies. I must also thank Dr. David Schultz and the UPenn High-Throughput Screening Core for the thoughtful discussions surrounding the conception, performance, and analysis of our combination drug screen. I must also thank the Thomas Jefferson University Laboratory for Cancer Genetics for performing the library preparation and next-generation sequencing for our RNA seq experiment.

I would also like to thank the Pharmacology Graduate Group for providing the opportunity to earn this degree. Thank you to the members of my dissertation committee: Dr. Xianxin Hua, Dr. Margaret Chou, Dr. Jeffrey Field, and Dr. Yael Mossé. Thank you for pushing me to question my assumptions, providing guidance, and offering helpful solutions during this thesis work. I must also thank Sarah Squire and Julie Blendy for managing all aspects of the Pharmacology Graduate Group training program.

Words cannot adequately express my deepest gratitude to my family throughout my entire education journey. Thank you to my parents, John and Melissa Coggins, for always reminding me to “take your time and check your work.” Your never-ending love and encouragement gave me the motivation to strive to do

my best in anything I attempted. Thank you for listening to my rambling phone calls and for never doubting my ability to earn this degree. Thank you to my sister, Sarah, for being my best friend and role model. I feel incredibly lucky to have experienced life together throughout our parallel journeys that led us both to Philadelphia. Thank you to my grandmother, Erin Coggins, as well as my late grandparents, Jack Coggins Sr. and Bernard and Helen Ferguson, for their love and support at every stage. Finally, thank you to David for the happiest two and a half years of my life.

ABSTRACT

EXPLOITING ACQUIRED RESISTANCE MECHANISMS TO MEK INHIBITION IN RAS- ACTIVATED NEUROBLASTOMA

Grace E. Coggins

Dr. John M. Maris

High-risk neuroblastoma is characterized by an aggressively metastatic phenotype and five-year survival rates of approximately 40%. Half of all high-risk patients experience disease relapse which remains incurable. Recent studies have identified an enrichment of mutations in the RAS-MAPK pathway upon relapse that are potentially sensitive to MEK1/2 inhibition with drugs such as trametinib. Although trametinib is a potent MEK1/2 inhibitor, single-agent therapy invariably encounters *de novo* or acquired bypass mechanisms that allow for disease progression. The central goal of this dissertation was to contribute to the understanding of compensatory signaling mechanisms adopted by RAS-MAPK aberrant neuroblastomas in response to MEK1/2 inhibition. Here, we interrogated the role of the Hippo pathway protein YAP in intrinsic trametinib resistance and discovered that *YAP1* gene knockout sensitized neuroblastoma cells to trametinib. Further exploration into this mechanism showed that significantly reduced expression of *E2F* and *MYCN* gene signatures promoted G₁ phase cell cycle arrest. This study also investigated novel TEAD palmitoylation inhibitors as inhibitors of YAP activity in combination with trametinib. Of the three compounds tested, one showed synergy with trametinib across three RAS-hyperactivated neuroblastoma cell lines. To evaluate other signaling adaptations driving

trametinib resistance, we performed a high-throughput screen to identify synergistic trametinib drug combinations in six RAS-hyperactivated neuroblastoma cell lines. The top drug targets with broad efficacy in at least three cell lines were HMG-CoA reductase inhibitors, or statins, and three epigenetic inhibitors. The principal finding of these studies was the observation of synergy between trametinib and two statins in two neuroblastoma cell lines. However, no synergy was detected between trametinib and epigenetic inhibitors, suggesting a false positive result. Altogether, this dissertation provides evidence of two synergistic trametinib drug combinations in RAS-hyperactivated neuroblastoma that can be explored in the clinic. These findings underscore the importance of YAP activity in response to trametinib in RAS-driven neuroblastomas, as well as the potential for harnessing the pleiotropic effects of TEAD palmytoilation inhibition and/or statins in a trametinib combination. Continued functional characterization of potential targets of resistance will build upon these efforts to improve clinical responses of relapsed neuroblastoma to trametinib combinatorial therapies and contribute to the larger field of MEK inhibitor bypass mechanisms in cancer.

TABLE OF CONTENTS

ACKNOWLEDGMENTS	iii
ABSTRACT	vi
TABLE OF CONTENTS	viii
LIST OF TABLES	x
LIST OF ILLUSTRATIONS	xi
LIST OF ABBREVIATIONS	xiv
CHAPTER 1: INTRODUCTION	1
I. Neuroblastoma	1
II. Mutational Landscape in Neuroblastoma	4
III. RAS-MAPK Pathway	6
IV. MEK Inhibitor Drug Combination Design	11
V. YAP-Hippo Pathway	13
VI. Research Aims	19
CHAPTER 2: ROLE OF HIPPO PATHWAY PROTEIN YAP1 IN RESISTANCE TO MEK1/2 INHIBITION IN RAS ACTIVATED NEUROBLASTOMAS	23
I. Abstract	23
II. Introduction	24
III. Methods and Materials	26
IV. Results	33
V. Discussion	50
CHAPTER 3: COMBINATORIAL TARGETING OF THE RAS-MAPK AND HIPPO PATHWAYS WITH MEK1/2 AND TEAD PALMITOYLATION INHIBITORS	54
I. Abstract	54
II. Introduction	55
III. Methods and Materials	58
IV. Results	59
V. Discussion	72
CHAPTER 4: HIGH-THROUGHPUT APPROACH TO DESIGNING ALTERNATE MEK1/2 DRUG COMBINATIONS FOR RAS ACTIVATED NEUROBLASTOMA	75
I. Abstract	75

II. Introduction	76
III. Materials and Methods	77
IV. Results	81
V. Discussion	90
CHAPTER 5: OVERALL DISCUSSION AND FUTURE DIRECTIONS.....	93
I. YAP1 modulation of MEK inhibitor sensitivity	94
II. YAP1-TEAD as a therapeutic target	97
III. Alternate MEK inhibitor drug combinations.....	99
IV. Future Directions	102
APPENDIX: Additional Published Manuscript.....	106
I. Genetic Susceptibility to Neuroblastoma.....	106
REFERENCES.....	146

LIST OF TABLES

TABLE 2-S1: *MYCN* amplification and chromosome 11q status across a panel of 16 neuroblastoma cell lines.

LIST OF ILLUSTRATIONS

FIGURE 1-1: The RAS-MAPK signaling pathway in cancer.

FIGURE 1-2: The Hippo signaling pathway in cancer.

FIGURE 2-1: Trametinib causes nuclear accumulation of unphosphorylated yap1 protein.

FIGURE 2-2: *YAP1* knockout sensitizes neuroblastoma cell lines to trametinib.

FIGURE 2-3: YAP-5SA overexpression induces trametinib resistance in low yap-expressing neuroblastoma cell lines.

FIGURE 2-4: Increased trametinib sensitivity upon *YAP1* loss is due to loss of E2F and MYCN target gene expression.

FIGURE 2-5: Trametinib treatment of *YAP1*^{-/-} cells causes G₁ cell cycle arrest.

FIGURE 2-S1: Sanger sequencing of NLF *YAP1*^{-/-} isogenic lines confirm mutational status.

FIGURE 2-S2: *YAP1* knockout pools in neuroblastoma cell lines are sensitized to trametinib.

FIGURE 2-S3: Growth rates of NLF *YAP1* null clones are slower than NLF sgCon.

Figures 2-S4: YAP-5SA overexpression induces trametinib resistance in NLF *YAP1*^{-/-} neuroblastoma cell lines.

FIGURE 2-S5: Confirming differential gene expression between RNA seq samples.

FIGURE 2-S6: TEAD1-4 transcription factor consensus sites at the *MYCN* gene locus.

FIGURE 2-S7: Gene Ontology analysis between control-treated *YAP1*^{-/-} #1 and #4 cell lines.

FIGURE 3-1: Dose-response curves of VT101, VT102, and VT103 in NLF.

FIGURE 3-2: Dose-response curves of VT101, VT102, and VT103 in SKNAS.

FIGURE 3-3: Dose-response curves of VT101, VT102, and VT103 in SKNFI.

FIGURE 3-4: Dose-response curves of VT101, VT102, and VT103 in Kelly.

FIGURE 3-5: Dose-response curves of VT101, VT102, and VT103 in COG-N-519.

FIGURE 3-6: Synergy observed between trametinib and VT101 in NLF, SKNAS, and SKNFI.

FIGURE 3-7: No synergy observed between VT102 and trametinib in NLF, SKNAS, OR SKNFI.

FIGURE 4-1: High-throughput trametinib combination screen design.

FIGURE 4-2: SSMD analysis reveals top drug targets for trametinib combination.

FIGURE 4-3: Single-agent activity of statins in neuroblastoma cell lines.

FIGURE 4-4: Synergy observed between statins and trametinib in NLF and NB-EBc1.

FIGURE 4-S1: Z-factor scores for each plate for quality assessment.

FIGURE 4-S2: Comparison of SSMD and Z-scores in response to compound library treatment in SKNFI.

LIST OF ABBREVIATIONS

ALK	anaplastic lymphoma kinase
CDK	cyclin-dependent kinase
ERK	extracellular signal-regulated kinase
DMSO	dimethyl sulfoxide
FTI	farnesyl transferase inhibitor
GSEA	gene set enrichment analysis
GO	gene ontology
GAP	GTP-ase activating protein
GEF	guanine nucleotide exchange factor
GPCR	G-protein coupled receptor
HRAS	Harvey rat sarcoma viral oncogene homolog
KRAS	Kirsten rat sarcoma viral oncogene homolog
LATS1/2	large tumor suppressor kinases
MAPK	mitogen-activated protein kinase
MYCN	v-myc avian myelocytomatosis viral oncogene neuroblastoma derived homolog
NF1	neurofibromin 1
NPI	normalized percent inhibition
NRAS	neuroblastoma rat sarcoma viral oncogene homolog
NSCLC	non-small cell lung cancer
PDX	patient-derived xenograft
RB	retinoblastoma protein
RTK	receptor tyrosine kinase
SAV	Salvador protein kinase
SH2	sequence homology 2 domain
SSMD	strictly standardized mean difference
TAZ	transcriptional coactivator with PDZ-binding motif

TEAD	TEA domain family member
WTS	Warts protein kinase
YAP	Yes-associated protein

CHAPTER 1: INTRODUCTION

I. Neuroblastoma

A pediatric cancer of the developing sympathetic nervous system, neuroblastoma arises from the neural crest during early embryogenesis (Hoehner JC, 1996). The neural crest is a temporary structure that forms along the dorsal neural plate during gastrulation. This structure is comprised of highly migratory pluripotent neural crest stem cells that give rise to a variety of cell types in four anatomical categories: cardiac, enteric, trunk, and head (Liu and Cheung, 2016, Gammill and Roffers-Agarwal, 2010). Neuroblastoma originates along the migratory route of sympathoadrenal precursor cells that differentiate into adrenal chromaffin cells and sympathetic ganglion cells of the trunk, ultimately forming neurons that line the ventral roots of the spinal cord and chromaffin cells of the adrenal medulla and melanocytes (Matthay, 2016, Liu and Cheung, 2016, Gammill and Roffers-Agarwal, 2010). As a result, primary tumors can be located anywhere located along the sympathetic nervous system, but the most common site is the adrenal gland in 40% of cases.

Neuroblastoma is characterized by remarkable clinical heterogeneity, with survival rates varying widely based on the age of diagnosis, initial disease burden, and biological characteristics of the tumor. Although neuroblastoma is classified as an ultra-orphan disease, with <1,000 newly diagnosed cases each year in North America, it is the most common extracranial solid tumor diagnosed in childhood (Howlader N, 2011; Maris, 2007). The biological features of neuroblastoma tumors

can be used to stratify cases and predict overall prognosis. At diagnosis, neuroblastoma typically has a low somatic mutational burden and is instead considered a copy number-driven malignancy. Tumors frequently harbor genomic instability in the form of segmental chromosomal copy number alterations and focal copy number alterations, particularly *MYCN* gene amplification. Copy number gain of 17q and loss of 1p are correlated with *MYCN* amplification, while loss of 11q is inversely correlated with *MYCN* amplification (Matthay 2016, Maris 2007). However, both *MYCN* amplification and 11q loss are both associated with high-risk disease and poor prognosis (Schwab M, 1983; Brodeur GM, 1984; Seeger RC, 1985). According to the International Neuroblastoma Risk Group Staging System, neuroblastomas are stratified according to the overall risk of relapse (Cohn SL, 2009). Low-risk neuroblastomas are localized and biologically favorable tumors (see below) with no other sites of disease. Intermediate-risk neuroblastoma is a heterogeneous group that does not fall neatly into low- or high-risk. Rather, it includes unresectable solid tumors with favorable biological characteristics as well as metastatic disease without *MYCN* amplification in infancy. Approximately 50% of all neuroblastomas are classified as high-risk, typically presenting as a primary tumor with widely distant metastases. Approximately 99% and 95% of low- and intermediate-risk neuroblastomas, respectively, are cured with little to no cytotoxic therapy, whereas <50% of high-risk neuroblastomas are cured despite intensive therapy (Maris JM, 2007, Matthay, 2016). Disease burden is combined with other prognostic indicators, such as age, to further define risk groups. The median age

of diagnosis is 18 months, which serves as a demarcation of overall prognosis. Patients younger than 18 months generally have better overall survival rates and are associated with lower risk, while patients >18 months are typically categorized as high-risk (Maris, 2007, Matthay, 2016).

The diversity inherent to neuroblastoma necessitates distinct treatment guidelines, ranging from little to no therapeutic intervention to intense, multi-modal therapy with toxic side effects. Low risk neuroblastomas frequently only require surgery, and intermediate risk neuroblastomas are typically treated with surgery and low-dose chemotherapy. These interventional methods are highly effective, achieving survival rates of nearly 90% (Oberthuer A, 2015; Maris JM, 2010). High risk neuroblastomas, however, require aggressive therapy that begins with high-dose chemotherapy and surgery, followed by consolidation therapy consisting of autologous hematopoietic stem cell transplantation and radiotherapy to induce the remaining disease into remission (Matthay, 2016, Maris, 2007). Patients then receive maintenance chemotherapy to prevent a relapse from recurring. In spite of this therapy regimen, high-risk neuroblastoma has a survival rate of only 40%. This devastating statistic is largely due to the high rate of relapse, with over half of high-risk neuroblastomas recurring and becoming incurable (Oberthuer A, 2015; Maris JM, 2010). Patients receiving treatment for high-risk neuroblastoma experience serious side effects, including myelosuppression, insufficient weight gain, and renal dysfunction. This is compounded by the neurological and musculoskeletal long-term side effects, as well as the increased risk of a secondary malignancy,

impaired growth, chronic kidney disease, and infertility (Maris JM, 2010). Altogether, the physical toll of the treatment for high-risk disease combined with a poor prognosis presents a clear rationale for the design of novel therapeutic approaches.

II. Mutational Landscape in Neuroblastoma

Novel targeted therapies have shown immense promise in some cancers with “druggable” oncogenic drivers. Broader access to and advances in sequencing technologies has exponentially increased our ability to detect and identify germline and somatic mutations. Defining the landscape of somatic and germline mutations has enabled the clinical development of targeted inhibitors for treating neuroblastoma.

Hereditary neuroblastoma is extremely rare and accounts for 1-2% of all neuroblastoma cases. In 80-90% of familial cases of neuroblastoma, gain-of-function germline mutations in the receptor tyrosine kinase *ALK* are drivers of tumorigenesis (Mosse, 2008). For patients with identified *ALK* driver mutations, *ALK* inhibitor therapy has produced impressive results (Bresler SC, 2011; Schonherr C, 2011; Heuckmann JM, 2011; Carpenter EL, 2012). Loss of function mutations in *PHOX2B*, a master regulator neural crest development, causes 5% hereditary cases of neuroblastoma that is associated with other comorbidities of nervous system development including congenital central hypoventilation

syndrome and Hirschsprung disease (Maris, 2007). The remaining ~5% of hereditary cases remain unexplained.

A series of major efforts to define the spectrum of genetic mutations in high-risk neuroblastoma identified *ALK*, *PTPN11*, and *ATRX* as the most commonly mutated genes and additional low-frequency mutations in *MYCN* and *NRAS*. (Cheung NV, 2012; Molenaar JJ, 2012; Pugh TJ, 2013; Sausen M, 2013). In a follow-up study, whole genome sequencing of 23 paired diagnosis and relapse tumor samples identified mutations in both primary and relapse samples, with an average of 28% of shared mutations in the primary and relapse tumors (Eleveld, 2015). Unbiased pathway analysis of the relapse samples indicated an enrichment for mutations in genes associated with the RAS-MAPK signaling pathway in 18/23 relapse samples (78%) (Eleveld, 2015). These mutations included two RTKS, *ALK* and *FGFR1*, a RAS-GAP, *NF1*, an oncogenic tyrosine phosphatase, *PTPN11*, and four pathway kinases, *HRAS*, *KRAS*, *NRAS*, and *BRAF*. Subsequent clonality analyses determined that RAS-MAPK pathway mutations were present in subclonal populations in the majority of primary tumors and were retained upon relapse, suggesting that positive selection in response to standard of care therapy set the stage for eventual relapse (Eleveld, 2015). This discovery not only expanded our understanding of neuroblastoma genetics between diagnosis and relapse, but also offered new hope for the treatment of patients with relapsed neuroblastoma.

III. RAS-MAPK Pathway

The RAS-MAPK pathway is a complex and critical cellular signaling network that regulates proliferation, growth, survival, differentiation, and apoptosis. This pathway has been extensively studied for its role in oncogenic signaling and tumorigenesis. The primary downstream effector proteins of the RAS-MAPK pathway are ERK1/2 kinases, which exert their function on a variety of substrates such as transcription factors, cell cycle components, kinases, and membrane proteins (Fig. 1-1) Negative regulation of the RAS-MAPK pathway also serves an important role in regulating normal pathway function, and loss of this tumor suppressive function can promote RAS hyperactivation.

Germline mutations in RAS-MAPK pathway genes cause several important cancer predisposition syndromes. Noonan Syndrome and neurofibromatosis type 1 are both autosomal dominant disorders that predisposes individuals to developing pediatric cancers (Tidyman, 2010). In Noonan Syndrome, germline mutations in four genes have been identified (*PTPN11*, *KRAS*, *SOS1*, and *CRAF*), although more genes are expected to be identified as drivers in this disease. Of these four genes, *PTPN11* (SHP2) is associated with approximately 50% of all Noonan Syndrome cases and promotes RAS hyperactivation when activating mutations are present (Fig. 1-1) (Tidyman WE, 2009). In a smaller subset of Noonan's Syndrome cases, gain-of-function mutations in *SOS1*, as RAS-GEF, *KRAS*, and *CRAF* directly promote hyperactivation of RAS-MAPK pathway signaling (Tidyman WE, 2009). In addition, neurofibromatosis 1 is one among the

most common genetic conditions and is caused by inactivation of the *NF1* gene (Tidyman WE, 2009). The NF1 tumor suppressor protein functions as a RAS-GAP, but loss-of-function germline mutations render the protein unable to promote the conversion of RAS-GTP to the inactive form, leading to RAS hyperactivation (Williams VC, 2009).

Somatic mutations causing constitutive activation of one or more pathway components are extremely common in many types of human cancer, including pancreas, colon, lung, and ovary organ sites (Santarpia, 2012). Two adult neural-crest derived cancers, non-small cell lung cancer (NSCLC) and melanoma, also frequently show RAS-MAPK pathway mutations. Melanomas frequently present BRAF V600E (66%) mutations and NRAS (15%), whereas one-third of NSCLCs are NRAS-mutated (Liu, 2018).

Efforts to target the RAS-MAPK pathway pharmacologically have been met with mixed results. Until recently, the RAS proteins were largely considered to be “undruggable” based on its function as a molecular switch with no clear cleft or groove for inhibitor binding. Furthermore, the extremely high affinity of RAS for GTP renders competitive inhibition nearly impossible. Early approaches to pharmacologically inhibit RAS focus on targeting the post-translational farnesylation that is required for RAS function and tethering to the plasma membrane. Farnesyl transferase inhibitors (FTI) were developed to prevent this enzymatic modification and showed promising early preclinical results. After two different FTIs failed to show clinical efficacy, it was discovered that geranyl-

geranylation could compensate for the loss of NRAS and KRAS farneylation (Basso AD, 2006; Berndt N, 2011; Ryan MB and Corcoran RB, 2018). The failure of FTIs underscores the difficulty of targeting a small G-protein and highlights the promising potential for inhibiting downstream RAF and MEK proteins.

Two RAF inhibitors have been approved for single-agent treatment of BRAF V600E/K mutant melanoma: vemurafenib and dabrafenib. Both second-generation RAF inhibitors show improved selectivity for mutant BRAF but are limited by the phenomenon of paradoxical ERK activation (Lorentzen HF, 2019). If the RAF inhibitor is at a non-saturating concentration, drug-free RAF proteins can interact with MEK and promote downstream activation of ERK. Furthermore, in the case of non-V600E BRAF mutants, dimeric RAF complexes can evade inhibition due to decreased binding affinity for the second partner (Poulikakos PI, 2010; Liu, 2018; Durrant and Morrison, 2018). Thus, the inherent redundancy within the function of RAF proteins allows the pathway to bypass BRAF inhibition.

For this reason, the development of MEK inhibitors has accelerated despite the rarity of MEK1/2 mutations in human cancers. Three MEK1/2 inhibitors are approved for combination with RAF inhibitors to treat cancer, but the only MEK1/2 inhibitor approved for single-agent use is trametinib (Yaeger R and Corcoran RB, 2019). Trametinib is a non-competitive inhibitor of MEK1/2 that functions by binding to an allosteric pocket adjacent to the ATP-binding site. Binding of trametinib causes a conformational change in the MEK1/2 protein structure that occludes the ATP binding pocket and prevents kinase activation. Not only does

trametinib have sub-nanomolar affinity for both MEK1 and MEK2, but it also has fewer off-target interactions compared to other ATP mimetic kinase inhibitors.

Trametinib was the first FDA-approved MEK inhibitor in 2013 and was indicated for the treatment of BRAF V600E/K-mutated metastatic melanoma (Liu, 2018). In the METRIC trial (NCT01245062), single agent trametinib significantly increased progression-free survival by over 3 months compared to standard chemotherapy, as well as improved overall survival rate (81% vs. 67%) and complete or partial responses (22% vs. 8%) (Wright and McCormack, 2013). Beyond overall survival, the effects of single-agent RAF or MEK1/2 inhibition shows dramatic but transient clinical responses. While trametinib remains the only MEK1/2 inhibitor indicated for single-agent treatment of BRAF V600E/K-mutant melanoma, two additional MEK1/2 inhibitors, binimetinib and cobimetinib, have also reached FDA-approval. Combination therapy has shown the ability to overcome drug cytostasis and is preferentially used to treat RAS- or RAF-mutant cancers over single-agent therapy.

Based on this early success of in melanoma, the efficacy of trametinib was assessed in preclinical neuroblastoma models. Although gain-of-function *ALK* mutations activate RAS-MAPK pathway signaling, cell lines with *ALK* mutations were the least sensitive to trametinib *in vitro* and *in vivo* of all RAS-MAPK pathway mutated cell lines (Eleveld, 2015, Umapathy, 2017). Trametinib was most potent in *RAS*-mutated cell lines, followed closely by *NF1*-mutated cell lines and xenograft

models. However, this activity is transient and cytostatic *in vitro*, necessitating further therapeutic approaches to achieve sufficient antiproliferative effect.

Figure 1-1. The RAS-MAPK signaling pathway in cancer.

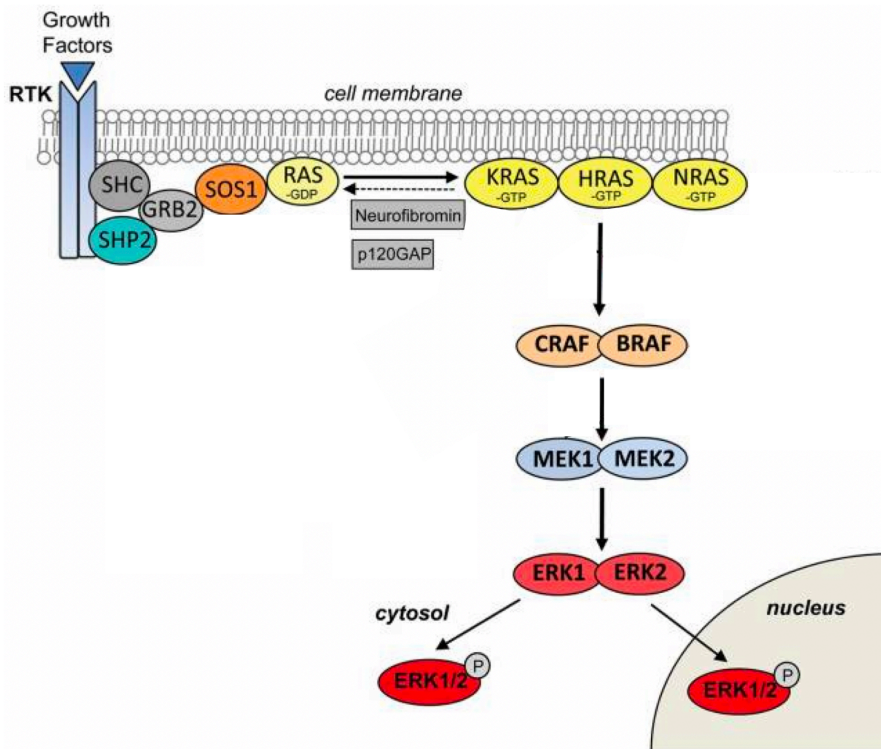


Figure 1-1: Pathway activation is initiated by the binding of an extracellular ligand to receptor tyrosine kinases (RTKs) and receptor dimerization and transautophosphorylation. These phosphorylation sites serve as docking sites for adapter proteins which recruit guanine nucleotide exchange factors (GEFs) to the plasma membrane. The interaction of RAS proteins with GEFs accelerates the conversion of RAS from the inactive GDP-bound to the active GTP-bound state. Activated RAS is able to initiate an array of important downstream pathways, including the canonical RAF-MEK-ERK kinase cascade. RAS (NRAS, KRAS, HRAS) phosphorylates and activates RAF (ARAF, BRAF, and CRAF), which then phosphorylates and activate MEK1/2 (MAPK kinase). MEK1/2 phosphorylate ERK1/2 (MAPK), which serve as the ultimate effector kinases.

IV. MEK Inhibitor Drug Combination Design

Encouraged by the prolonged survival achieved by MEK1/2 inhibition, continued efforts have focused on combining trametinib with rationale targeted inhibitors to improve survival outcomes. The goal of combination therapy is to eliminate alternate routes of survival to single-agent therapy, thereby crippling the ability of a cancer cell to develop therapeutic resistance. Although MEK1/2 inhibition has proven to be effective in the context of RAS-MAPK pathway hyperactivation, the efficacy of individual drug combinations appears to be much more dependent on the signaling milieu of specific cancer cell types.

One approach to developing MEK1/2 inhibitor drug combinations has been to target alternate kinases within the RAS-MAPK pathway. This double-hit approach is predicated on the assumption that resistance occurs through ERK reactivation and loss of feedback inhibition. In BRAF V600E/K malignant melanoma, the combination of BRAF and MEK1/2 inhibition has been proven effective and is now FDA-approved. Vemurafenib, dabrafenib, and the most recent RAF inhibitor to gain FDA-approval, encorafenib, are approved for combination treatment with MEK1/2 inhibitors cobimetinib, trametinib, and binimetinib, respectively (Lorentzen HF, 2019). In a randomized phase III clinical study (NCT01597908) of BRAF V600E/K metastatic melanoma, patients were randomly assigned to receive either a combination of trametinib and RAF inhibitor, dabrafenib, or single-agent RAF inhibitor, vemurafenib (Robert, 2015). The objective response rate was 64% in the combination group and 51% in the single-

agent vemurafenib group alone. Based on these results, combined BRAF and MEK1/2 inhibition was able to overcome pathway reactivation to improve upon overall survival. Unfortunately, a vast amount of survival data collected from many clinical trials suggests that BRAF inhibitors are largely ineffective in models with wild-type BRAF alleles (Robert, 2015). BRAF mutations are rare in neuroblastoma, so combined inhibition of BRAF and MEK1/2 is unlikely to be efficacious in the vast majority of neuroblastomas.

Another mechanism implicated in resistance to MEK1/2 inhibition is collateral activation of PI3K/AKT pathway signalling, seemingly due to upstream RTK activation promoting parallel pathway activation. In KRAS-mutant preclinical models of colon, pancreatic, lung, and melanoma cancer cell lines, synergy was observed between an AKT inhibitor, MK-2206, and MEK1/2 inhibitor, selumetinib (Tolcher, 2014). This effect was also observed in a KRAS-mutant colorectal cancer xenograft model, but not in a BRAF V600E melanoma xenograft model. Building on these results, numerous clinical trials have been established to test the combination of a MEK1/2 inhibitor and PI3K inhibitor in cancer. One study in particular, a phase I study of the combination of MK-2206 and selumetinib, was conducted and showed partial responses in 3/13 KRAS-mutant NSCLC patients and 1/2 ovarian cancer patients, but no objective responses were seen in KRAS-mutant colorectal cancer (Tolcher, 2014). These results underscore the complex heterogeneity between cancer types with similar driver mutations

In neuroblastoma specifically, there have also been ongoing efforts to identify drug combinations partners in models with RAS-MAPK pathway hyperactivation. Deregulation of cyclin-dependent kinases 4 and 6 (CDK4/6) was shown to confer resistance MEK1/2 inhibition. A MEK1/2 inhibitor, binimetinib, and a CDK4/6 inhibitor, ribociclib, were observed to have therapeutic synergy across a panel of neuroblastoma cell line models (Hart, 2016). In murine xenograft models, the combination of binimetinib and ribociclib contributed to tumor growth delay and prolonged survival over single-agent or vehicle treatment (Hart, 2016). Based on this preliminary evidence, the Next Generation Personalized Neuroblastoma Therapy (NEPENTHE, NCT02780128) Phase I clinical trial was devised to sequence each patient's individual tumor to identify actionable genetic mutations. If a mutation in either *ALK*, CDK4/6, or the RAS-MAPK pathway is discovered, they receive targeted therapy (with ceritinib, ribociclib, and/or trametinib). Despite the preclinical success of MEK1/2 and CDK4/6 dual inhibition, it was not well-tolerated in the clinic and was abandoned by Novartis. This project aims to build upon previous progress by investigating alternate MEK1/2 inhibitor drug combination strategies to achieve better clinical responses and improve survival outcomes for relapsed neuroblastoma.

V. YAP-Hippo Pathway

In this dissertation, Chapters 2 and 3 focus on the involvement of the Hippo pathway protein YAP in promoting *de novo* resistance to trametinib in RAS driven

neuroblastoma. The Hippo pathway was first identified in *Drosophila* to control organ growth during development. Overexpression of *Yki*, the *Drosophila* ortholog of the human Yes-associated protein (YAP), caused massive overgrowth of epithelial structures (Huang, 2005). In humans, YAP is the primary effector protein regulated by the upstream Hippo pathway (Fig. 1-2). The Hippo pathway can be activated by a host of upstream signals, including mechanotransduction (the process by which cells sense and convert mechanical stimuli into biochemical signals), cell density, mitogen-activated signaling, and cell-cell contact. As a co-activator, YAP can bind to transcription factors such as the TEAD family of transcription factors, to promote transcription of YAP target genes, including *CTGF* (connective tissue growth factor) and *CYR61* (cysteine-rich angiogenic inducer 6) (Zhao, 2007; Zhang, 2011). TAZ, a paralog of YAP, is known to have both overlapping and independent functions as YAP and is regulated by similar mechanisms via phosphorylation.

Figure 1-2. YAP and the Hippo signaling pathway in cancer.

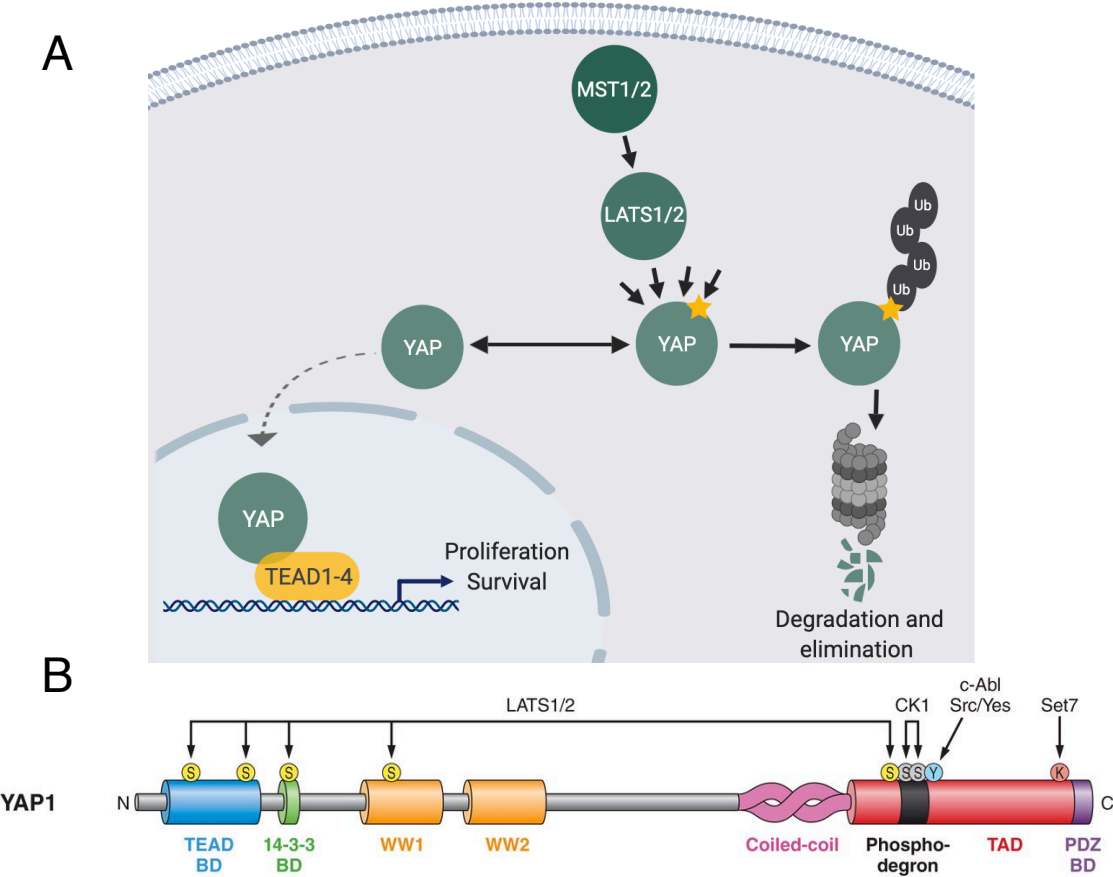


Figure 1-2. A) Mechanotransduction, cell density, mitogen-activated signaling, and cell-cell contact can activate MST1/2 kinases, which phosphorylate and activate LATS1/2 kinases. LATS1/2 then phosphorylate YAP at S127, which recruits 14-3-3 protein binding and is retained in the cytoplasm. Subsequent YAP phosphorylation events recruit SCF, an E3 ubiquitin ligase. Upon poly-ubiquitination, YAP is flagged for proteasomal degradation and elimination. If the upstream Hippo pathway is inactive and YAP remains in an unphosphorylated state, it is able to translocate into the nucleus. The YAP protein structure lacks nuclear localization signal and translocates into the nucleus through nuclear pores, although the regulation of YAP nuclear transport has not been fully described (Wang, 2016b). Upon entering the nucleus, YAP can function as a co-activator or co-repressor of transcription. B) LATS1/2 phosphorylate YAP at five serine residues in the YAP protein, indicated by yellow circles with “S” in the center.

In cancer, YAP has been described as both an oncogene and a tumor suppressor in a cell type-specific manner. YAP has been described as a stemness-promoting factor in liver, intestinal, and skin stem cell populations (Hindley CJ, 2016). In other nervous system cancers, increased activation of YAP has been shown to promote proliferation and tumorigenesis (Fernandez-L 2009; Orr, 2011). High expression of YAP in breast cancer and colorectal cancer correlates with high histological grade, metastasis, and poor overall survival (Zanconato, 2016). Furthermore, liver-specific overexpression of YAP in mice causes hepatomegaly and hepatocellular carcinoma tumor formation (Dong, 2007). Reduced LATS-mediated phosphorylation and inactivation of the Hippo pathway is well-supported, but the rarity of inactivating pathway mutations in human cancers suggests that alternate regulatory mechanisms may be at play (Harvey, 2013; Wang Y, 2018). YAP can also be regulated by Rho-GTPases, actin dynamics, G-protein coupled receptor (GPCR) signaling, and metabolism, all of which may be altered in a cancer cell (Zanconato, 2016). Nevertheless, loss of LATS1/2 diminishes the ability of each of these signaling modalities to regulate YAP activity via phosphorylation, suggesting that the LATS1/2 is the primary upstream regulator of YAP regardless of the causal signaling input (Zanconato, 2016).

The extent of oncogenic YAP signaling as a driver of tumorigenesis has only recently been elucidated with the advent of omics tools to study somatic Hippo pathway alterations (Wang Y, 2018). Molecular profiling of data from the Cancer

Genome Atlas (TCGA) identified 19 Hippo core pathway gene alterations. Amplification of *STK3* (MST2) and *WWTR1* (TAZ) were the most frequent somatic copy number alterations, followed by *TEAD4*, *YAP1*, and *STK4* (MST1) (Wang Y, 2018). In fact, the most frequently amplified gene in cervical squamous cell carcinoma was *YAP1*. The tumor suppressive function of *LATS1/2* was consistent with the observation of deep deletions in *LATS1/2*. However, somatic mutations in *YAP1* and *WWTR1* (TAZ) are rarely found but have been discovered at low frequencies (Wang Y, 2018). Furthermore, loss-of-function truncating mutations in neurofibromatosis type 2 gene, *NF2*, were observed and have been shown to drive oncogenic Hippo pathway activation (Bianchi AB, 1995; Li W, 2014; Sekido Y, 1995; Wang Y, 2018).

Investigation of YAP in neuroblastoma had not been extensively explored until very recently, but literature suggests that YAP functions as an oncogene to promote cellular proliferation, survival, and, metastasis (Yang, 2017, Seong, 2017). Although YAP expression was not diagnostic across a large cohort of neuroblastoma patients, a YAP pathway signature was prognostic of patient outcome (Seong, 2017). This observation is supported by evidence of upregulated YAP transcriptional activity in relapsed neuroblastomas compared to matched primary tumors (Schramm, 2015). Further, mice injected with YAP/TAZ-depleted neuroblastoma cells experienced a significant reduction in metastases and an increase in survival compared to control cells (Seong, 2017). Altogether, these

data suggest that YAP signaling may be particularly relevant to relapsed neuroblastoma.

Although YAP is not predicted to be a primary driver of neuroblastoma development, recent literature suggests that it may be highly relevant in the context of RAS-MAPK mutated cancers. Using a pooled shRNA screen, YAP was discovered as genetic dependency in response to MEK1/2 inhibition in BRAF V600E-mutated NSCLC cells (Lin, 2015). In response to trametinib, growth inhibition of these cells increased by approximately 30% upon YAP1 knockdown (Lin, 2015). In this study, investigators focused primarily on BRAF V600E-mutated cells from a variety of cancers, including neural-crest derived NSCLC and melanoma, but discovered that cells with KRAS and NRAS mutations were also more sensitive to trametinib upon YAP knockdown (Lin, 2015). In two KRAS-addicted colon cancer and lung cancer cell lines, YAP was shown to rescue cell viability and promote resistance in response to inducible KRAS knockdown. KRAS and YAP were shown to converge on the transcriptional regulation of a subset of genes promoting epithelial-mesenchymal transition (EMT) (Shao, 2014). Despite this evidence for YAP playing a role in RAS-activated cancer cell response to MEK1/2 inhibition, the precise signaling mechanisms remain inconclusive.

VI. Research Aims

Innovation Statement

Although there have been incremental improvement in long-term outcomes for patients with neuroblastoma, there is an ongoing and urgent need for more precise and effective therapies. Here, we sought to identify intrinsic resistance mechanisms to MEK1/2 inhibition through parallel oncogenic pathways in RAS-driven neuroblastoma, with the major ultimate goal of discovering synergetic drug combinations. This project evaluates YAP as a potential contributing factor to acquired trametinib resistance in neuroblastoma and the utility of novel YAP activity inhibitors as potential partners of a therapeutic combination. We hypothesized that reducing YAP transcriptional activity would improve sensitivity to trametinib in RAS-driven neuroblastoma cell lines. In addition, this project utilized a high-throughput drug screen for alternate drug combinations for the treatment of a variety of RAS-MAPK pathway aberrant neuroblastomas. We hypothesized that a large-scale survey of pharmacological compounds would define potentially unknown compensatory mechanisms in response to trametinib treatment. Overall, the goal of the project was to identify potential trametinib drug combinations for translation to the NEPENTHE Phase I clinical trial at the Children's Hospital of Philadelphia (CHOP). The functional characterization of potential targets of acquired resistance builds upon ongoing efforts to better understand clinical responses of relapsed neuroblastomas to trametinib;

furthermore, this project aims to contribute to the larger field of MEK1/2 inhibitor bypass mechanisms in cancer.

Specific Aim 1: Evaluate the role of Hippo pathway protein YAP as a major modulator of resistance to MEK1/2 inhibition in relapsed neuroblastoma

Specific Aim 1A: Investigate the contribution of YAP-Hippo pathway signaling to trametinib efficacy in RAS-driven neuroblastoma cell lines

I observed the effect of trametinib on YAP phosphorylation and cellular localization. Using CRISPR-Cas9 genetic editing and lentiviral overexpression, I modulated YAP expression in neuroblastoma cell lines to assess sensitivity and determine underlying signaling mechanisms. I hypothesized that YAP knockout would sensitize RAS-driven neuroblastoma cell lines to trametinib and improve overall efficacy.

Specific Aim 1B: Determine if combined MEK1/2 inhibition and YAP activity inhibition is synergetic in RAS-driven neuroblastoma cell lines

I tested novel inhibitors of TEAD palmitoylation, which is critical for YAP/TEAD transcriptional activity, in combination with trametinib in two RAS-driven neuroblastoma cell lines to evaluate synergy. I analyzed the effect of TEAD palmitoylation inhibitors on YAP target gene expression as a single-agent and in combination with trametinib. I hypothesized that inhibiting YAP/TEAD

transcriptional activity in combination with trametinib would produce synergy in RAS-driven neuroblastoma cell lines.

Specific Aim 2: Identify synergistic drug combinations with trametinib for preclinical validation

I designed and performed a high-throughput drug screen using a library of >3,000 compounds to identify effective trametinib drug combinations across a panel of RAS-MAPK aberrant neuroblastoma cell lines. I performed data analysis to narrow down the list of possible drug combinations for preclinical validation. I hypothesized that profiling a large drug library would reveal specific and potentially unknown signaling dependencies in response to trametinib in RAS-driven neuroblastoma cell lines.

Significance

The proposed work is innovative because it is the first study to comprehensively explore druggable routes of intrinsic resistance to trametinib in RAS-driven neuroblastomas for preclinical validation and clinical application. The functional characterization of potential targets of resistance builds upon ongoing efforts to better understand clinical responses of relapsed neuroblastoma to trametinib and contributing to the larger field of MEK inhibitor bypass mechanisms in cancer. This dissertation contributes to the larger field of trametinib treatment

regimen design in cancer and has immediate relevance to ongoing and future therapies for relapsed neuroblastoma patients.

CHAPTER 2: ROLE OF HIPPO PATHWAY PROTEIN YAP1 IN RESISTANCE TO MEK1/2 INHIBITION IN RAS ACTIVATED NEUROBLASTOMAS

This chapter presents work featured in article: Coggins, G.E., Farrel, A., Rathi, K.S., Hayes, C.M., Scolaro, L., Rokita, J.L., Maris, J.M. (2019). The Hippo pathway effector protein YAP1 modulated resistance to MEK1/2 inhibition in neuroblastomas with hyperactivated RAS pathway signaling. Cancer Research. Accepted for publication 9/24/19.

Please see end of chapter for all figures and tables.

I. Abstract

Relapsed neuroblastomas harbor an enrichment in mutations activating RAS-MAPK signaling pathway. The MEK1/2 inhibitor trametinib has shown tumor growth delay, but not sustained regressions, in neuroblastoma preclinical models. Recent studies have implicated the Hippo pathway transcriptional coactivator protein YAP1 as an additional driver of relapsed neuroblastomas, as well as a mediator of trametinib resistance in other cancers. We hypothesized that increased YAP1 transcriptional activity is a mechanism of MEK1/2 inhibition resistance in RAS-driven neuroblastomas. Here, we used a highly annotated set of high-risk neuroblastoma cellular models to modulate YAP1 expression and RAS pathway activation to test our hypothesis. In NLF (biallelic *NF1* inactivation) and SK-N-AS (NRAS Q61K) cell lines, trametinib caused a near-complete translocation of YAP1 protein into the nucleus at 72 hours. YAP1 depletion sensitized neuroblastoma cells to trametinib, while overexpression of constitutively active YAP1 protein induced trametinib resistance. The mechanism explaining YAP1 deletion

sensitizing RAS-driven neuroblastomas to trametinib was significant enhancement of G₁/S cell cycle arrest, mediated through a depletion of MYC/MYCN and E2F transcriptional output.

II. Introduction

Neuroblastoma is a malignancy of the developing sympathetic nervous system (Hoehner JC, 2010; Park JR, 2010; Maris JM, 1999; Maris JM, 2007; Park JR, 2013; Maris JM, 2010). Half of all diagnosed neuroblastomas are classified as “high-risk”, for which cure rates remain low. Aggressive empiric multimodal therapy, including surgery, chemotherapy, radiation therapy and more recently immunotherapy have shown incremental improvements in survival rates at the cost of a host of chronic health comorbidities in survivors. Relapse after standard of care remains largely incurable (Maris JM, 2010; Cohn SL, 2009). Thus, there is an urgent need for more effective and precise therapies.

The development of novel treatments has been hindered by the relative lack of molecularly targetable genomic lesions. Recurrent kinase domain gain-of-function mutations in the *ALK* oncogene occur in 8-15% of all newly-diagnosed neuroblastomas (Maris JM, 2007; Park JR, 2013; Maris JM, 2010; Cohn SL, 2009; Mosse YP, 2008), but may be present in a much larger percentage of relapse specimens (Eleveld TF, 2015; Padovan-Merhar OM, 2016; Schleiermacher G, 2014; Schramm A, 2015). Indeed, compared to matched primary tumors, relapsed neuroblastomas have a significantly higher mutational burden, with clonal

enrichment in mutations in RAS-MAPK pathway genes beyond *ALK* such as *NRAS*, *KRAS*, *BRAF*, *PTPN11* and *NF1* (Eleveld TF, 2015; Padovan-Merhar OM, 2016; Schramm A, 2015). Neuroblastoma cellular models with these genetic aberrations have elevated levels of phosphorylated ERK1/2 and are extremely sensitive to the MEK1/2 noncompetitive inhibitor trametinib *in vitro*, with low nanomolar IC50s (Eleveld TF, 2015, Rader J, 2013). However, single agent MEK inhibition is cytostatic and results only in tumor growth delay in neuroblastoma xenotransplantation models with RAS hyperactivation (Eleveld TF, 2015; Hart LS, 2017; Umapathy G, 2017), similar to the experience in multiple preclinical and clinical settings with single agent inhibition of MAPK pathway mutated cancers (Lugowska I, 2015; Lito P, 2014; Lito P, 2013; Zhao Y, 2014). For this reason, combination strategies are being pursued to avoid tumor escape from therapy and improve long-term responses. Dual inhibition of MEK1/2 and rational targets, such as BRAF, PI3K/AKT, and CDK4/6, have shown promise in other tumor types, including neuroblastoma (Rader J, 2013; Hart LS, 2017; Lugowska I, 2015; Lito P, 2014; Lito P, 2013; Zhao Y, 2014; Yao Z, 2015), but in the latter case all xenografts eventually escaped dual MEK and CDK4/6 inhibition (Lito P, 2013).

The hippo signaling pathway is considered tumor suppressive through cytosolic sequestration of the transcriptional co-activator protein YAP1 (Huang J, 2005; Dong J, 2007; Overholtzer M, 2006). Activated YAP1 mediates diverse biologic functions such as organ size, cellular proliferation, and cell survival (Chan SW, 2011; Chen Q, 2015; Zhao B, 2007; Pan D, 2010; Yu FX, 2012; Wu S, 2003;

Wei X, 2007). YAP1 dephosphorylation allows translocation into the nucleus and interaction with TEAD family and other transcription factors to initiate transcription of a multiple gene targets (Lei QY, 2008; Steinhardt AA, 2008; Chen L, 2010; Liu-Chittenden Y, 2012; Cottini F, 2014; Adler JJ, 2013; Rayego-Mateos S, 2015). Several groups have reported that YAP1 may be involved in resistance to trametinib in RAS-driven cancers (Kapoor A, 2014; Lin L, 2015; Shao DD, 2014; Hong X, 2014; Slemmons KK, 2015). Recently, increased YAP1 activity was reported as a hallmark of relapsed neuroblastoma after intensive chemoradiotherapy (Schramm A, 2015; Zhao B, 2007). In addition, inhibition of YAP1 signaling has also been shown to abrogate neuroblastoma metastasis in preclinical models (Seong BK, 2017). Paradoxically, the *YAP1* gene is located on chromosome arm 11q, a region that shows frequent hemizygous deletion, particularly in high-risk neuroblastomas without MYCN amplification (Attieyeh EF, 2005; Mlakar V, 2017). Here we explore the hypothesis that derepression of YAP1 is a critical mediator of resistance to MEK inhibition in neuroblastomas with hyperactivated MAPK signalling.

III. Methods and Materials

Cell Culture and Chemicals

Human-derived neuroblastoma cell lines were obtained from the Children's Hospital of Philadelphia cell line bank, the Children's Oncology Group, and the ATCC (Harenza JL, 2017). Cells were cultured in RPMI-1640 medium containing

10% FBS, 2 mM L-Glutamine at 37 °C under 5% CO₂. The genomic identity of the cell lines was confirmed using the GenePrint 24 (Promega, Guardian Forensic Sciences) and cell lines were free of mycoplasma contamination. Trametinib dissolved in DMSO (Cellagen Technologies #C4112-5s) was used for *in vitro* assays, with 0.1% DMSO as a negative control treatment. All cell lines were derived from deidentified neuroblastoma patient tumor samples and the Children's Hospital of Philadelphia Institutional Review Board agreed with the investigators that this work is not considered human subjects research.

Cell Viability Assays

Cells were seeded in 96-well cell culture plates at 2,500-4,000 cells per well depending on growth kinetics. Drug treatments were performed in triplicate 24 hours later over a six-log dose range (0.01-10,000 nM). IC₅₀ values for trametinib were calculated using area under the curve at 72 hours post-treatment. Cell viability was assessed using CellTiter-Glo (Promega). Cell growth assays were performed using the IncuCyte Live Cell Analysis System (IncuCyte ZOOM, Essen Bioscience) with the 20x objective lens during a 72-hour treatment.

CRISPR-Cas9, Plasmids and Lentiviral Delivery

To produce *YAP1*-targeting CRISPR-Cas9 knockout cell lines, scrambled sgRNA CRISPR/Cas9 All-in-One Lentivirus (ABM #K011) and the *YAP1* sgRNA CRISPR All-in-One Lentivirus Set (Human) (ABM #K2653115) targeting the *YAP1* gene (Accession Number: NM_1006106.4) were used. Virus with sgRNA targeting sequence #1 (5'-GTGCACGATCTGATGCCCGG-3') and sequence #2 (5'-

CGCCGTCATGAACCCCAAGA-3') of the YAP1 TEAD binding domain were selected for these experiments. To produce *YAP1* knockout pools in SKNAS and NLF, cells were transduced with lentivirus for the sgRNA against sequence #1 according to the manufacturer's protocol. For NLF isogenic cell lines, a second *YAP1* knockout pool was produced using lentivirus targeting sequence #2. Two single-cell clones were selected from each *YAP1* knockout pool and grown into stable isogenic cell lines. Antibiotic selection was performed using 1 µg puromycin (Sigma, #P9620).

The lentiviral YAP-5SA overexpressing plasmid was produced by inserting the YAP-5SA sequence from the MYC-YAP-5SA plasmid (Zhao B, 2007) (Addgene #33091) into a lentiviral CMV-puro DEST vector (Campeau E, 2009) (Addgene #39481) using the PCR Cloning System with Gateway™ Technology with pDONR™221 & OmniMAX™2 Competent Cells (Invitrogen #12535029) according to the manufacturer's recommended protocol. For lentiviral production, the YAP-5SA lentiviral plasmid was transfected in combination with the pMD2.G VSV-G envelope expressing plasmid (Addgene #12260) and psPAX2 lentiviral packaging plasmid (Addgene #12259). Plasmids were transduced at equimolar concentrations of 3 µM into HEK-293T cells (ATCC, CRL-3216) using Lipofectamine 3000 (Thermo Fisher Scientific #L3000008). Viral supernatant was harvested at 48 hours and was filtered using a 0.45 µm filter and added to cells with 3 µg polybrene. Antibiotic selection was performed using 1 µg puromycin.

Primers

Sequencing primers for endogenous to detect mutations in both of the target sequences in the endogenous YAP1 protein TEAD binding domain: YAP1_F (5'-TAAAGAGAAAGGGGAGGCGG-3') and YAP1_R (5'-CCGGGAAGAAAGAAAGGAAGA-3'). Primers for Gateway cloning were designed according to the manufacturer's recommendations to remove the YAP-5SA sequence from the MYC-YAP-5SA retroviral plasmid with flanking *attB* sites. These primer sequences were: YAP-5SA_F (5'-GGGGACAAGTTTGTACAAAAAAGCAGGCTTCACCATGGAACAAAACTCATCTCA-3') and YAP-5SA_R (5'-GGGGACCACTTTGTACAAGAAAGCTGGGTCTATAACCATGTAAGAAAGCTTTCTTT-3').

Western Blotting

Protein was isolated from whole cell lysates using lysis buffer containing 1X Cell Lysis Buffer (10X from Cell Signaling, #9803), 2 mM PMSF (Cell Signaling, #8553S), in 100% isopropanol, and 1% phosphatase inhibitor cocktails 2 (Sigma, #P5726) and 3 (Sigma, #P0044). Protein concentration was determined using the Bradford protein assay (Bio-Rad). Approximately 20 µg of protein were run on 4-15% gradient Tris-Glycine gels (Bio-Rad, #5671085) and transferred using the Bio-Rad transfer system. Antibodies used for western blotting include (Cell Signaling, unless otherwise indicated): YAP1 (D8H1X) (1:1000, #14074), p-YAP1 (S127) (D9W2I) (1:500, #13008S), p-ERK (1:2000, #4370), ERK (1:2000, #4695), β-Actin (1:5000, #4967S), RB (1:2000, #9309), p-RB (S807-811) (1:1000, #9307), PARP

(1:1000, #9532), cleaved PARP (1:1000, #5625S), MYCN (1:2000, #9405S), Caspase-3 (1:1000, #9662), TATA Box binding protein (TBP) (1:1000, Abcam #ab818). Western blots were visualized using SuperSignal West Femto Maximum sensitivity substrate (Thermo Fisher Scientific, #34095) and the FluorChem Q chemiluminescent imaging system and FluorChemQ software v3.4.0 (ProteinSimple).

RNA isolation and RT-qPCR

RNA was isolated using the Qiagen miRNEasy Mini Kit (Qiagen). Reverse transcription was performed using the iScript Select cDNA Synthesis Kit (Bio-Rad #1708897). Quantitative PCR was performed using the Taqman 2X Master Mix (Thermo Fisher #4304437) on 384-well plates using the 7900HT Fast Real-Time PCR instrument (Applied Biosystems) and the SDS v2.4 software (Applied Biosystems). Taqman probes (Thermo Fisher Scientific, #4331182) used included: *YAP1* (Hs00902712_g1) *HPRT1* (Hs02800695_m1), *GAPDH* (Hs03929097_g1), *CTGF* (Hs01026927_g1), *CYR61* (Hs00155497_m1), *CDK1* (Hs00938777_m1), *MCM4* (Hs00907398_m1), *MCM6* (Hs00195504_m1), *POLA1* (Hs00213524_m1), *CCNE1* (Hs01026536_m1), *E2F1* (Hs00153451_m1).

Flow Cytometry

Samples for cell cycle analysis were collected after 72 hours of trametinib treatment at the IC₅₀ concentration of NLF (20 nM) and SKNAS (10 nM). Cells were detached with versene (0.02% EDTA in HBSS), washed with PBS + 1% FBS, fixed for approximately 10 seconds by adding ice cold 70% ethanol dropwise with

constant vortexing, and stored at -20°C. Cells were stained using 1 uL FxCycle Violet (Invitrogen #F10347) per 1 mL PBS and analyzed using the CytoFLEX LX with 6 lasers (Beckman Coulter). Data analysis was performed using the FlowJo v10 software as described previously (Hart LS, 2017).

RNA Sequencing

Cells were plated in triplicate and treated with 20 nM trametinib for 72 hours prior to collection. Cells were lysed on the plate using the QIAzol lysis reagent (Qiagen #79306) and homogenized with Qiashrepper tubes (Qiagen #79654). RNA was then isolated using the RNeasy Mini Kit (Qiagen #74104) according to the manufacturer's protocol and quality was determined using the TapeStation 2200 (Agilent Technologies). All 18 samples were of optimal quality and achieved RIN scores of 10.0. RNA synthetic spike-ins were added to each sample (Hardwick SA, 2016), with Mix A added to the NLF sgCon samples and Mix B added to the NLF *YAP1*^{-/-} #1 and #4 samples. Library preparation was done using 1 µg of RNA using the TruSeq Total mRNA Kit with Gold rRNA Removal Mix as recommended (Illumina #15031048). All 18 samples were sequenced using v2 chemistry, 2x150bp, and run on one high-output flow-cell of an Illumina NextSeq 500 instrument. Libraries were demultiplexed, Illumina adapters were trimmed, and FASTQ file generated using the Illumina NextSeq Control Software version 2.02.

Raw fastq files (n = 18) from RNA-sequencing data with an average sequencing depth of 22 million reads were aligned to human hg19 primary assembly reference

genome using the STAR aligner v2.5.3a (Dobin A, 2013). Gene expression was quantified as Fragments Per Kilobase of transcript per Million mapped reads (FPKM) and transcript per million (TPM) using RSEM v1.2.28 normalization and Gencode v23 gene annotation (Li B, 2011). On an average, 88.05% reads were uniquely mapped to the reference genome. Normalization of RNA expression between samples was performed by analyzing the synthetic spike-in standards using Anaquin software toolkit distributed by Bioconductor (Wong T, 2017).

Differential expression analysis was performed using the R package, DESeq2. Values were \log_2 -transformed and biological replicates (N=3) were averaged within each cell line and treatment group. Differentially-expressed genes underwent Gene Ontology analysis using the ToppFun tool from the ToppGene Suite and the top 5 ontologies were chosen (Chen J, 2009). GSEA was performed using the Molecular Signatures Database Hallmarks Gene Set collection and run for 1,000 iterations with a FWER p value cutoff of <0.01 . All RNA-sequencing data have been deposited in the Gene Expression Omnibus under Accession Number GSE130401.

Statistics

Group comparisons were determined with a two-tailed t-test with a significance cutoff of $p < 0.05$. Data analysis was performed using GraphPad Prism and R Studio.

IV. Results

Trametinib causes YAP1 nuclear translocation in RAS-MAPK activated neuroblastoma cell lines

We selected 16 of the 39 cell lines recently profiled and reported by our group based on *YAP1* mRNA expression and mutation status (Harenza JL, 2017) (Fig 2-1A). The majority, but certainly not all, of the lines with mutations in the canonical MAPK pathway showed *YAP1* mRNA and protein expression, but only one of the seven *ALK* mutated lines, and this line (SKNSH) showed robust protein expression in the absence of detectable *YAP1* mRNA. *MYCN* amplification and 11q copy number alterations for each cell line can be found in Supplemental Table S1. Given that phosphorylation status and subcellular location are inherent to *YAP1* transcriptional activity, we investigated whether trametinib alters *YAP1* nuclear localization in two high *YAP1* expressing cell lines, NLF and SKNAS. Nuclear and cytoplasmic extracts of NLF and SKNAS were collected after 72 hours of exposure to trametinib. We observed a reduction in cytoplasmic phosphorylated *YAP1* across the time course, and a concomitant enrichment of nuclear *YAP1* (Fig. 2-1B and C). Together, these data suggest that trametinib treatment in *YAP1*-expressing and MAPK mutant neuroblastoma models causes depression of the hippo pathway resulting in rapid (days) translocation of *YAP1* to the nucleus.

Figure 2-1. Trametinib causes nuclear accumulation of unphosphorylated YAP1 protein.

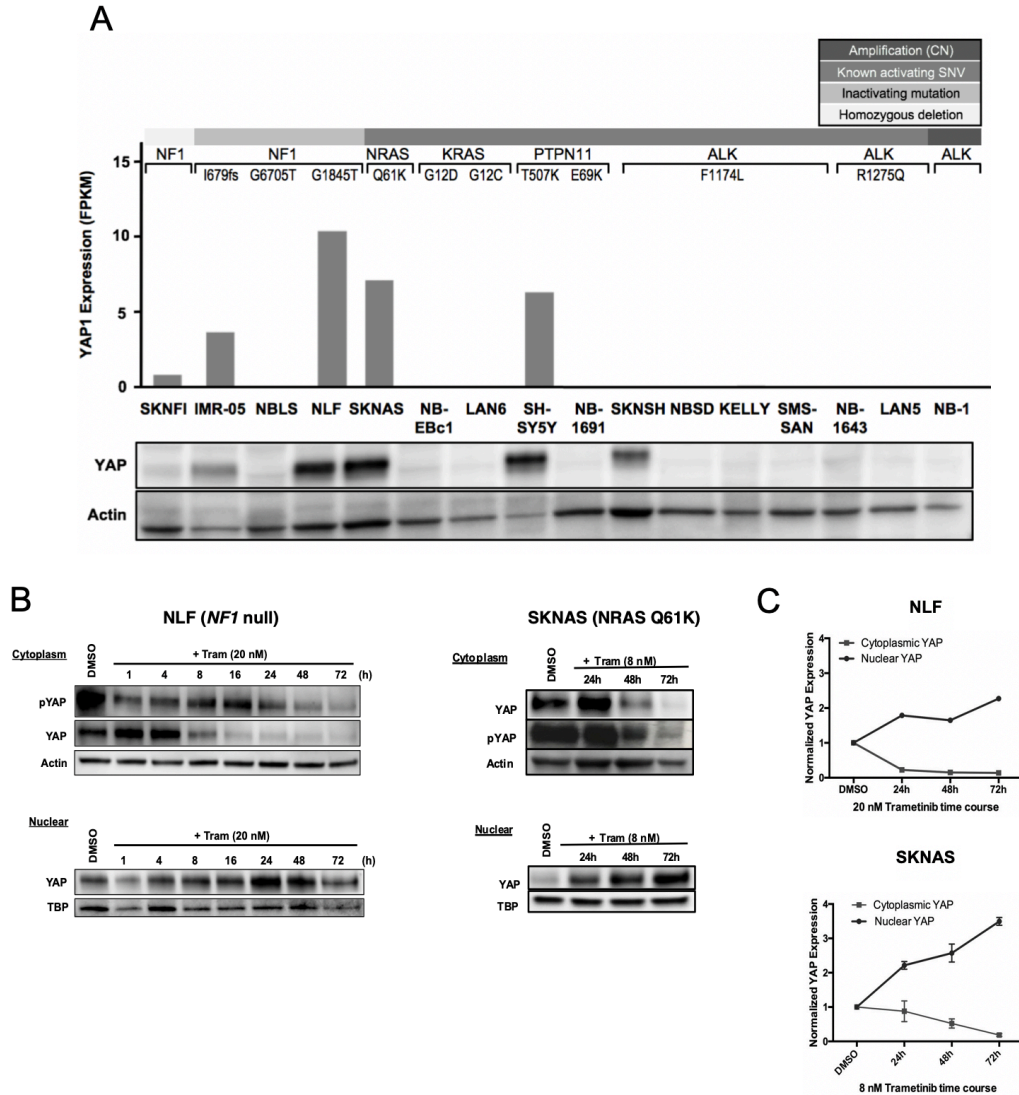


Figure 2-1 Legend: **(A)** Expression of *YAP1* mRNA (FPKM) across a panel of neuroblastoma cell lines with known RAS-MAPK pathway mutations indicated above. Below, YAP1 (70 kD) is expressed in a subset of RAS-driven neuroblastoma cell lines with a beta-actin (40 kD) loading control. **(B-C)** 72-hour trametinib treatment of NLF (20 nM) and SKNAS (10 nM) causes nuclear

translocation of YAP1 (70 kD) protein compared to TATA Box-binding protein (TBP, 40 kD) (B), which was quantified using densitometry (C).

Loss of YAP1 expression sensitizes neuroblastoma cell lines to trametinib

To determine whether YAP1 plays a role in sensitivity to trametinib in neuroblastoma, we selected two neuroblastoma cell lines, NLF (biallelic *NF1* inactivation) and SKNAS (NRAS Q61K), which both harbor endogenous hemizygous deletions of 11q and thus *YAP1* (Harenza JL, 2017). We employed lentiviral CRISPR-Cas9 gene editing to produce pools of *YAP1* null NLF and SKNAS cells. Lentivirus containing sgRNA targeted to the *YAP1* TEAD binding domain or a scrambled control (sgCon) were used to transduce cells (Supplementary Fig. 2-S1A). We observed incomplete reduction of *YAP1* mRNA and protein expression in both NLF and SKNAS sg*YAP1* pools (Supplementary Fig. 2-S2A and B). Despite this modest reduction in expression, we next showed that the canonical YAP1 target genes *CTGF* and *CYR61* (Chan SW, 2011) were significantly downregulated in NLF and SKNAS *YAP1*-depleted cells (Supplementary Fig. 2-S2C), suggesting a significant impact on YAP1-mediated transcription. We next sought to determine the impact of trametinib exposure on cell viability in the isogenic pairs differing in YAP1 transcriptional activity. We observed that the response of these cell lines to trametinib treatment was directly related to the degree of modulation of YAP1 target genes (Supplementary Fig. 2-S2D). Sensitivity to trametinib shifted in both NLF and SKNAS upon *YAP1*

depletion, with IC50s in SKNAS shifting from 6.57 nM in sgCon) to 0.81 nM in sgYAP1 ($p=0.0255$), as well as in NLF, with IC50s shifting from 15.98 nM in sgCon to 7.76 nM in sgYAP1 ($p=0.0019$) (Supplementary Fig. 2-S2D). The growth curves for the sgCon and sgYAP1 lines plateau at 35% viability for both NLF and SKNAS, which is expected for the control lines due to the cytostatic nature of trametinib. However, it is clear that the modest reduction of YAP1 expression was not sufficient to reduce viability at the highest dose of trametinib in neither NLF nor SKNAS sgYAP1 lines (Supplementary Fig. 2-S2D).

We next selected for clonal YAP1 null NLF cell lines after serial dilution of CRISPR/Cas9 edited cells and isolated four isogenic clones. Indel mutations were confirmed by Sanger sequencing of genomic DNA, with single nucleotide insertions present in NLF YAP1^{-/-} lines #1 and #2, and a single nucleotide deletion in NLF YAP1^{-/-} line #4 (Supplementary Fig. 2-S1B). Conversely, NLF YAP1^{-/-} line #3 showed a mixed population flanking the PAM site. We investigated the effect of YAP1 loss on cellular growth and observed a modest growth delay of 20% in the NLF sgYAP1 line compared to the sgCon line (Supplementary Fig. 2-S3). NLF YAP1^{-/-} #2 and #3 mixed clone had comparable growth rates, but the mixed clone reached a similar confluence as sgYAP1. NLF YAP1^{-/-} #1 and #4 cells grew at the slowest rate and only reached to 30-40% of sgCon confluence. All four NLF YAP1^{-/-} cell lines showed reduced mRNA expression, and three showed no detectable protein by immunoblotting (Fig. 2-2A-B). The NLF YAP1^{-/-} #3 mixed clone showed reduced, but detectable, YAP1 protein expression but displayed increased

phospho-ERK expression. Based on the Sanger sequencing results and protein expression, the NLF *YAP1*^{-/-} #3 mixed clone was excluded from subsequent assays. After confirming repression of *CTGF* and *CYR61* mRNA (Fig. 2-2C), we determined trametinib IC₅₀ values in the isogenic *YAP1*^{-/-} cell lines. All three *YAP1*^{-/-} lines were significantly more sensitive to trametinib than NLF sgCon or NLF sg*YAP1* pool, with IC₅₀ values reduced from a median of 0.79 – 2.18 nM for the three *YAP1*^{-/-} (p<0.0001) versus 7.62 nM for the pooled sg*YAP1* (p<0.0038) compared to 15.58 nM for the sgCon (Fig. 2-2D and E).

Figure 2-2. YAP1 knockout sensitizes neuroblastoma cell lines to trametinib.

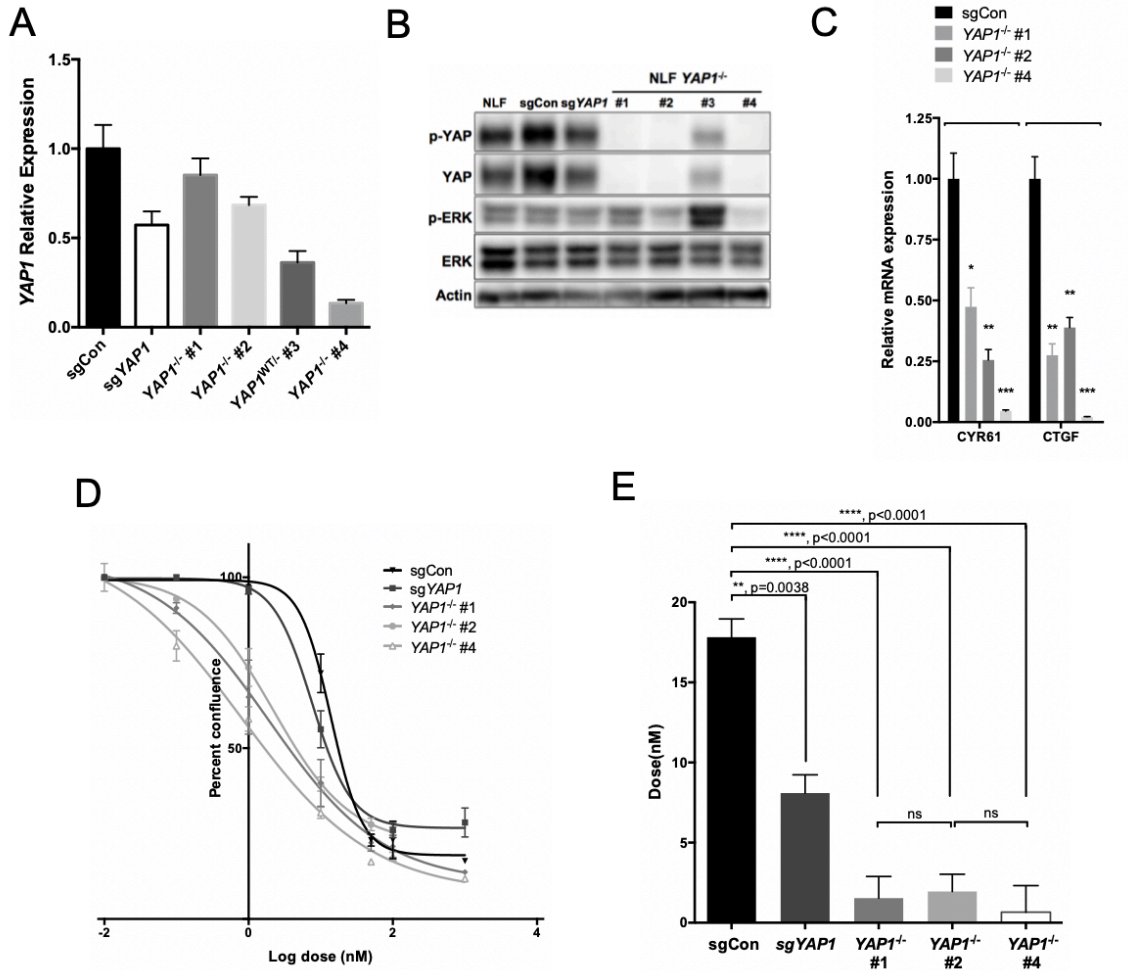


Figure 2-2 Legend: **A)** Four isogenic lines were established from the NLF sgYAP1 CRISPR pooled cell line. YAP1 expression is shown for NLF sgCon, sgYAP1 pool, and YAP1^{-/-} #1-4 (N=3). **B)** Immunoblots of NLF sgCon, sgYAP1 pool, and YAP1^{-/-} #1-4 for YAP, p-YAP, p-ERK, ERK, and beta-actin. **C)** Expression of YAP1 target genes, CTGF and CYR61, in NLF sgCon, sgYAP1 pool, and YAP1^{-/-} #1-4. **D-E)** IC₅₀ curves for trametinib in NLF sgCon, sgYAP1 pool, and YAP1^{-/-} #1-4 over a 6-log dose range (D) and a graphical representation of IC₅₀ values (E) of trametinib

(N=3). Student's t-test, * = $P < 0.05$, ** = $P < 0.01$, *** = $P < 0.001$, **** = $P < 0.0001$.

Constitutively active YAP1 overexpression induces resistance to trametinib in MAPK pathway activated neuroblastoma cells

The YAP1 protein contains five HXRXXS motifs that are recognized and phosphorylated by LATS1/2. Of these five sites, phosphorylation of S127 on YAP1 promotes binding with 14-3-3 which causes cytoplasmic retention of YAP1. Mutating all five serine residues to alanine ablates the LATS1/2 phosphorylation sites and yields a constitutively-active YAP-5SA protein (Zhao B, 2007). In order to observe the effect of increased YAP activity in response to trametinib, we overexpressed YAP-5SA cDNA in NB-EBc1 (KRAS G12D) and SKNFI (*NF1* homozygous inactivation), which are both *de novo* YAP1 protein null cell lines (Fig. 2-1A, Fig. 2-3A). Forced high overexpression of YAP-5SA protein resulted in variable changes in these cells with different genotypes, in terms of a slight increase in p-YAP1 in the NB-EBc1, and p-ERK in SKNFI. We next confirmed the upregulation of *CTGF* and *CYR61* in both lines (Fig. 2-3B and C). YAP-5SA overexpression induced resistance to trametinib, in which cell viability did not reach 50% in either YAP-5SA overexpressing line compared to the control IC50s in both NB-EBc1 (73.03 nM, $p < 0.001$), and SKNFI (16.94 nM, $p < 0.0001$) (Fig. 2-3D and E). We then forced YAP-5SA overexpression in NLF *YAP1*^{-/-} #1 and #4 cell lines, despite the known limitation that the YAP-5SA construct would be recognized and

cut by the CRISPR-Cas9 machinery. Despite this, we were able to obtain modest overexpression of constitutively active YAP1, and a likewise (albeit subtler) induction of relative resistance to trametinib, partially rescuing the *YAP1*^{-/-} phenotype (Supplementary Fig. 2-S4A-C).

Figure 2-3. YAP-5SA overexpression induces trametinib resistance in low YAP-expressing neuroblastoma cell lines.

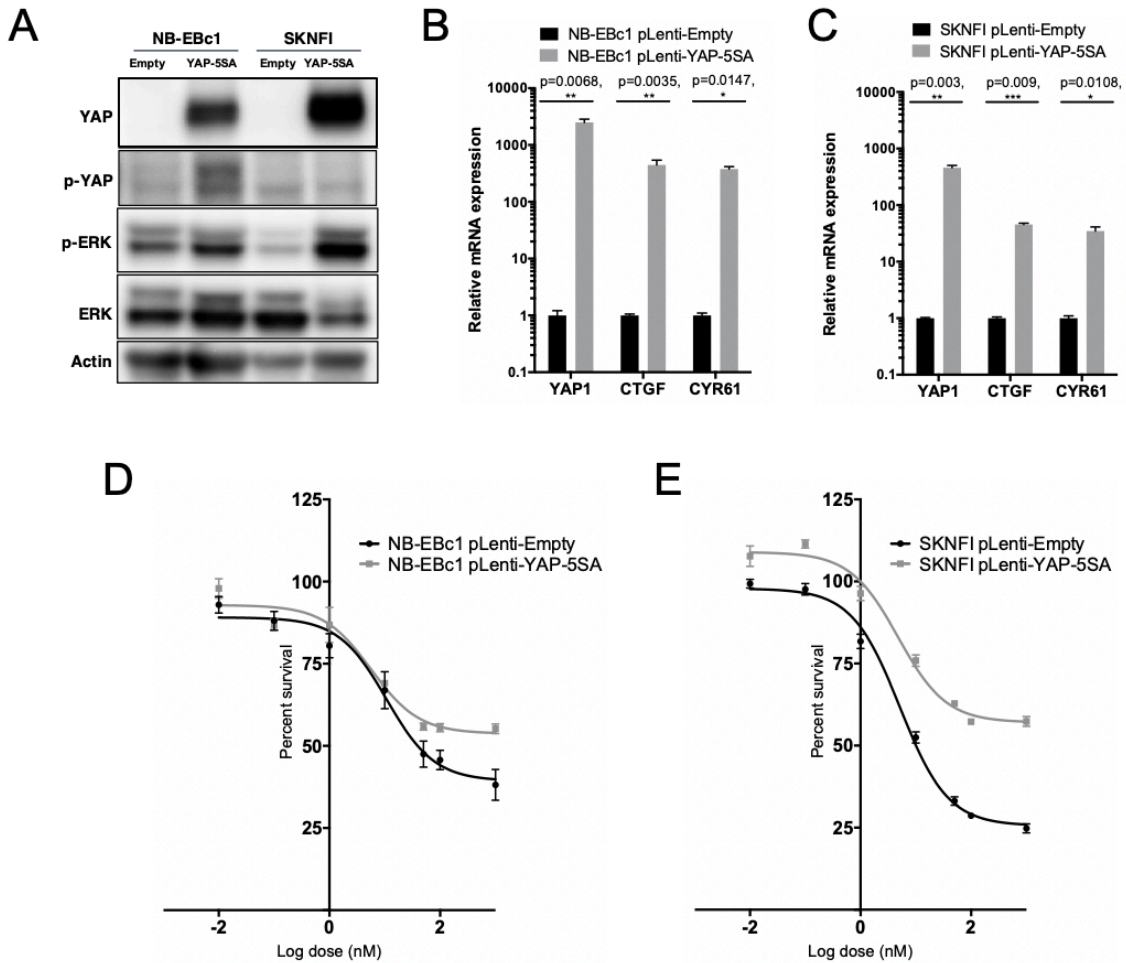


Figure 2-3 Legend: **A)** Immunoblots of NB-EBc1 and SKNF1 empty vector and YAP-5SA-overexpressing cells. Immunoblots were probed for p-YAP1 S127 (70 kD), total YAP1 (70 kD), phospho-ERK (42, 44 kD), total ERK (42, 44 kD), and beta-actin (40kD). **B-C)** *YAP1*, *CTGF*, and *CYR61* expression in NB-EBc1 (B) and SKNF1 (C) empty vector- and YAP-5SA-overexpressing cells. Relative mRNA expression is represented on a log scale (N=3). Student's t-test, * = P < 0.05, ** = P < 0.01, *** = P < 0.001, **** = P < 0.0001. **D-E)** IC₅₀ curves for trametinib between

empty vector and YAP-5SA overexpressing NB-EBc1 ($P < 0.001$) (D) and SKNFI ($P < 0.0001$) (D) cells ($N=3$). One-way ANOVA ($F(3,74) = 18.69$, $P < 0.0001$) with Sidak multiple comparisons test.

YAP1 mediates resistance to trametinib in neuroblastoma cells with hyperactivated MAPK signalling through transcriptional activation of E2F and MYC(N)

To better understand how YAP1 plays a role in trametinib sensitivity, we performed RNA sequencing of NLF sgCon and two isogenic cell lines, NLF *YAP1*^{-/-} #1 and #4. All three cell lines were treated in triplicate with 20 nM trametinib or DMSO for 72 hours, at which time total RNA was isolated (Fig. 2-4A). After total mRNA sequencing, we confirmed that the biological replicates clustered together by principal component analysis (Supplementary Fig. 2-S5A). We next confirmed that *YAP1* and downstream transcriptional targets *CTGF*, and *CYR61* mRNA expression was suppressed as predicted in the RNA sequencing data (Supplementary Fig. 2-S5B). Of note, expression of *WWTR1*, the gene encoding the YAP1 paralog TAZ, follows the same trend as *YAP1* and its target genes, which confirms that TAZ expression is not being upregulated to compensate for *YAP1* loss (Supplementary Fig. 2-S5B).

We next performed three distinct differential expression analyses using the R package DESeq2 (Fig. 2-4B). Differentially-expressed genes were identified between three distinct sets: 1) sgCon treated with either DMSO or trametinib (Trametinib-specific), 2) sgCon and NLF *YAP1*^{-/-} #4 treated with DMSO (*YAP1*^{-/-} specific), 3) sgCon + DMSO and NLF *YAP1*^{-/-} #4 + trametinib (Combination of

YAP1 loss and MEK inhibition). Differentially expressed genes in the Trametinib-specific and *YAP1*^{-/-}-specific groups were subtracted from the trametinib-treated *YAP1*^{-/-} gene list. This final dataset represented the 1,474 differentially expressed genes that were unique to the combination of trametinib treatment in a *YAP1*^{-/-} model. Gene ontology analysis of the transcripts downregulated within this dataset revealed cell cycle and DNA repair pathways as most significantly enriched (Fig. 2-4C). Gene set enrichment analysis (GSEA) of the 1,474 genes produced only two significantly enriched gene sets with a family-wise error rate of <0.01: E2F and MYC targets (Fig. 2-4D). Heatmaps of E2F and MYC target genes show reduced expression of target genes in NLF *YAP1*^{-/-} #1 and #4 compared to sgCon (Fig. 2-4E). The most striking decrease in expression occurred with trametinib treatment, particularly in the NLF *YAP1*^{-/-} #4 cell line (Fig. 2-4E). Importantly, NLF neuroblastoma cells do not express MYC but do express MYCN, suggesting that this gene set actually refers to MYCN gene targets. To test this, we performed an additional GSEA using the WEI_MYCN_TARGETS_WITH_E_BOX gene set (Wei JS, 2008) (Fig. 2-4F). We confirmed that MYCN gene targets are significantly enriched in the list of differentially expressed genes, with a family-wise error rate of <0.01 and a normalized enrichment score of -3.22. Expression of relevant cell cycle and DNA replication and repair genes follow a pattern similar to the E2F and MYC heatmaps (Fig. 2-4G). Changes in expression of *E2F1* were more modest, but *MYCN* expression increases upon *YAP1* loss in control-treated NLF *YAP1*^{-/-} #1 and #4. In response to trametinib, expression in NLF *YAP1*^{-/-} #1 and #4 decreases

to similar levels of control- and trametinib-treated NLF sgCon samples. We also confirmed the change in MYCN protein expression, which follows a similar pattern observed in the differential expression results in response to YAP1 loss and trametinib treatment (Supplementary Fig. 2-S5C). In an effort to connect the changes in *MYCN* expression to YAP-TEAD signaling, we identified the conserved DNA-binding motif *CATTCC* which is shared by all four TEAD1-4 transcription factors using the online JASPER tool (7th release, 2018 version) (Supplementary Fig. 2-S6A). We queried the region surrounding the *MYCN* gene locus using Integrated Genomics Viewer (IGV) and identified *CATTCC* sense sequences in the *MYCN* promoter and the first intron, as well as an antisense *CATTCC* sequence in the *MYCN* promoter (Supplementary Fig. 2-S6B). This observation confirms that the TEADs are able to bind at the *MYCN* locus and the loss of YAP-TEAD transcriptional activity upon *YAP1* knockout may account for these changes in *MYCN* expression.

To understand the differences in differential expression between the *YAP1*^{-/-} #1 and #4 cell lines, a differential expression analysis was performed between DMSO-treated *YAP1*^{-/-} #1 and *YAP1*^{-/-} #4. Gene ontology analysis identified an enrichment of genes upregulated in *YAP1*^{-/-} #4 related to mRNA splicing and cell morphogenesis as the primary biological processes, whereas downregulated genes *YAP1*^{-/-} #4 compared to *YAP1*^{-/-} #1 were relevant to adhesion and angiogenesis (Supplementary Fig. 2-S7). GSEA was performed against the MSigDB hallmark gene sets but it identified no significant gene set enrichment.

Taken together, these results suggest that there are major cancer signaling-related gene expression differences between the two *YAP1*^{-/-} cell lines. Rather, it suggests that the *YAP1*^{-/-} #4 cell line is a more differentiated line with reduced adhesion and angiogenic capacity.

Figure 2-4. Increased trametinib sensitivity upon YAP1 loss is due to loss of E2F and MYC target gene expression.

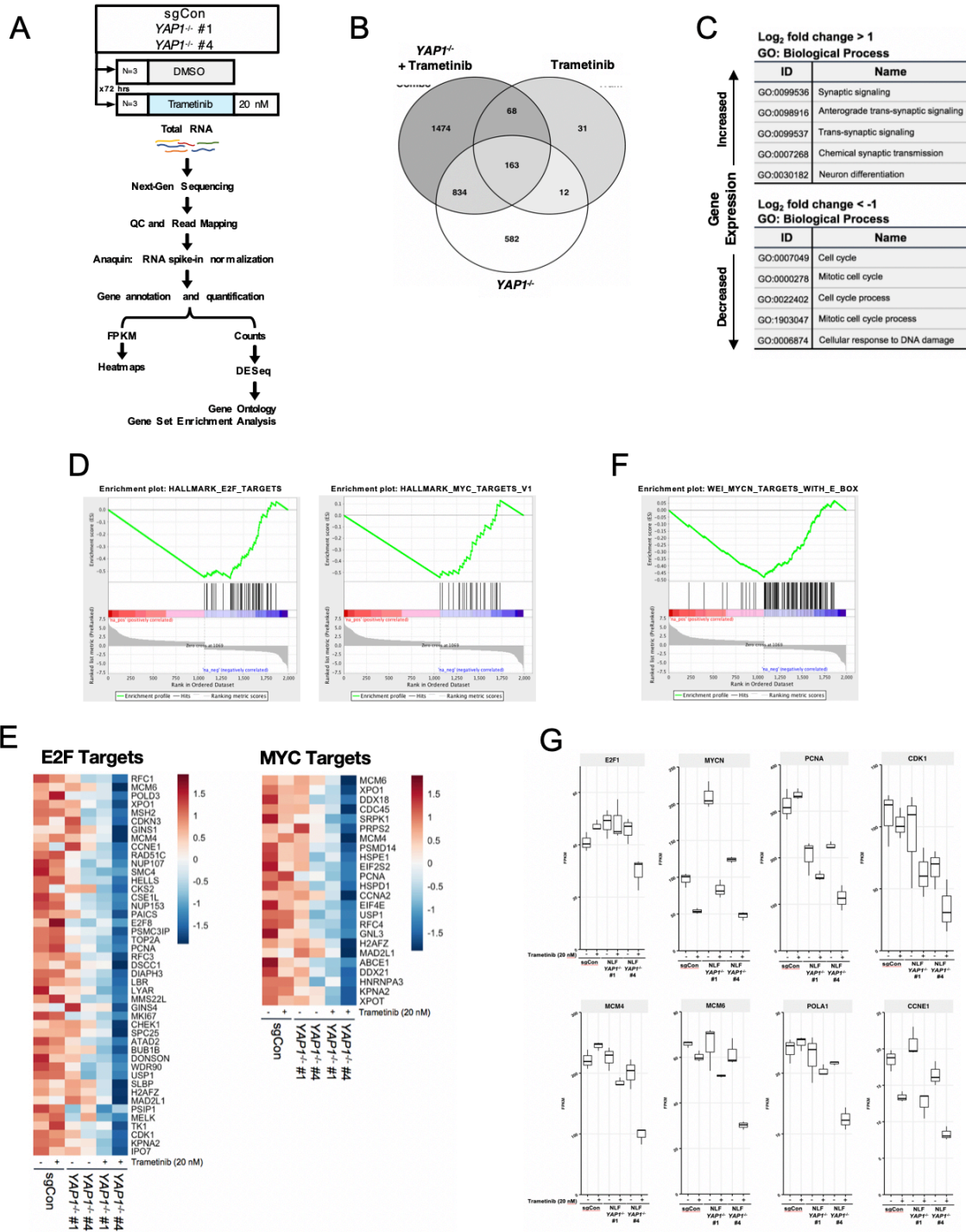


Figure 2-4 Legend: **A)** Workflow of RNA sequencing experiment. NLF sgCon, *YAP1*^{-/-} #1 and #4 were treated in triplicate with either DMSO or 20 nM trametinib for 72 hours and total RNA was isolated. **B)** Venn diagram showing shared genes among three differential expression analyses: 1) Trametinib-specific: sgCon DMSO vs. sgCon Tram, 2) *YAP1*^{-/-} #4-specific: sgCon + DMSO vs. *YAP1*^{-/-} #4 + DMSO, and 3) *YAP1*^{-/-} #4 + trametinib: sgCon + DMSO vs. *YAP1*^{-/-} #4 + trametinib. **C)** Top 5 gene ontologies represented among the 1,474 unique trametinib-treated *YAP1*^{-/-} #4 genes. **D)** Gene set enrichment analysis of the 1,474 unique trametinib-treated *YAP1*^{-/-} #4 genes with a FWER p value cutoff of <0.01. **E)** Heatmaps of FPKM values normalized by row for each gene represented in the E2F and MYC target gene sets. **F)** Gene set enrichment analysis of the 1,474 unique trametinib-treated *YAP1*^{-/-} #4 genes against the WEI_MYCN_TARGETS_WITH_E_BOX gene set. **G)** FPKM values among all 6 groups for a subset of E2F and MYC target genes.

In order to validate these RNA sequencing results, we performed RT-qPCR of five gene targets from Fig. 2-4G and expression follows the expected pattern (Fig. 2-5A). We also tested this using the SKNAS sgCon and sg*YAP1* pooled lines treated with trametinib (or DMSO), which followed a similar pattern (Fig. 2-5B). The reduction of target gene expression was less robust than in the NLF *YAP1*^{-/-} isogenic lines likely due to the mosaic *YAP1* expression in the pooled CRISPR line. Since many of the E2F and MYC target genes are involved in the cell cycle

and DNA replication, we performed flow cytometry to examine DNA content after 72 hours of trametinib treatment. In response to trametinib, the NLF sgCon cells displayed a minor increase in G₁ arrest (Fig. 2-5C). Loss of *YAP1* expression caused a further increase in G₁ arrest and an even greater increase in G₁ arrest upon trametinib treatment. In the NLF *YAP1*^{-/-} #4, which had the most significant decrease in YAP1 target gene expression, we observed that 90% of the cells were arrested at G₁ in response to trametinib (Fig. 2-5C). These data were verified in the SKNAS pooled cells, but to a lesser degree as expected (Fig. 2-5D). We further investigated whether or not the combination of YAP1 loss and trametinib treatment causes apoptosis. We did not observe increases in cleaved PARP or cleaved caspase 3 in the *YAP1*^{-/-} cell lines treated with or without trametinib (Supplementary Fig. S5C). From these data, we propose that trametinib induces a change in cellular signaling that causes a reduction in YAP1 protein phosphorylation and induces YAP1 nuclear translocation, where it can promote the transcription of E2F and MYCN target genes. In the absence of nuclear YAP1, trametinib treatment induces a significant reduction in E2F and MYCN target gene expression. As a consequence, we have shown G₀/G₁ cell cycle arrest, thus impairing the proliferative capacity of neuroblastoma cell lines (Fig. 2-5E).

Figure 2-5. Trametinib treatment of *YAP1*^{-/-} cells causes G₁ cell cycle arrest.

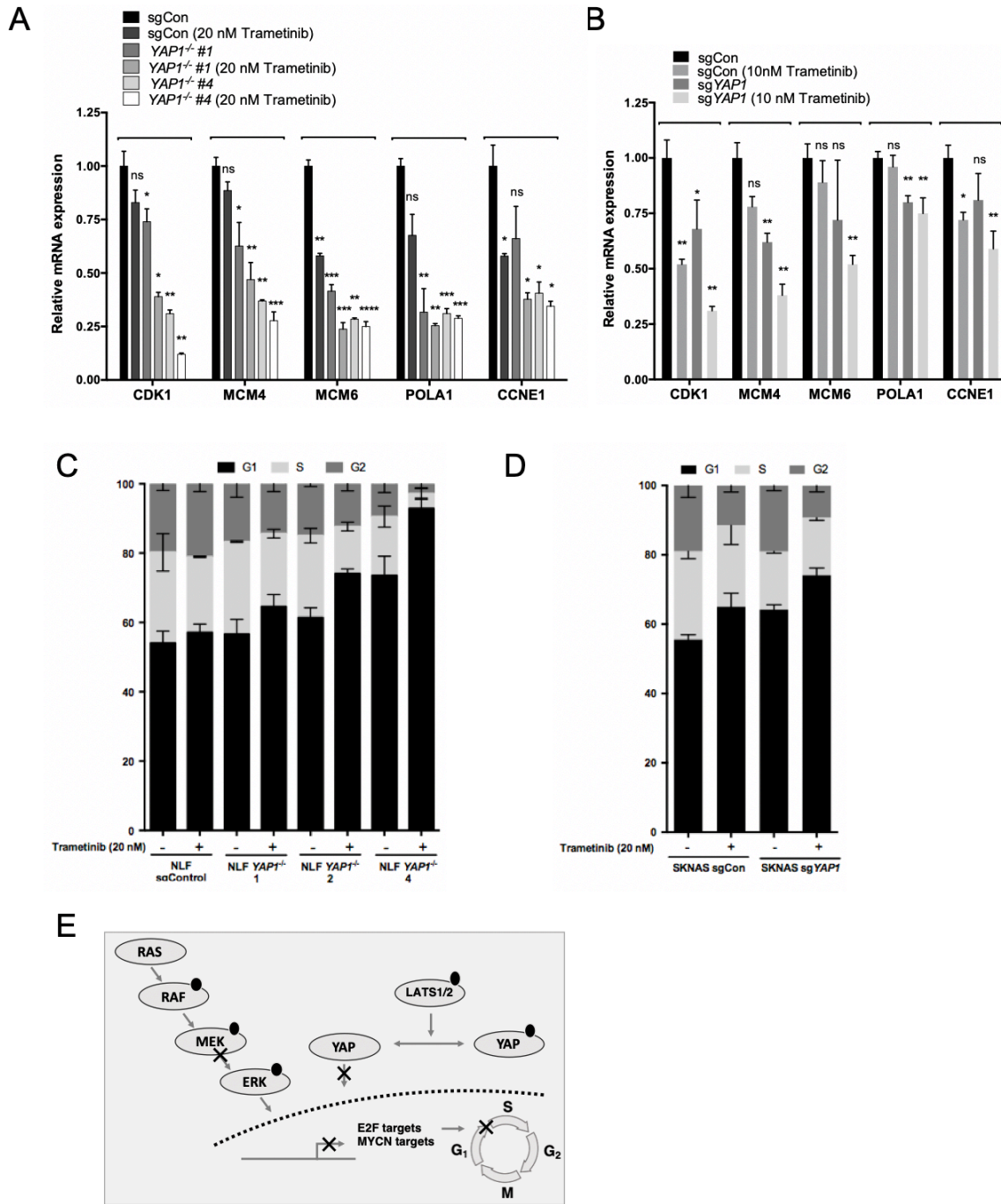


Figure 2-5 Legend: (A-B) Expression of *CDK1*, *MCM4*, *MCM6*, *POLA1*, and *CCNE1* in NLF sgCon and *YAP1*^{-/-} #1 and 4 (N=3) (A) and SKNAS sgCon and

sgYAP1 (N=3)(B). Cells were treated with DMSO or trametinib (NLF 20 nM, SKNAS: 10 nM). **(C-D)** Cell cycle analysis of NLF sgCon and YAP1^{-/-} #1-4 (N=3) (C) and SKNAS sgCon and sgYAP1 (N=3) (D) treated with DMSO or trametinib (NLF: 20 nM, SKNAS: 10 nM) for 72 hours. Flow cytometry was performed to detect the proportion of cells present in G₁, S, and G₂. **(E)** Proposed mechanism of inhibiting MEK1/2 signaling and YAP1 activity in RAS-driven neuroblastoma. Dot = phosphorylation. Student's t-test, * = p<0.05, ** = p<0.01, *** = p<0.001, **** = p<0.0001.

V. Discussion

Relapsed neuroblastomas remain largely incurable, but recent insight into relapse-specific mutations provide an opportunity to develop targeted therapies (Eleveld TF, 2015; Schramm A, 2015). Hyperactivation of the RAS pathway is a common finding in relapsed neuroblastomas, suggesting this contributes to resistance to standard up front chemoradiotherapy. MEK inhibition shows cytostasis and eventual tumor outgrowth in neuroblastoma preclinical models, highlighting the need to identify combination therapies for this subset of patients.

Here, we identify enhanced activation of Hippo pathway protein YAP1 as a cellular adaptation to MEK1/2 inhibition in RAS-driven neuroblastomas. We show that while only a subset of RAS-driven neuroblastoma cell lines express detectable YAP1 protein, short-term exposure to trametinib induces the translocation of unphosphorylated “active” YAP1 into the nucleus. The exact mechanism causing

the reduction in YAP1 protein phosphorylation, as well as the mechanism for nuclear translocation, remains to be defined. The latter may be a result of reduced phosphorylated YAP1, although actin stress fiber formation has been reported to cause nuclear translocation in response to BRAF inhibitor resistance (Kim MH, 2016). Therefore, there may be multiple mechanisms involved in the YAP1 protein dynamics in response to MEK inhibition. In the YAP1-expressing neuroblastoma cell lines, we discovered that YAP1 protein expression levels were directly related to trametinib sensitivity. In YAP1 expressing cell lines, genetic depletion of *YAP1* expression sensitized to trametinib, while overexpression of constitutively active YAP1 induced trametinib resistance in neuroblastoma cell lines with undetectable YAP1. This observation may be clinically useful, as *YAP1* transcriptional activity may explain the cytostatic effects of MEK inhibition in RAS-driven neuroblastoma. This finding also supports the purported clinical relevance of YAP1 in this disease, as neuroblastomas have been shown to acquire increased *YAP1* transcriptional activity upon relapse (Schramm A, 2015).

Our findings show that in cells with YAP1 edited out, E2F and MYCN target gene sets were downregulated when MEK1/2 was inhibited. This result provides additional biological value to the importance of the hippo pathway in conferring resistance to RAS-MAPK pathway inhibition. Due to the low MYC expression in NLF cells, we demonstrated that MYCN gene targets were differentially expressed and that MYCN expression increased in response to YAP1 loss but decreased when combined with MEK inhibition. TEAD4 has been reported to bind to a

consensus site in the MYCN promoter and function in a YAP1-independent manner in neuroblastoma cells (Rajbhandari P, 2018). It is possible that the absence of YAP1 may allow the TEAD proteins to initiate an alternate gene expression program. However, we observed that this effect is lost when combined with MEK inhibition. Alternatively, MYCN has been shown to be regulated by E2F proteins in neuroblastoma (Strieder V, 2003), which may indicate E2F1 target gene expression as the primary cause of the gene expression changes causing the observed G₁ cell cycle arrest. The exact mechanism causing E2F gene target expression to decrease remains unclear. YAP and TEAD have been reported to cooperate with E2F by ChIP analyses to coordinate cell cycle gene expression (Kapoor A, 2014). The loss of both MEK-activated and YAP-activated E2F-related gene expression may contribute to the differential gene expression observed in response to MEK1/2 inhibition and *YAP1* depletion. Recent literature has also shown that BRAF-inhibitor resistance can induce YAP activated E2F-related cell cycle gene expression in an actin-dependent manner (Kim MH, 2016). Here, we present data suggesting a similar effect may occur in the context of MEK inhibition in neuroblastomas with RAS activation.

This study has important clinical implications because combinatorial inhibition of MEK1/2 and YAP1 signaling could be an effective combination to circumvent cellular reprogramming. While no hippo pathway modulating drugs are currently be tested in the clinic, there is increasing interest within academia and industry to develop inhibitors of YAP1 activity (Chan P, 2016). It is important to

note that the clinical relevance of the combination of YAP1 and MEK inhibition in neuroblastoma would be limited to tumors that both harbor RAS-MAPK pathway mutations and express YAP1 (*de novo* and/or induced by MEK inhibition). As inhibitors of YAP1 activity are developed, our data support the development of combined MEK1/2 and YAP1 inhibition for neuroblastomas with hyperactivated MAPK signalling.

Acknowledgements

This work was supported in part by NIH grants R35 CA220500 and P01CA217959 (JMM), 1F31CA220844-01A1 (GEC) and T32GM008076 (GEC), grants from Cookies for Kids Cancer (GEC, JMM), the Press On Foundation (JMM), the Giulio D'Angio Endowed Chair (JMM), and an Alex's Lemonade Stand Foundation Young Investigator Award (JLR). We are grateful to Tim Mercer for providing RNA sequins for RNA sequencing and to the Jefferson Cancer Genomics Laboratory for library preparation and next-generation sequencing. pQCXIH-Myc-YAP-5SA was a gift from Kunliang Guan (Addgene plasmid # 33093; <http://n2t.net/addgene:33093>; RRID:Addgene_33093). pLenti CMV Puro DEST (w118-1) was a gift from Eric Campeau & Paul Kaufman (Addgene plasmid # 17452; <http://n2t.net/addgene:17452>; RRID:Addgene_17452).

CHAPTER 3: COMBINATORIAL TARGETING OF THE RAS-MAPK AND HIPPO PATHWAYS WITH MEK1/2 AND TEAD PALMITOYLATION INHIBITORS

We will refrain from pursuing publication of this work until we receive compounds optimized for *in vivo* mouse studies. This work was included in an AACR abstract (#2886): Coggins GE, Scolaro L, Hart LS, Tang, TT, Post, LE, Maris, JM. The Hippo pathway protein YAP mediates resistance to MEK1/2 inhibition in neuroblastoma. Poster presented at: AACR Annual Meeting; 2019 Apr 2; Atlanta, GA.

I. Abstract

TEAD autopalmitoylation has recently been discovered to be required for binding to the Hippo pathway protein YAP to TEAD1-4 proteins and promoting transcription of YAP-TEAD gene targets. Vivace Therapeutics has developed first in-class potent small molecule inhibitors of TEAD palmitoylation. Based on our findings in Chapter 2, we hypothesized that inhibitors of TEAD palmitoylation would have synergistic anti-tumor activity with trametinib in RAS-hyperactivated neuroblastomas. I tested the efficacy of TEAD palmitoylation inhibitor tool compounds as single-agents and in combination with the MEK1/2 inhibitor trametinib in a panel of RAS hyperactivated and control neuroblastoma cell lines. To determine single-agent activity, cells were treated with a 4-log dose range of three TEAD palmitoylation inhibitors: VT101, VT102, and VT103. As expected, no single agent activity was observed in the cell lines tested, regardless of RAS-MAPK pathway status. Synergy studies were performed in three RAS hyperactive

cell lines (NLF, SKNAS, and SKNFI) with combinations of VT101 or VT102 and trametinib. Cells were treated in duplicate in a matrix format over a 5-dose constant ratio range of either drug based on the IC₅₀ (here denoted as X; 1/4X, 1/2X, X, 2X, 4X). Since no IC₅₀ was able to be calculated for the TEAD palmytoilation inhibitors, we empirically assigned X=1 uM. The combination of VT101 and trametinib showed synergy across all three cell lines, but the combination of VT102 and trametinib did not. This difference in sensitivity is likely due to differential TEAD1-4 specificity or promiscuity. These results further support the hypothesis that YAP promotes intrinsic resistance to MEK1/2 inhibition in neuroblastoma models with Ras-MAPK pathway mutations.

II. Introduction

The previous chapter provided the rationale for investigating the combination of a MEK1/2 inhibitor and a YAP inhibitor in preclinical models of relapsed neuroblastoma. Efforts to pharmacologically inhibit YAP in cancer models have been largely unsuccessful. Verteporfin (VP) is a protoporphyrin compound, which is FDA-approved as a photodynamic therapy for treatment of blood vessel disorders of the eye, such as macular degeneration and myopia. VP was observed to disrupt the YAP-TEAD interaction by selectively binding to YAP (Liu-Chittenden Y, 2012). In addition, VP has been reported to function as a scaffold to increase YAP interaction with 14-3-3 leading to cytoplasmic sequestration (Wang, 2015). Subsequent *in vitro* studies showed that VP treatment caused a reduction in YAP,

phospho-YAP (S127), CYR61, and CTGF protein expression in uveal melanoma cells (Ma Y.-W, 2016). However, there are drawbacks to pursuing VP as a feasible therapeutic candidate for treating YAP-driven cancers. *In vitro* studies in a melanoma cell line suggested that VP could cause YAP protein degradation, but this effect disappeared in VP-treated tumors from a transgenic melanoma mouse model (Liu JW, 2019). Furthermore, VP is a porphyrin compound and facilitates the formation of protein aggregates, which could cause cellular toxicity and undesirable side effects in patients.

Rather than targeting YAP directly, recent progress has been made towards understanding the dynamics of the protein-protein interaction between TEAD and YAP. Autopalmitoylation was discovered to regulate the transcriptional activity of the Hippo pathway and was shown to be necessary for TEAD binding to YAP but not other transcriptional binding partners, such as the Vgll4 tumor suppressor (Chan P, 2016). Furthermore, palmitoylation status did not affect TEAD localization and therefore does not function as a membrane anchor like RAS farnesylation (Chan P, 2016). Rather, autopalmitoylation was observed within a deep pocket within the TEAD protein structure but did not interact with the YAP protein upon binding. Chan P, et al. postulate that the palmitate group induces a TEAD conformational change that is required for YAP binding.

The discovery of TEAD autopalmitoylation revealed a novel avenue for inhibiting oncogenic YAP transcriptional activity. Vivace Therapeutics has developed small molecule inhibitors of YAP-TEAD activity by selectively blocking

the palmitoylation of TEAD1-4 proteins via high-throughput phenotypic profiling (Tang TT, 2019). Subsequent optimization produced extremely potent compounds with IC₅₀s at single digit nM levels in cell-based assays and demonstrated reduced palmitoylation in presence of purified recombinant TEAD proteins. Vivace Therapeutics validated this mechanism in NF2-deficient mesothelioma cells with YAP hyperactivity and discovered that the novel compounds reduced proliferation *in vitro* and *in vivo* and were well-tolerated in murine models (Tang TT, 2019). The efficacy of these compounds in a YAP-driven preclinical cancer model serves as a strong foundation for the continued exploration of TEAD palmitoylation inhibitors for clinical development. The company is continually evolving a series of compounds with varying selectivity for individual TEAD proteins as well as pan-TEAD inhibitors for eventual application across a spectrum YAP- and TEAD-driven diseases.

In collaboration with Vivace Therapeutics, we performed the first exploration of the efficacy of TEAD palmitoylation inhibitors in combination with trametinib in human cancer. This chapter builds on the conclusions from Chapter 2 and observes the predicted lack of single-agent activity of TEAD palmitoylation inhibitors in a panel of neuroblastoma cell lines. This study also demonstrates combination drug synergy between trametinib and TEAD palmitoylation inhibitors in three neuroblastoma cell lines, NLF (*NF1* splice variant), SKNAS (NRas Q61K), and SKNFI (*NF1* null). I hypothesized that inhibiting YAP activity using TEAD

palmitoylation inhibitors in combination with trametinib would be synergistic in Ras-driven neuroblastoma cell lines.

III. Methods and Materials

Cell Culture and Chemicals

Human-derived neuroblastoma cell lines were obtained from the Children's Hospital of Philadelphia cell line bank, the Children's Oncology Group, and the ATCC (Harenza JL, 2017). Cells were cultured in RPMI-1640 medium containing 10% FBS, 2 mM L-Glutamine at 37 °C under 5% CO₂. The genomic identity of the cell lines was confirmed using the GenePrint 24 (Promega, Guardian Forensic Sciences) and cell lines were free of mycoplasma contamination. Trametinib dissolved in DMSO (Cellagen Technologies #C4112-5s) was used for *in vitro* assays, with 0.1% DMSO as a negative control treatment. Vivace Therapeutics provided the TEAD palmitoylation inhibitors (VT101, VT102, and VT103), which were received dissolved in DMSO to a stock concentration of 10 mM. All cell lines were derived from deidentified neuroblastoma patient tumor samples and the Children's Hospital of Philadelphia Institutional Review Board agreed with the investigators that this work is not considered human subjects research.

Cell Viability Assays

Cell growth assays were performed using the IncuCyte Live Cell Analysis System (IncuCyte ZOOM, Essen Bioscience) with the 20x objective lens during a 72-hour

treatment. IC₅₀ values for trametinib were calculated using area under the curve at 7 days post-treatment. To detect cell viability, cells were seeded in 96-well cell culture plates at 1,500-3,000 cells per well depending on growth kinetics. Drug treatments were performed in duplicate 24 hours later over a 5 dose range based on the cell line IC₅₀ value at a constant ratio (DMSO, 1/4X, 1/2X, X, 2X, 4X, where X = IC₅₀). By plating the drugs in a matrix format, the efficacy of each combination of drug concentrations was measured. Cell viability was assessed using CellTiter-Glo (Promega).

Statistics

Drug combination synergy was calculated using Compusyn software based on the Chou method of calculating drug synergy (Chou TC, 2006; Chou TC, 2010). IC₅₀ values were determined using GraphPad Prism (v6) and performing a nonlinear regression analysis using the “log(inhibitor) vs. response –Variable slope (four parameters)” dose response equation at the 7-day time point for each concentration.

IV. Results

TEAD palmitoylation inhibitors are not effective as single-agents in Ras-hyperactivated neuroblastoma cell lines

Based on the data shown in Chapter 2, we did not expect to see single-agent activity with TEAD palmitoylation inhibitors of YAP activity. In order to

establish a baseline level of activity of TEAD palmitoylation inhibitors for subsequent synergy assays, we selected three Ras-hyperactivated neuroblastoma cell lines used in Chapter 2: NLF, SKNAS, SKNFI. We received three TEAD palmitoylation inhibitors from Vivace Therapeutics that were identified as VT101, VT102, and VT103. Cells were treated with over a 4-log dose range of each drug and percent confluence was compared to a topotecan positive control. In NLF cells, topotecan was potent in the low nanomolar range, but VT101 produced only a minimal response in the highest doses (Fig. 3-1A and B). However, VT102 and VT103 had no effect on cellular growth in NLF (Fig. 3-1C and D). Topotecan was similarly potent in SKNAS, but no effect on cellular confluence was induced by any of the TEAD palmitoylation inhibitors (Fig.3-2A-D). With these results in two high YAP-expressing cell lines, we selected a third low YAP-expressing cell line, SKNFI, to test whether YAP expression levels affect single-agent potency of TEAD palmitoylation inhibitors. Although topotecan potency remained consistent, none of the TEAD palmitoylation inhibitors had a significant effect on SKNFI confluence (Fig. 3-3A-D). In response to VT101 and VT102, the effect of the 1nM treatment appeared to be an outlier in SKNFI due to the lack of a response at higher concentrations (Fig. 3-3C-D). These results suggest that single-agent inhibition of YAP activity in Ras-addicted neuroblastoma cells is not an effective treatment.

Figure 3-1. Dose-response curves of VT101, VT102, and VT103 in NLF

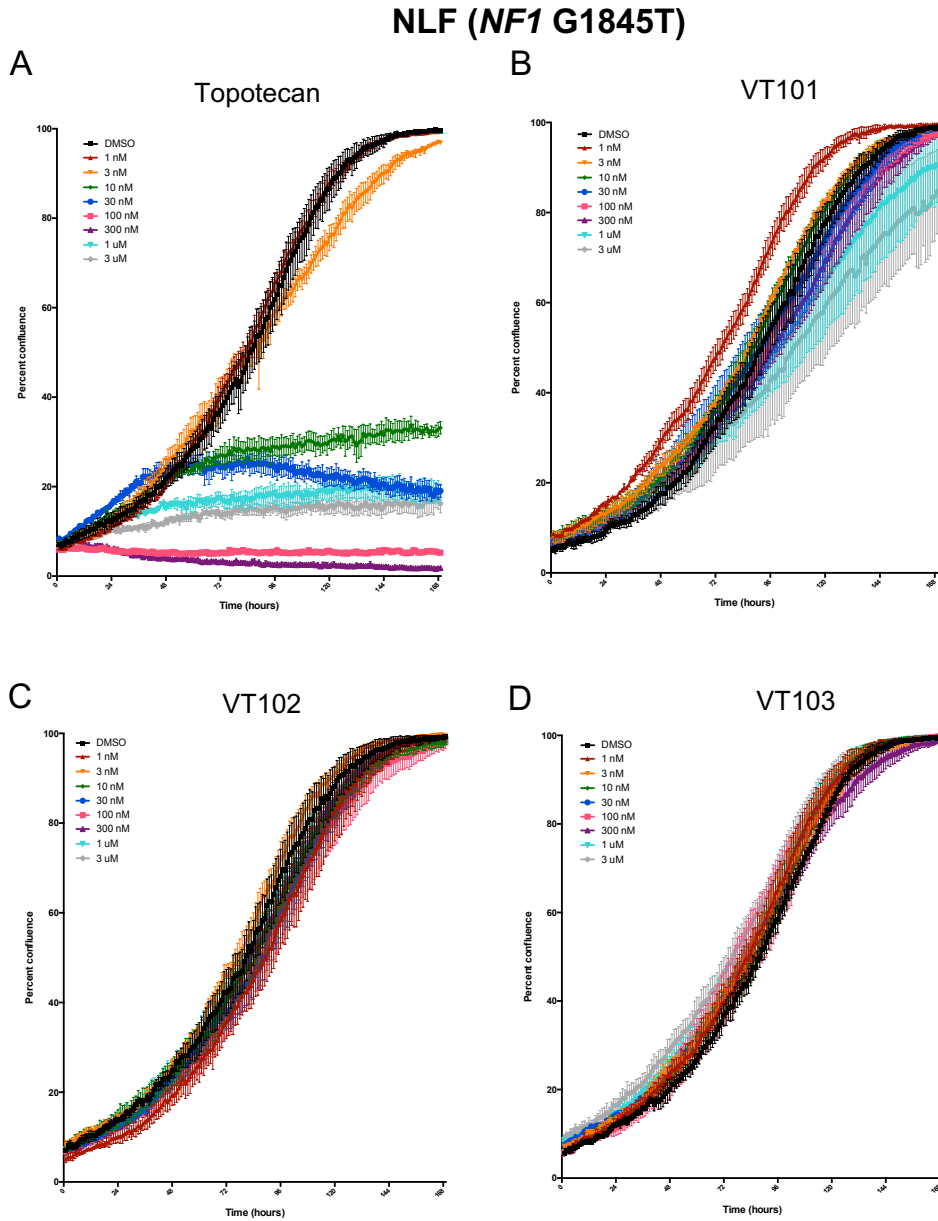


Figure 3-1 Legend: Dose-response curves performed in NLF over a 4-log dose range of A) topotecan, B) VT101, C) VT102, and D) VT103. Percent confluence over a 7-day assay was determined using a confluence mask in the IncuCyte ZOOM software.

Figure 3-2. Dose-response curves of VT101, VT102, and VT103 in SKNAS

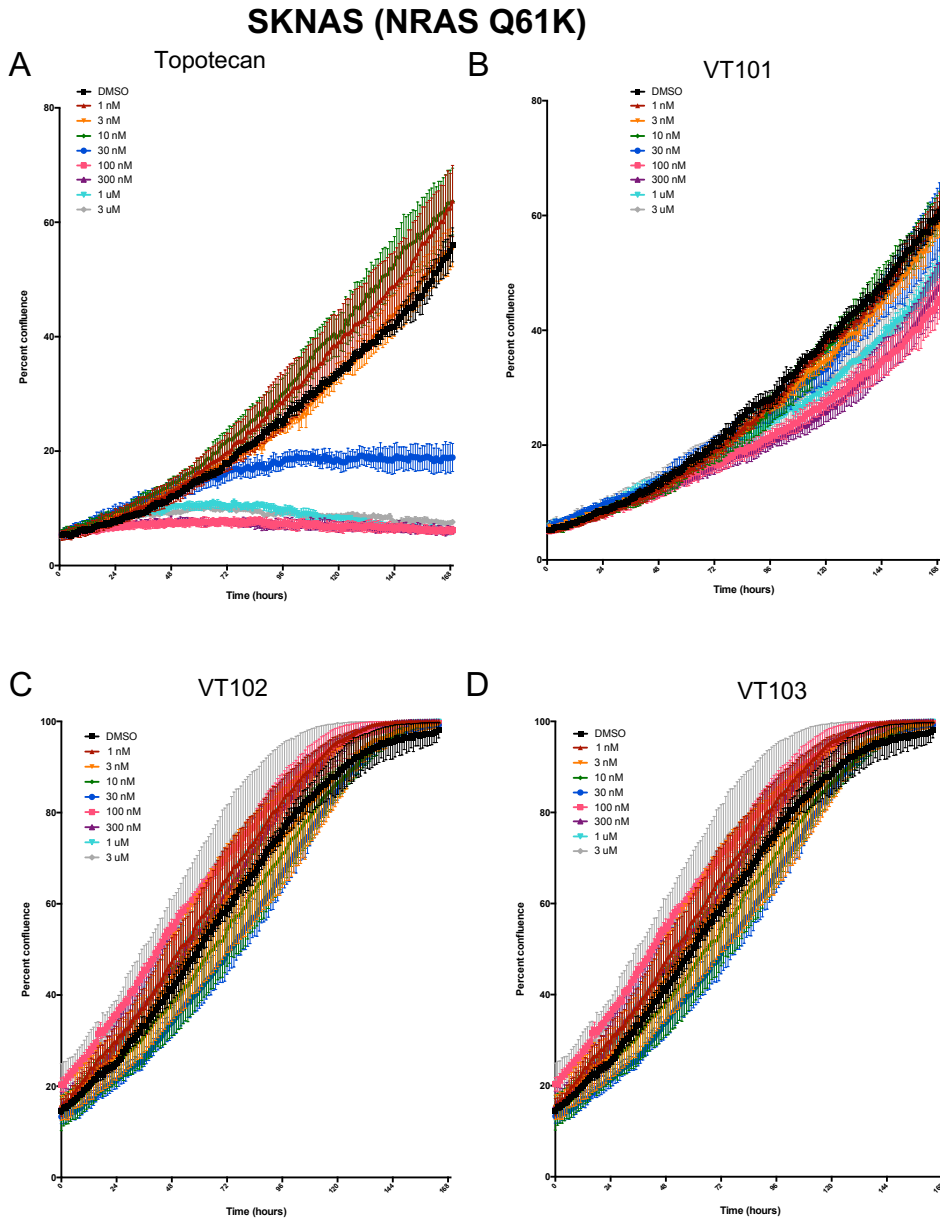


Figure 3-2 Legend: Dose-response curves performed in SKNAS over a 4-log dose range of A) topotecan, B) VT101, C) VT102, and D) VT103. Percent confluence over a 7-day assay was determined using a confluence mask in the IncuCyte ZOOM software.

Figure 3-3. Dose-response curves of VT101, VT102, and VT103 in SKNFI
SKNFI (*NF1* null)

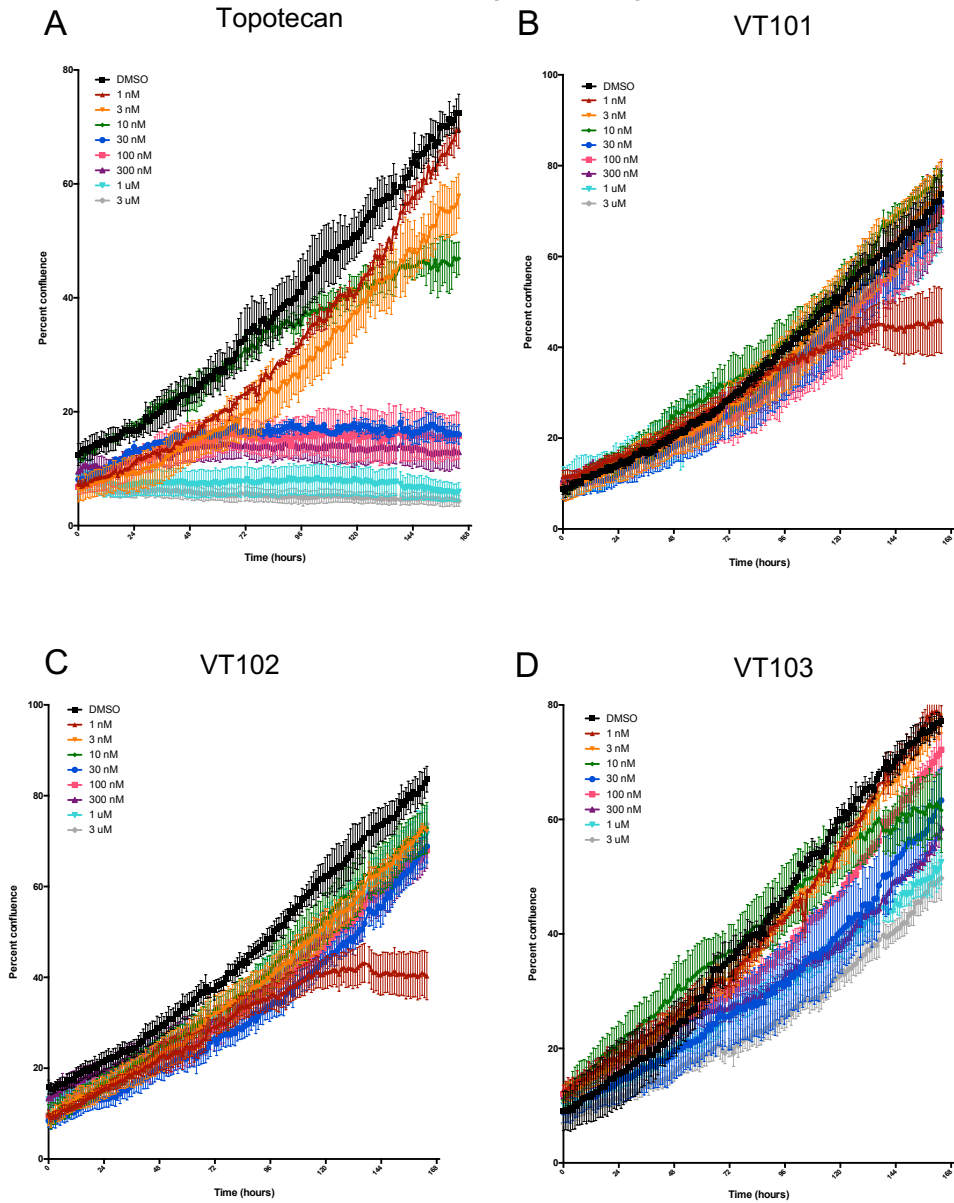


Figure 3-3 Legend: Dose-response curves performed in SKNFI over a 4-log dose range of A) topotecan, B) VT101, C) VT102, and D) VT103. Percent confluence over a 7-day assay was determined using a confluence mask in the IncuCyte ZOOM software.

We next sought to validate the observation that TEAD palmitoylation is necessary for interaction with YAP but not other binding partners (Chan P, 2016). TEAD4 has been reported to function in a YAP-independent manner to promote survival in the context of *MYCN*-amplification (Rajbhandari P, 2018). Knockdown of TEAD4 caused a significant reduction in proliferation and colony formation (Rajbhandari P, 2018). To test whether VT101, VT102, and VT103 harbor single-agent activity in RAS wild-type, *MYCN*-amplified neuroblastoma, we selected two cell lines, Kelly and COG-N-519, for dose-response assays. Compared to topotecan, no effect of percent confluence was observed in response to VT101, VT102, or VT103 in Kelly (Fig. 3-4A-D). Similarly, the three TEAD palmitoylation inhibitors had no effect on percent confluence in COG-N-519 (Fig. 3-5A-D). Although these data look strikingly similar to that of the RAS hyperactivated cell lines, we have validated the observation that inhibiting TEAD palmitoylation does not affect YAP-independent signaling in *MYCN*-amplified neuroblastomas.

Figure 3-4. Dose-response curves of VT101, VT102, and VT103 in Kelly

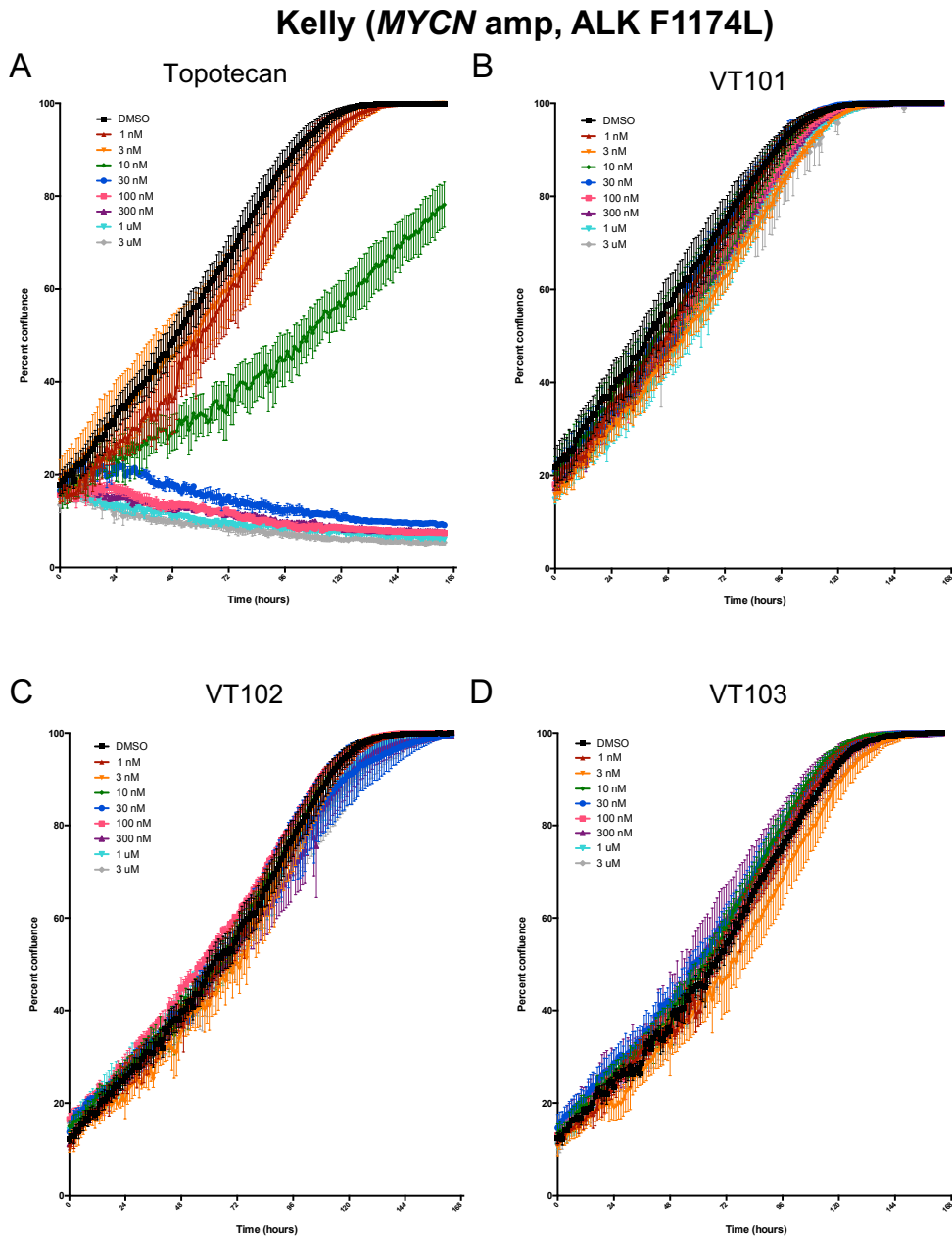


Figure 3-4 Legend: Dose-response curves performed in Kelly over a 4-log dose range of A) topotecan, B) VT101, C) VT102, and D) VT103. Percent confluence

over a 7-day assay was determined using a confluence mask in the IncuCyte ZOOM software.

Figure 3-5. Dose-response curves of VT101, VT102, and VT103 in COG-N-519

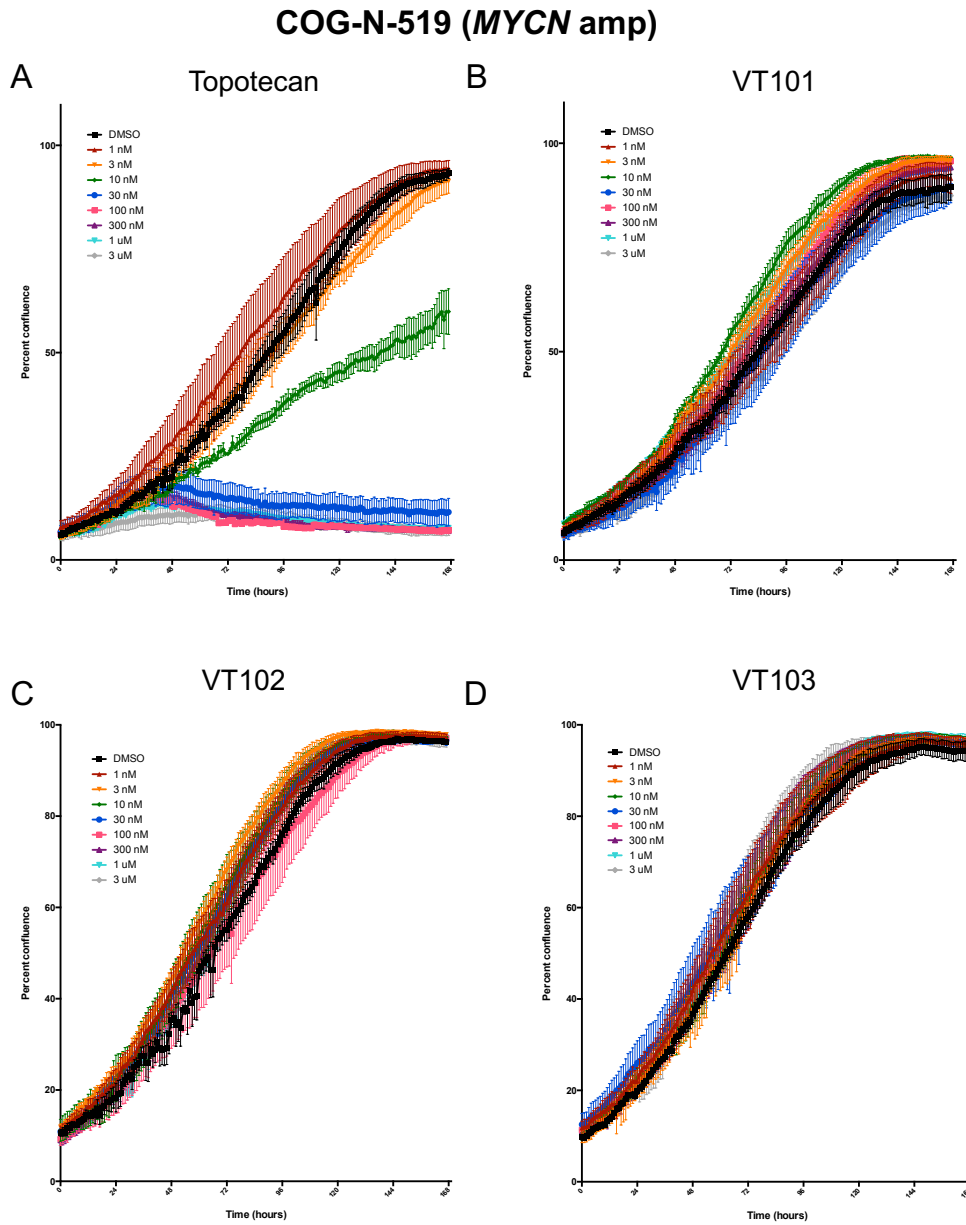


Figure 3-5 Legend: Dose-response curves performed in COG-N-519 over a 4-log dose range of A) topotecan, B) VT101, C) VT102, and D) VT103. Percent confluence over a 7-day assay was determined using a confluence mask in the IncuCyte ZOOM software.

TEAD palmitoylation inhibitors and trametinib are synergistic in vitro

Building upon the observation in Chapter 2 that knocking down YAP sensitized Ras-MAPK pathway mutated neuroblastoma cells to trametinib, we tested whether TEAD palmitoylation inhibitors could recapitulate that effect. In conversations with Vivace Therapeutics, VT103 was determined to be undesirable for continued preclinical testing due to a lack of potency and an undesirable pharmacological profile, so only VT101 and VT102 were tested for synergy with trametinib. NLF, SKNAS, SKNFI cells were treated in a matrix format with increasing doses of each drug at a constant ratio (1/4X, 1/2X, X, 2X, 4X, with $X=IC_{50}$). Due to the lack of potency of VT101 and VT102 as single-agents, no IC_{50} could be calculated and a concentration of $X=1$ μ M. In all three cell lines, synergy was tested between VT101 and trametinib, with synergy defined as a combination index (CI) values <1 . In NLF, the series of CI values corresponding to the equal ratios of VT101 and trametinib were plotted against fraction of cells affected (Fig. 3-6A). Although this spread of CI values across the fraction affected is large, the highest fraction affected value was produced by the highest concentration combination. Importantly, all CI values analyzed in NLF were <1 and synergistic

(Fig. 3-6B). Similar results were seen in SKNAS, in which all combinations were synergetic, including the 5 equal ratio CI values (Fig. 3-6C and D). In SKNFI, all of the CI values were below 1, but the fraction affected was high in all five equal ratio combinations (Fig. 3-6E and F). This result suggests that the combination of YAP and MEK1/2 inhibition in SKNFI is particularly potent.

Figure 3-6. Synergy observed between trametinib and VT101 in NLF, SKNAS, and SKNFI

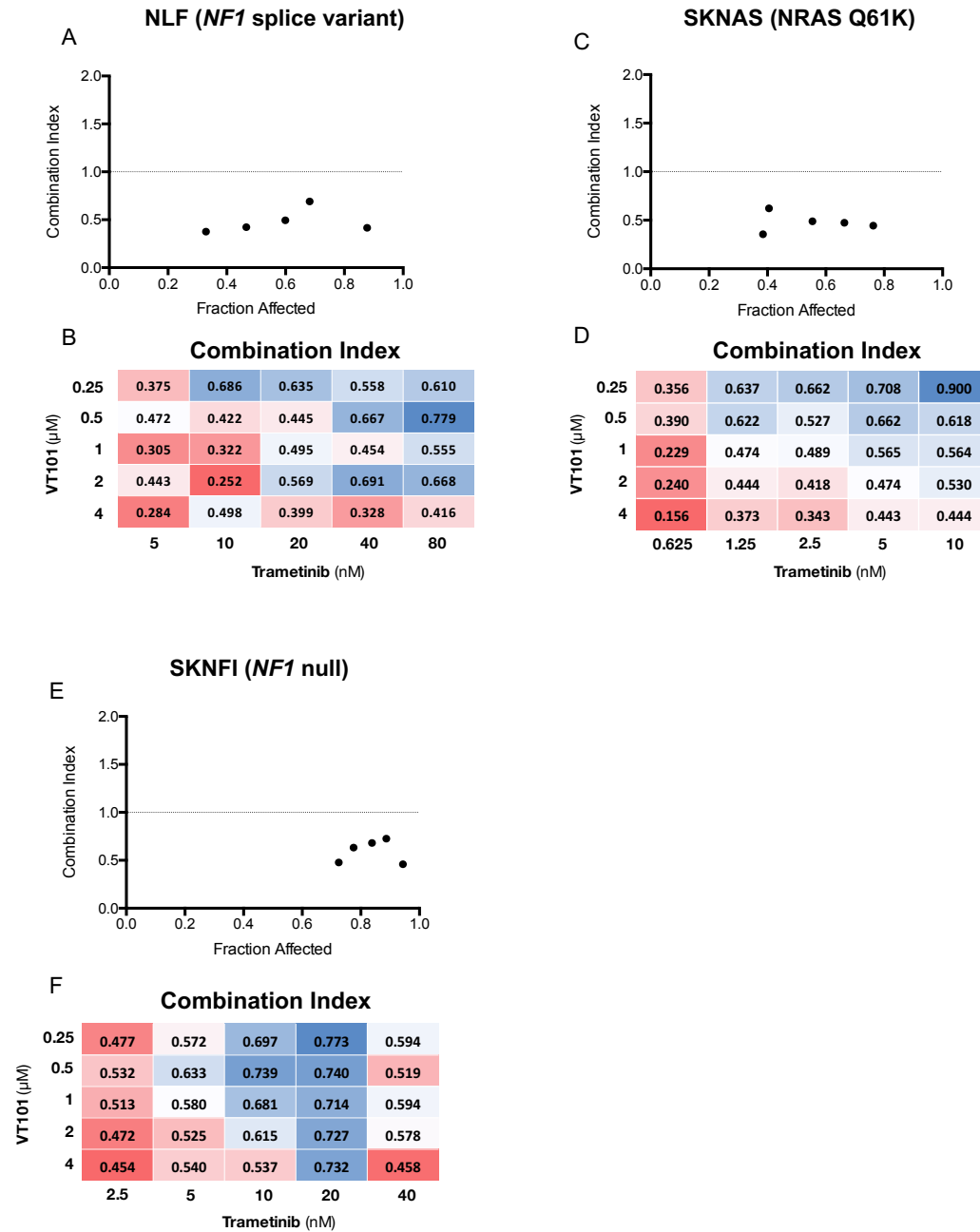


Figure 3-6 Legend: Synergy assays were performed by plating cells onto 96-well plates and treating cells in a matrix format with 1/4X, 1/2X, X, 2X, and 4X dilutions

of either trametinib or VT101, where $X=IC_{50}$. For VT101, $X=1$ μ M. Combination index (CI) values were quantified based on cell viability using Compusyn. A) CI values of equal ratio combinations are plotted against the cell viability fraction affected in NLF. B) CI values are shown for each combination of trametinib and VT101 in NLF. C) CI values of equal ratio combinations are plotted against the cell viability fraction affected in SKNAS. D) CI values are shown for each combination of trametinib and VT101 in NLF. E) CI values of equal ratio combinations are plotted against the cell viability fraction affected in SKNFI. F) CI values are shown for each combination of trametinib and VT101 in SKNFI.

In contrast to the synergy observed between VT101 and trametinib, no synergy was detected between VT102 and trametinib (Fig. 3-7A-C). In fact, the CI values were so exponentially large that they could not be calculated. In looking at the fraction affected in NLF and SKNAS, it is clear that VT102 imposes no additional effect on cell viability in combination with trametinib and appears to be antagonistic (Fig. 3-7A and B). In SKNFI, combination of VT102 and trametinib appeared to be antagonist based on the fraction of cells affected, although VT102 did appear to be more potent as a single-agent than in NLF or SKNAS (Fig. 3-7C). Our data confirm that inhibiting YAP-TEAD activity with TEAD palmitoylation inhibitors in combination with trametinib is synergistic, but that there are functional differences between VT101 and VT102 that affect this synergistic relationship with trametinib. Under our confidentiality agreement with Vivace Therapeutics, we are

unable to disclose the specificity of TEAD palmitoylation inhibitor but we postulate that the differences in synergistic activity may be related to inhibitor specificity for TEAD1-4. To further validate the effect of combination of trametinib and VT101 in RAS-hyperactive neuroblastoma, synergy assays in RAS wild-type, *MYCN* amplified lines is planned but not yet completed.

Figure 3-7. No synergy observed between VT102 and trametinib in NLF, SKNAS, or SKNFI

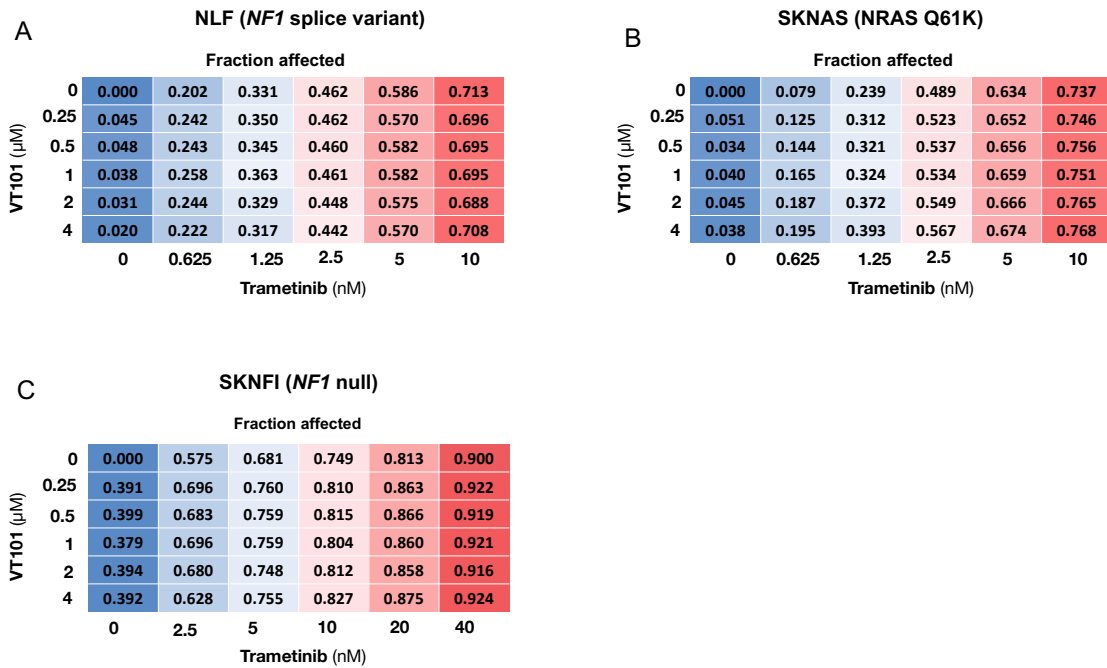


Figure 3-7 Legend: Synergy assays were performed by plating cells onto 96-well plates and treating cells in a matrix format with 1/4X, 1/2X, X, 2X, and 4X dilutions of either trametinib or VT102, where X=IC₅₀. For VT102, X=1 μ M. Combination index (CI) values were quantified based on cell viability using Compusyn but were extraordinarily high and considered antagonistic. To demonstrate the lack of

synergy between trametinib and VT102, values representing the fraction affected are shown for each combination of trametinib and VT102 in A)NLF, B) SKNAS, and C) SKNFI.

V. Discussion

In this chapter, I assessed the efficacy of combined MEK1/2 and TEAD palmitoylation inhibition on cell viability of Ras-hyperactivated neuroblastoma cell lines. RAS wild-type controls are ongoing. I first performed dose-response assays in a panel of Ras-hyperactivated neuroblastoma cell lines to determine a baseline activity measurement of the three compounds as single-agents. Inhibiting YAP-TEAD activity alone did not significantly decrease cellular growth or confluence over the seven-day period. This was not entirely surprising based on the growth rates of the sg*YAP1* and *YAP1*^{-/-} #2 cell lines (Supplementary Fig. 2-S3), in which the decrease in proliferation was not proportional to the degree of YAP knockdown. In consultation with Vivace Therapeutics, VT103 was determined to be inferior to the other two compounds due to a lack of potency and was not included in subsequent experiments. I next validated previous reports of YAP-independent TEAD activity in *MYCN*-amplified neuroblastoma by showing that inhibiting the YAP-TEAD interaction via TEAD palmitoylation does not affect growth or survival in RAS wild-type, *MYCN*-amplified Kelly and COG-N-519 neuroblastoma cell lines.

To assess whether inhibiting TEAD palmitoylation would recapitulate the YAP knockout from Chapter 2, I also tested for synergy between VT101 or VT102 and trametinib in a subset of RAS-hyperactivated neuroblastoma cell lines in a seven-day period. Synergy was detected between VT101 and trametinib in NLF, SKNAS, and SKNFI, but not between VT102 and trametinib. Furthermore, with increasing concentrations of VT101 and trametinib, the fraction affected in each cell line increased. Our findings suggest that TEAD palmitoylation inhibition is a candidate for combination with trametinib in RAS-MAPK aberrant neuroblastomas. As discussed in Chapter 2, this drug combination would only benefit patients with tumors expressing YAP and harboring RAS hyperactivity.

The striking difference between VT101 and VT102 in combination with trametinib suggests that the predicted differential sensitivity of each compound for TEAD1-4 may be biologically relevant. If one or more TEAD transcription factors are more relevant to intrinsic MEK1/2 inhibitor resistance than others, this could expand upon our current mechanistic understanding. Understanding the exact specificity of each compound will be immensely important for further studies of this drug combination. In addition, investigating the effect of this combination on YAP and phospho-YAP protein expression and cellular localization would provide important context into YAP protein dynamics in response to abolished YAP-TEAD binding capability. Further studies should also examine the effects of combined TEAD palmitoylation and MEK1/2 inhibition on cell cycle arrest and apoptosis, which would serve to validate our findings in Fig. 2-5C and D and Supplementary

Fig. 2-S5C. Ultimately, an *in vivo* study using Ras-hyperactivated patient-derived xenografts (PDX) will be an important means to test of the clinical potential of this combination based on the efficacy and tolerability observed in mice.

This study represents a proof-of-concept validation of the relationship between YAP and MEK1/2 in RAS hyperactive neuroblastoma. Our lab is continuing to work closely with Vivace Therapeutics as they optimize compounds with the proper pharmacokinetic and pharmacodynamic properties. We aim to test these lead compounds in combination with trametinib *in vitro* and *in vivo* and submit this story for publication.

**CHAPTER 4: HIGH-THROUGHPUT APPROACH TO DESIGNING
ALTERNATE MEK1/2 DRUG COMBINATIONS FOR RAS ACTIVATED
NEUROBLASTOMA**

I. Abstract

I hypothesized that high-throughput profiling of a large drug library for trametinib drug combination partners would reveal novel mechanisms of intrinsic resistance to MEK1/2 in a panel of RAS-MAPK pathway hyperactivated neuroblastoma. Cells were plated onto 384-well plates and treated with a library of FDA-approved and investigational anti-cancer agents and either DMSO or trametinib. By comparing the effect of the library compounds alone and combined with trametinib, the strictly standardized mean difference (SSMD) for each combination was used to rank and filter the top drug combinations in each cell line. To identify a drug combination that would be broadly effective across the spectrum of RAS-MAPK pathway mutations in neuroblastoma, I prioritized candidates that were potent across a majority of the cell lines screened. HMG-CoA Reductase inhibitors, including atorvastatin and lovastatin, were identified as the top drug candidates in three cell lines. Synergy was observed in the combination of the statins and trametinib in multiple cell lines, although the most synergistic combinations required statin concentrations in the micromolar range, which is typically not considered clinically relevant. These results suggest that statins may be useful candidates for combination with trametinib, but additional validation of other drug screen combinations is necessary. In summary, continued exploration

of potential drug combinations will be critical for the preclinical development of trametinib drug combinations and will help improve our understanding of the cellular reprogramming events that drive *de novo* trametinib resistance in neuroblastoma.

II. Introduction

In Chapters 2 & 3, I presented evidence that YAP expression determines sensitivity to MEK1/2 inhibition in RAS driven neuroblastoma cell lines. Furthermore, I showed that the combination of MEK1/2 and YAP activity inhibition produced synergy. While we think this combination could improve survival rates of children with relapsed neuroblastoma, the Vivace compounds are early in development and there are many potential obstacles before first-in-human studies. In order to identify other potential targeted inhibitors for combination with trametinib (or other MEK1/2 inhibitors), we conducted a high-throughput screen (HTS) to test the efficacy of combinations across five neuroblastoma cell lines with unique RAS-MAPK pathway aberrations, all resulting in hyperphosphorylated MEK and ERK.

In the wake of developments in genomics technologies, oncogenic driver mutations and signaling pathway addictions have been characterized and identified as putative therapeutic targets (Lawrence MS, 2014; Al-Lazikani B, 2012). Single-agent drug screens have produced expansive databases of anticancer agents with activity in distinct cell lines and genomic profiles (Weinstein JN, 1997; Greshock J, 2010; Barretina J, 2012; Garnett MJ, 2012). However, the

potential for superior activity of a drug combination rather than a single-drug therapy serves as the motivating force for developing a dual treatment strategy. To this end, high-throughput screening offers an efficient and robust method of uncovering novel signaling dependencies in response to single-drug treatment (Sun X, 2013). Many screening approaches have been utilized to identify targets for combination therapy, including CRISPR-based knockout, short-hairpin RNA, as well as directly testing drug-drug combinations (Sun X, 2013; Han K, 2017; Manchado E, 2016; Williams SP, 2017). In this study, we profiled a library of 3,045 compounds for synergistic combination with the MEK1/2 inhibitor trametinib.

I hypothesized that profiling a large library of drug compounds in combination with trametinib would reveal previously unknown drivers of intrinsic resistance to trametinib in a panel of neuroblastoma cell lines. By profiling a five neuroblastoma cell lines, our goal was to capture a potential trametinib drug combination that would exhibit potency in models with unique RAS-MAPK pathway aberrations.

III. Materials and Methods

Cell culture

Cells were cultured in RPMI-1640 medium containing 10% FBS, 2 mM L-Glutamine at 37 °C under 5% CO₂. Cells were detached with versene (0.02% EDTA in HBSS), washed with PBS + 1% FBS, and resuspended in culture media for plating.

Cell Viability Assays

Cells were seeded in 96-well cell culture plates at 2,500-4,000 cells per well depending on growth kinetics. Drug treatments were performed in triplicate 24 hours later over a six-log dose range (0.01-10,000 nM). IC₅₀ values for trametinib were calculated using area under the curve at 72 hours post-treatment. Cell viability was assessed using CellTiter-Glo (Promega).

Compound library and storage

The screening drug library was comprised of 3,045 compounds and was pre-plated on 10 individual 384-well plates (Selleckchem). A complete list of drugs can be found in Table 4-S1. On each plate, columns 1 and 23 contained 100% DMSO as a negative control and column 24 contained bortezomib as a positive control. Stock plates were stored at -40°C and freeze-thaw cycles were kept below 10 to prevent compound degradation. Trametinib dissolved in DMSO (Cellagen Technologies #C4112-5s) was maintained at 10 mM concentration at -20°C.

High-throughput screening

Cells were plated onto 20 384-well assay plates using a Multidrop Combi Reagent Dispenser (Thermo Scientific) at pre-determined plating densities for a 96-hour assay for each cell line. Cells were incubated overnight in a humidity-controlled incubator at 37°C and 5% CO₂. Drugs from the compound library were plated at

50 nl using the slotted pin tool (V&P Scientific) within the JANUS Automated Workstation (Perkin Elmer). Each library plate was transferred to two assay plates, which were then treated with either 50 nl 100% DMSO or 50nl trametinib at the IC₂₀ concentration for each cell line (NLF: 1nM, SKNAS: 0.5 nM, SKNFI: 2 nM, NB-EBc1: 2 nM, and SKNSH: 1 nM). Altogether, 10 assay plates were treated with the library compounds and DMSO and 10 assay plates were treated with the combination of the library compounds and trametinib. Assay plates were incubated at 37°C for 72 hours and cell viability was assessed using the ATPlite Luminescence Assay (Perkin Elmer) and the EnVision Xcite Multilabel Plate Reader (Perkin Elmer).

Data analysis

Data was analyzed using the Strictly Standardized Mean Difference (SSMD) method of high-throughput screen analysis, in which the difference of the means and the standard deviation of the difference between two populations is quantified (Zhang XD, 2007; Williams SP, 2017). The following equation was used: SSMD =

$\frac{(\mu_1 - \mu_2)}{\sqrt{\sigma_1^2 + \sigma_2^2}}$. In this screen, 10 library plates were used to treat 20 assay plates that

then received either DMSO or trametinib. Because only one replicate of the screen was performed, $(\mu_1 - \mu_2)$ corresponded to difference between the raw values for each library compound treated in combination with DMSO (μ_1) and trametinib (μ_2). To control for the variability within each library plate, the plate standard deviation was determined using the standard deviations of all DMSO-treated (σ_1) and

trametinib-treated (σ_2) sample values treated with corresponding library plates. Altogether, 10 unique analyses were performed for each cell line specific to each library plate.

Z-scores were also calculated for each drug combination to compare to the SSMD method using the formula $Z = \frac{\mu_n - x}{\sigma_n}$, where μ_n refers to the mean of the trametinib-treated negative control wells on each assay plate and σ_n refers to the standard deviation of this mean.

Screen quality was assessed using a Z-factor measurement with the following equation: $Z\text{-factor} = 1 - \frac{3(\sigma_p + \sigma_n)}{|\mu_p - \mu_n|}$, with p denoting positive control values and n denoted negative control values. Z-factor scores between 0.5 – 1.0 were considered to be excellent assays, with 1.0 being ideal. Scores between 0 – 0.5 were considered marginal, while <0 was considered to have too much overlap between positive and negative controls to be useful.

For filtering, a set of guidelines were established to identify a synthetic lethal combination. First, a cutoff was set to SSMD >3 , indicating at least three standard deviations from the mean. Next, the cutoff for the difference in normalized percent inhibition (NPI) between the DMSO-treated and trametinib treated samples was set to $>20\%$, because the IC₂₀ trametinib concentration would be expected to reduce cell viability by 20%. Finally, the NPI of the library compounds treated with

DMSO cutoff was set to $-15 \leq 0 \leq 15$ to eliminate compounds that either induced excessive growth or cell death as single-agents.

Statistics

Drug combination synergy was calculated using Compusyn software based on the Chou method of calculating drug synergy (Chou TC, 2006; Chou TC, 2010). IC₅₀ values were determined using GraphPad Prism (v6) and performing a nonlinear regression analysis using the “log(inhibitor) vs. response –Variable slope (four parameters)” dose response equation at the 7-day time point for each concentration.

IV. Results

High-throughput combination screen design

We selected five neuroblastoma cell lines as representative models of the most frequent RAS-MAPK pathway aberrations detected in neuroblastoma patient samples: NLF (*NF1* splice variant), SKNAS (*NRAS* Q61K), SKNFI (*NF1* null), NB-EBc1 (*KRAS* G12D), SKNSH (*ALK* F1174L). These five cell lines all been shown to have basal hyperphosphorylation of ERK and are sensitive to trametinib in the low nanomolar range (Hart LS, 2017). Although MEK1/2 inhibition is not potent in most ALK-mutated neuroblastoma models, SKNSH is the most sensitive of the ALK-mutated cell lines and was included. In an effort to identify a synthetic lethal drug combination, we designed a HTS to test the effect of a library of 3,045 compounds, of which 27.8% are FDA-approved, 68.6% are not FDA-approved,

and 3.5% are discontinued (Fig. 4-1A). Within this library, drugs can be classified by their proposed class, including cancer, endocrine, epigenetic, GPCR, ion channel, kinase, metabolism, microbiology, NSAID, protease, and other. The compounds classified as “other” were largely inviable candidates for future use in humans but served as tool compounds within this library. The layout of each library plate included two DMSO negative control columns and one bortezomib positive control column, with the remaining wells on the 384-well plate containing library compounds (Fig. 4-1B).

Figure 4-1. High-throughput trametinib combination screen design

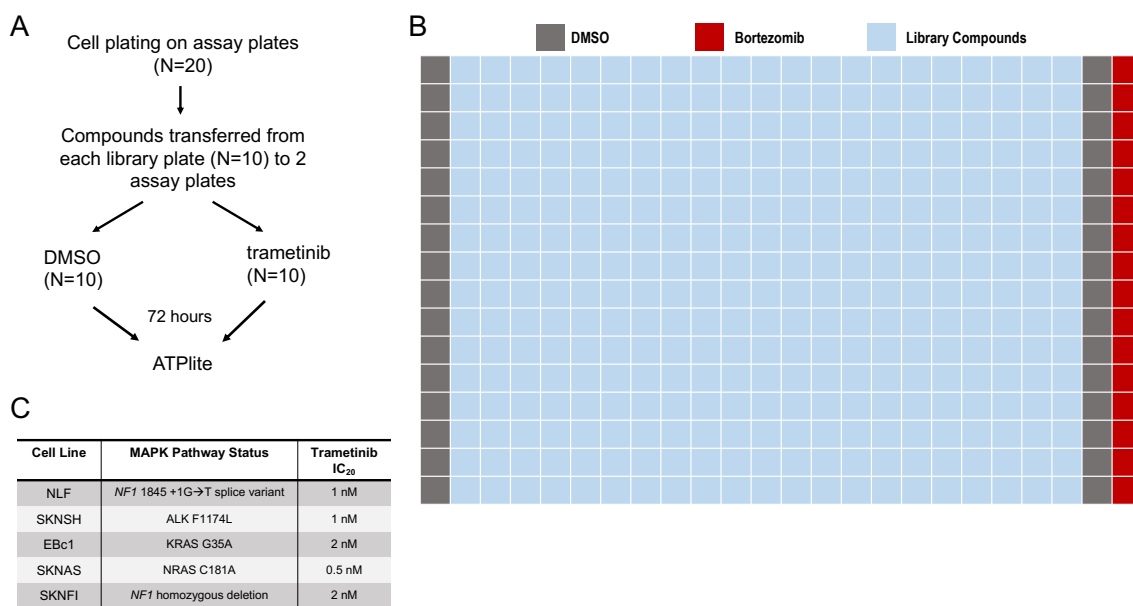


Figure 4-1 Legend: A) Schematic of high-throughput screen protocol. B) Library plate layout including negative control (DMSO), positive control (bortezomib) and sample library compounds on each plate. C) 72-hour IC₂₀ values for each cell line determined on a 384-well plate using ATPlite cell viability reagent.

In an effort to identify potent drug combinations, the trametinib dose for the HTS was determined by the trametinib IC₂₀ in each cell line (Fig. 4-1C). Cell viability results were analyzed to determine the quality of the data on each plate using a Z-factor measurement. This scale ranges from 0-1.0, with 0.5-1.0 indicating an excellent assay, 0-0.5 indicating a marginal assay, and scores <0 negating the usefulness of the data. Across 20 plates tested for each cell line, only 8 total plates were considered marginal assays and 92% (92/100 plates) of the screen being considered “excellent” (Supplementary Fig. 4-S1). The DMSO-treated SKNFI library plate 3 plate did receive a Z-factor score of 0, but because it was not <0, we included it in this analysis. We next calculated z-scores and strictly standardized mean difference (SSMD) scores as a dual method of analysis. The SSMD scoring is more robust because it is less sensitive to outliers than z-scoring. The SSMD was calculated using the difference of the DMSO and trametinib-treated values in combination with each compound and divided by the sample standard deviation of the entire assay plate. We compared the z-scores and SSMD scores for each cell line and determined that SSMD was a more robust indicator of quality. For example, the entirety of the trametinib-treated combinations in SKNFI was plotted using SSMD scores or Z-scores (Supplementary Fig. 4-S2A and B). When z-scores were overlaid according to highest SSMD value to lowest, it became clear that the high SSMD scores predicted activity in the trametinib combinations more uniformly and with greater accuracy than high z-scores

(Supplementary Fig. 4-S2C). Based on this comparison, SSMD scores were used for further “hit” determination.

We next instituted a series of filtering steps to narrow down the list of viability trametinib drug combinations. First, the cutoff for SSMD score was set to ≥ 3 , which corresponded to a value three standard deviations from the mean of the assay plate. However, only one compound in SKNSH achieved an SSMD score of >3 , so the cutoff for SKNSH was lowered to $SSMD > 2$. Next, the normalized percent inhibition (NPI) was calculated as the ratio of each sample to the negative control on each plate. The NPI cutoff for DMSO-treated samples was set to $-15 \leq 0 \leq 15$ to eliminate any compounds that caused excessive increases or decreases in cell viability as single-agents. Because the IC_{20} concentration of trametinib was used, we set a cutoff of $>20\%$ difference in NPI values between DMSO-treated and trametinib-treated samples. The final list of top trametinib drug combinations for each cell line was tabulated and further sorted by drug target, with one or more drugs acting on each drug target (Fig. 4-2A). In order to identify a drug combination that would be effective across cell lines with different RAS-MAPK pathway alterations, we selected drug targets that were shared between at least 3 or more cell lines (Fig. 4-2B).

Figure 4-2. SSMD analysis reveals top drug targets for trametinib combination

A

NLF	NB-EBc1	SKNAS	SKNFI	SKNSH
5-HT Receptor	AChR	Adrenergic Receptor	5-HT Receptor	Sodium Channel
AChR	ATGL	Androgen Receptor	AChR	
Adrenergic Receptor	ATPase	Cannabinoid Receptor	Adrenergic Receptor	
CETP	Autophagy,ROCK	COX	Adrenergic Receptor,Autophagy	
ClC-2 chloride channels	Beta Amyloid	Dehydrogenase	BET	
COX	Caspase	GPR	Dehydrogenase	
Dehydrogenase	COX	HDAC	Dopamine Receptor	
Dopamine Receptor	CXCR	Histone Methyltransferase	Epigenetic Reader Domain	
Estrogen/Progesterone Receptor,Autophagy	DNA/RNA Synthesis	HMG-CoA Reductase	Estrogen/Progesterone Receptor	
Factor Xa	EGFR	Integrase	FAAH	
GABA receptors	Histamine Receptor	MMP,Others	Factor Xa	
GluR	Integrin	Others	Ftase	
HDAC	IkB/IKK,PDK-1	PAFR	GluR	
Histamine Receptor	MAO	PI3K,mTOR	HDAC	
Histone Methyltransferase	MT Receptor	RAAS	Histamine Receptor	
HMG-CoA Reductase	Others	Reverse Transcriptase	Histone Acetyltransferase	
Hydroxyapatite	Phosphorylase		Histone Demethylase	
imidazoline receptor	RAAS		Histone Methyltransferase	
Liver alcohol dehydrogenases	Reverse Transcriptase		HMG-CoA Reductase	
MOR			IDO	
MTH			Kinesin	
NET, Histamine receptors			NOS	
NOD1			Others	
Others			p38 MAPK	
P2 Receptor			P450 (e.g. CYP17)	
PDE			PARP	
RAAS			PDE	
Sirtuin			RAAS	
Topoisomerase			Reverse Transcriptase	
			S1P Receptor	
			Sodium Channel	
			STAT, DNA/RNA Synthesis	

B

Common Drug Targets			
Between 4 cell lines	Number of Drugs	Between 3 cell lines	Number of Drugs
RAAS	9	AChR	7
Others	277	Adrenergic Receptor	12
		COX	14
		Dehydrogenase	4
		HDAC	2
		Histamine Receptor	10
		Histone Methyltransferase	5
		Reverse Transcriptase	3

Figure 4-2 Legend: SSMD scores were calculated to determine the top trametinib drug combinations on each plate and in each cell line, with a cutoff of SSMD>3. A) All combinations with SSMD>3 were compiled further categorized by unique drug

targets and listed within each cell line. B) To identify a combination with broad efficacy, drug targets that were present among the top combinations in 3 or more cell lines were filtered. For each drug target, the number of corresponding unique compounds are listed.

Validation of HMG-CoA Reductase inhibitors in combination with trametinib

HMG-CoA reductase is the rate-limiting enzyme of the mevalonate pathway, an essential metabolic pathway in the biosynthesis of cholesterol. For this reason, HMG-CoA reductase inhibitors, or statins, are commonly used to treat hypercholesterolemia and adults and familial hypercholesterolemia in children (Hindler K, 2006). Within the mevalonate pathway, statins prevent conversion of HMG-CoA to mevalonic acid, which is later converted to farnesyl and geranylgeranyl intermediates. Because small G-proteins require post-translational isoprenylation for membrane tethering and function, statins have been predicted to be useful against cancer models with hyperactivated Rho, Rac, and RAS (Hindler K, 2006).

To assess the value of a combination of trametinib and a statin, we first determined the single-agent activity of statins in the five RAS-hyperactive neuroblastoma cell lines tested in the screen (Fig. 4-3A and B). Both atorvastatin calcium and lovastatin were most potent in NLF, with IC_{50} values in the nanomolar range, while IC_{50} values in NB-EBc1, SKNAS, SKNFI, and SKNSH were in the

micromolar range (Fig. 4-3C). In general, all five cell lines were more sensitive to atorvastatin calcium than lovastatin, although the differences in IC₅₀ values did not exceed two-fold.

Figure 4-3. Single-agent activity of statins in neuroblastoma cell lines.

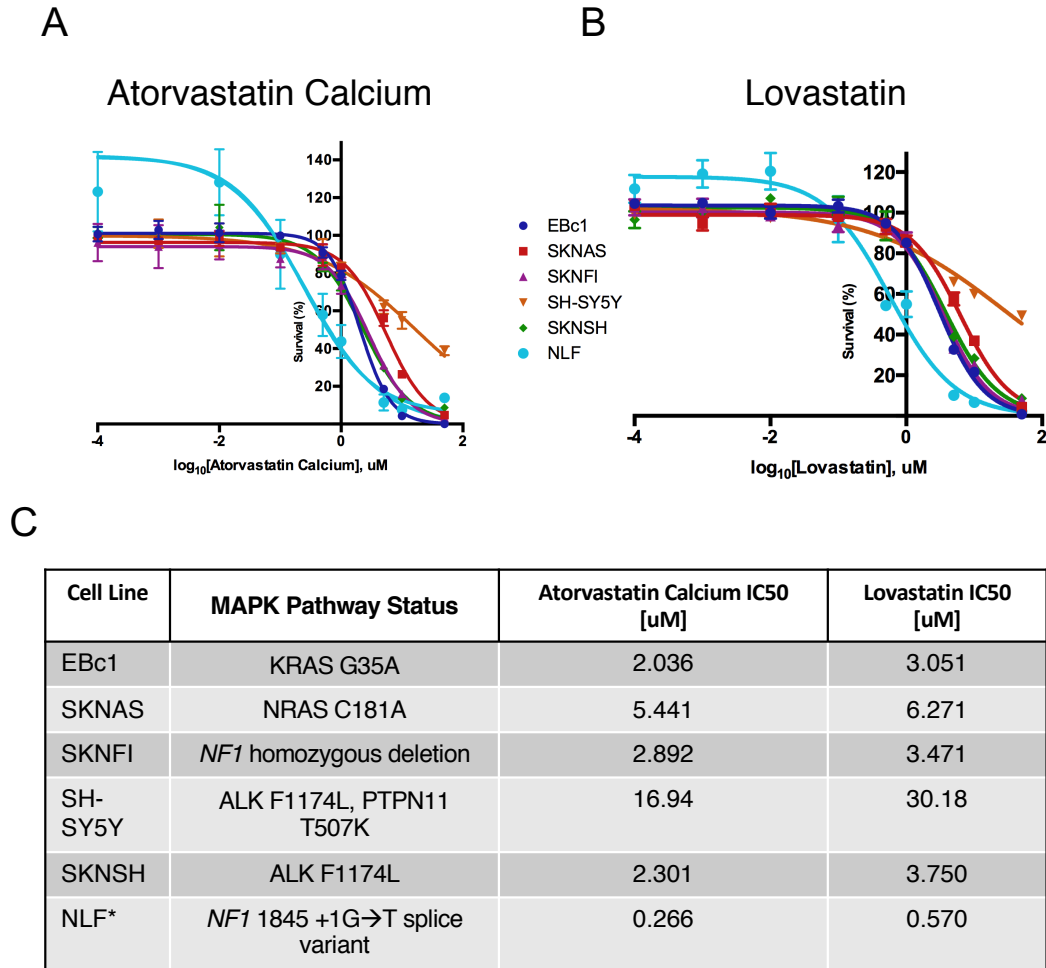


Figure 4-3 Legend: 72-hour dose-response curves performed over a 6-log dose range of in NB-EBc1, SKNAS, SKNFI, SH-SY5Y, SKNSH, and NLF treated with A) Atorvastatin calcium and B) lovastatin. C) IC₅₀ values calculated in

GraphPad Prism corresponding to atorvastatin calcium and lovastatin in six cell lines.

We next investigated whether the combination of trametinib and a statin is synergistic in RAS-hyperactivated neuroblastoma. The two most sensitive cell lines to single-agent atorvastatin calcium and lovastatin were NLF and NB-EBc1, which were selected for synergy analysis (Fig. 4-3B). Unlike the synergy assays performed in Chapter 2, only two trametinib concentrations (corresponding to the IC_{20} and IC_{50} in each line) were tested in combination with five concentrations of either atorvastatin calcium or lovastatin. Cell viability was analyzed, and synergy was quantified using CI values. In NLF, all combinations of trametinib and atorvastatin calcium were synergistic, as well as all combinations of trametinib and lovastatin, with CI values <1 . (Fig. 4-4A and B). Similarly, all combinations of trametinib and atorvastatin calcium showed synergy in NB-EBc1 (Fig. 4-4C). However, the combination of the IC_{20} trametinib dose and lower dose lovastatin in NB-EBc1 was not synergistic, but rather antagonistic with CI values >1 , while the high doses of lovastatin did show synergy (Fig. 4-4D). Upon increasing the trametinib dose to the IC_{50} concentration, all combinations of trametinib and lovastatin were considered synergistic (Fig. 4-4D). Altogether, these results suggest that combined inhibition of MEK1/2 and HMG-CoA Reductase is an effective combination in RAS-hyperactivated neuroblastoma cell lines.

Figure 4-4. Synergy observed between statins and trametinib in NLF and NB-EBc1.

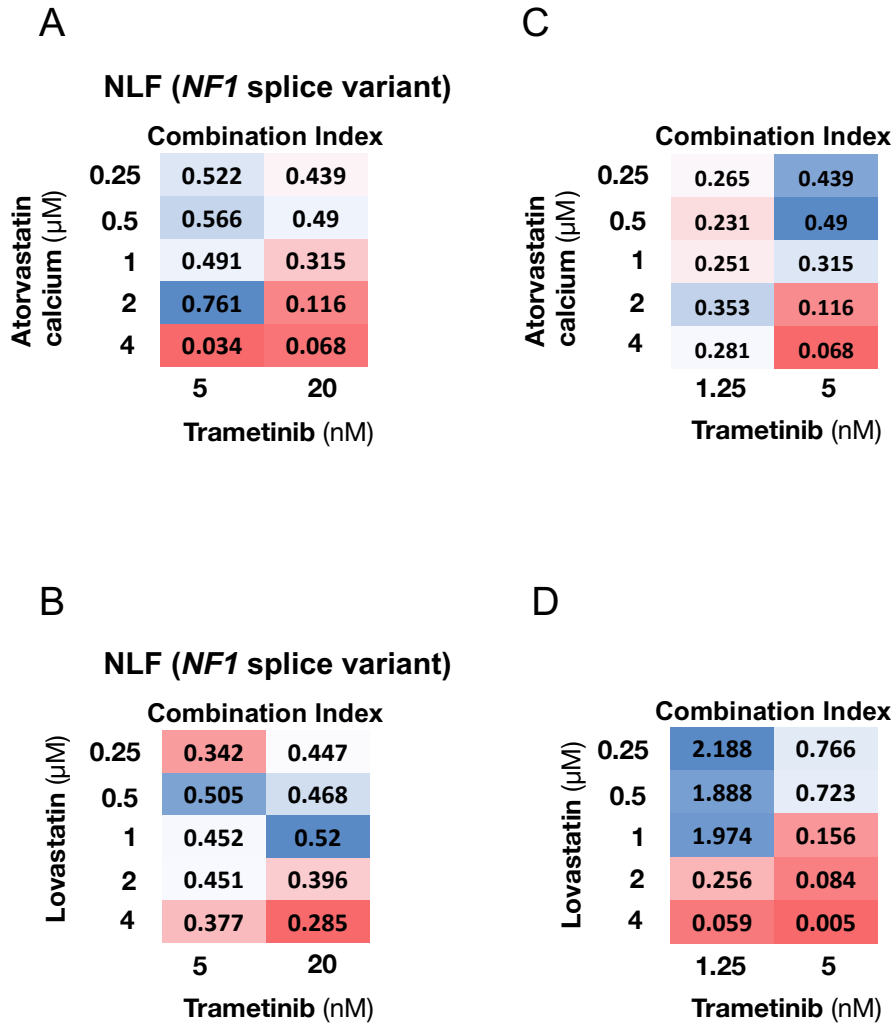


Figure 4-4 Legend: Synergy assays were performed by plating cells onto 96-well plates and treating cells in a matrix format with 1/4X, 1/2X, X, 2X, and 4X dilutions of either atorvastatin calcium or lovastatin, where X=IC₅₀. For both statins, X=1 μM . The IC₂₀ and IC₅₀ concentrations for trametinib in NLF (5 and 20 nM, respectively) and NB-EBc1 (1.25 and 5 nM, respectively) were used. Combination index (CI) values were quantified based on cell viability using Compusyn. A) CI

values are shown for each combination of trametinib and atorvastatin calcium in NLF. B) CI values are shown for each combination of trametinib and lovastatin in NLF. C) CI values are shown for each combination of trametinib and atorvastatin calcium in NB-EBc1. D) CI values are shown for each combination of trametinib and lovastatin in NB-EBc1.

V. Discussion

In this chapter, I profile a large drug library for potential combination with trametinib in RAS-hyperactivated neuroblastomas and assess the efficacy of trametinib in combination with HMG-CoA reductase inhibitors. Combined trametinib and atorvastatin calcium or lovastatin proved to be synergistic in RAS-addicted neuroblastoma cell lines. Overall, these findings suggest that while HMG-CoA reductase inhibitors may have potential in a trametinib drug combination, further work must be done to interrogate alternate combinations from the screen and validate drug combinations using patient-derived xenograft (PDX) mouse models.

Our findings suggest that dual inhibition of MEK1/2 and HMG-CoA reductase is consistent with reports from prior studies. One downstream implication of inhibiting isoprenylation of oncogenic G-proteins is the reported suppression of AKT activation, which can promote survival in response to MEK1/2 inhibitor therapy (Iizuka-Ohashi M, 2018). This evidence supports observations that targeting PI3K, the direct upstream of activator of AKT, with ribociclib shows

therapeutic synergy with trametinib in neuroblastoma models and causes tumor growth delay (Hart LS, 2016). Thus, statins may target multiple potential signaling pathways related to intrinsic trametinib resistance. Unfortunately, the statin concentrations required to achieve synergy with trametinib were in the low micromolar range, which are not considered clinically-relevant concentrations. Further testing with novel HMG-CoA Reductase inhibitors may yield improved synergy efficacy and potency with trametinib. In addition, investigating the pleiotropic effects of statins within cancer cells by assessing changes in gene expression and post-translational modifications will improve our understanding of trametinib-related therapy escape in neuroblastoma.

We also tested additional combinations of trametinib and epigenetic inhibitors of HDAC6, EZH2, and DOT1L. We elected not to present this data in this chapter based on the lack of efficacy observed. The three compounds showed no single-agent activity *in vitro* in NLF, SKNAS, SKNFI, or SKNSH. Meanwhile, the data obtained from our synergy assays were inconsistent and suggested that these combinations were highly antagonistic. This suggests that the combination of trametinib and an epigenetic inhibitor was likely a false positive finding and highlights the limitation of a HTS with only one replicate.

In conclusion, this study utilized an existing high-throughput screening platform to survey a large library of compounds to identify trametinib drug combinations for RAS-hyperactivated neuroblastoma. We had hoped to find novel and immediately translatable drug candidates, but none emerged to date, which is

unfortunately not limited to our system as combinatorial partners for MEK1/2 inhibition in other cancers have also been difficult to define. Of note, a potential weakness of this study was the single replicate of the combination drug screen. Edge effects on cell culture plates as well as natural biological variation could have caused fluctuations in data that could have been interpreted more easily with additional replicates. These data provide useful evidence for combinatorial efficacy, but additional replicates or a larger validation effort would be necessary to identify a viable trametinib drug combination for further preclinical evaluation. In addition, expanding the panel of cell lines to include more models with different RAS-MAPK aberrations would help define the broad usefulness of a combination. Taken together, our data represents a step forward in understanding the signaling adaptations in neuroblastoma cells in response to trametinib and supplementary investigation will be necessary to fully validate clinically-useful therapeutic combinations.

CHAPTER 5: OVERALL DISCUSSION AND FUTURE DIRECTIONS

Within the neuroblastoma research field, the paucity of recurrent druggable oncogenic driver mutations and genomic heterogeneity between and within tumors has impeded the development of broadly effective targeted therapies. Rather than focusing on low- or intermediate-risk neuroblastomas with good prognoses, or even high-risk neuroblastomas at diagnosis, the purpose of this research was to contribute meaningful insight into therapy design for relapsed neuroblastomas, for which survival rates remain abysmally low, with the future goal of integrating effective relapse therapies into frontline regimens to prevent relapse. This dissertation work was centered around our discovery that RAS hyperactivation is enriched in relapsed tumors and our assumption that mechanisms of *de novo* and acquired trametinib resistance would be tissue specific. The overall hypothesis of this dissertation was that identifying competitive adaptations of MAPK-active neuroblastoma cells in response to MEK1/2 inhibition will guide the design of novel combination therapies for relapsed neuroblastomas. Using a bimodal approach to combination therapy design, we have identified a role for YAP in *de novo* trametinib resistance, as well as validated a synergistic combination of novel inhibitors of YAP activity and trametinib. In addition, we catalogued the activity of 3,045 compounds as single-agents and in combination with trametinib in five RAS-MAPK hyperactivated neuroblastoma cell lines and have begun to characterize the efficacy of combined treatment with trametinib and statins. While these latter data are not yet fully exploited, the screen provides a major resource for future drug

development activities in the neuroblastoma research community (all data will be made freely available prior to any publication).

The approaches adopted to test our central hypothesis were carved out of lessons learned from the neuroblastoma field and the larger MEK1/2 inhibitor field. In addition, these findings presented herein support our approach to identifying novel combinations, both using innovative new compounds and FDA-approved compounds identified via screening. Collectively, this body of work advances what was known about neuroblastomas with hyperactivated RAS signaling and the rewiring of oncogenic signaling as a result of MEK1/2 inhibition.

I. YAP1 modulation of MEK inhibitor sensitivity

Here, we first define a role for the Hippo pathway protein YAP in determining trametinib sensitivity in RAS-MAPK aberrant neuroblastoma cell lines. While basal levels of YAP are low in the majority of neuroblastomas, we have definitively shown that YAP activity can be induced by trametinib. With respect to the YAP-expressing neuroblastoma cell lines, we present the first evidence of nuclear accumulation of YAP induced by trametinib exposure. The exact mechanism underlying this shift in cellular localization remains unclear. In BRAF V600E mutant melanoma cell lines, the BRAF inhibitor vemurafenib was shown to induce YAP nuclear translocation with concomitant formation of actin stress fibers (Kim, 2016). Actin remodeling and actin-associated proteins are known to regulate YAP-Hippo signaling via inputs including mechanical stress, contractile actomyosin,

extracellular matrix stiffness, cell-cell junctions, and nuclear pores (Seo and Kim, 2018). However, phosphorylation of YAP could also be performed by upstream core Hippo kinases or other cellular kinases such as Src; alternatively, dephosphorylation could be altered by phosphatases such as PTPN14, in which inactivating mutations have been identified in relapsed neuroblastomas (Seo and Kim, 2018; Eleveld, 2015). Further investigation of this mechanism of YAP phosphorylation and cellular localization will be critical to understanding the interplay between the RAS-MAPK and Hippo pathways in neuroblastoma.

Using CRISPR-Cas9 gene editing, we generated four isogenic clones in NLF cells (*NF1* splice variant) and observed an 8-10-fold increase in trametinib sensitivity over 72-hours. Conversely, we overexpressed a constitutively-active form of YAP (YAP-5SA) in low-YAP expressing RAS-hyperactive cell lines and demonstrated that YAP-5SA induced trametinib resistance. Taken together, these two observations show that YAP activity in RAS-MAPK cell lines is a predictive biomarker of trametinib sensitivity. However, we do not think that endogenous YAP expression dictates sensitivity to single-agent trametinib, but rather induction of YAP expression and nuclear translocation upon the selective pressure of MEK1/2 inhibition in hyperactivated RAS pathway cells. For example, SKNAS and NLF cells have moderate-high YAP expression, yet they are extremely sensitive to trametinib, with IC_{50} values of 10 nM and 20 nM, respectively. Rather, changes in the regulation of YAP can provide a competitive advantage to MEK1/2 inhibition that we seek to better understand.

Using RNA sequencing, we defined gene signatures enriched in trametinib-treated *YAP1* knockout cells. Using gene set enrichment analysis (GSEA), we determined that E2F and *MYCN* gene sets were significantly downregulated in response to combined *YAP1* knockout and MEK1/2 inhibition. The connection between E2F and YAP has been reported in other studies (Kapoor, 2014), although there are several important distinctions. First, ChIP-qPCR was used to confirm the co-occurrence of YAP/TEAD2 and E2F transcription factors at the promoters of cell cycle genes in KRAS G12D mutant pancreatic ductal adenocarcinoma cells (Kapoor, 2014). While we were not able to confirm the enrichment of YAP or TEAD at the promoter of E2F genes, previous reports in neuroblastomas that describe MYCN regulation of E2F expression suggests that MYCN may play a more central role in our findings (Strieder V, 2003). Although the model used for RNA seq does express MYCN, the majority of RAS-driven neuroblastomas express high MYC, which is likely why we detected an enrichment of the MYC gene signature in our RNA sequencing results. Furthermore, YAP knockdown in vemurafenib-resistant BRAF V600E mutant melanoma cells revealed enrichment of the E2F1 gene signature, as well as EGFR, EZH2, and MYC gene signatures (Kim, 2016). In our analyses, E2F and MYC were the top gene signatures enriched in the trametinib-treated *YAP1* null-specific dataset. While these results do point to a similar mechanism observed in Chapter 2, our findings are specific to MEK1/2 inhibition and has significant implications in the fields of neuroblastoma and MEK1/2 inhibitor research. In the same study that

identified E2F1 gene signature changes in response to YAP knockdown, the serine-threonine kinase TESK1, which promotes actin stress fiber formation via Cofilin phosphorylation, was identified as a synthetic lethal target in vemurafenib-resistant melanoma (Kim J, 2015). Further investigation of TESK1 and other potential intersections between the RAS-MAPK and Hippo-YAP pathways will be crucial to developing a deeper understanding of this mechanism in neuroblastoma and defining translatable combinatorial therapeutic strategies.

II. YAP1-TEAD as a therapeutic target

Our findings demonstrating the role of YAP in intrinsic trametinib resistance was further validated upon discovering synergy between dual inhibition of MEK1/2 and YAP activity. The innovative efforts by Vivace Therapeutics generated novel pharmacological inhibitors of TEAD palmitoylation as a proxy for the inhibiting YAP-TEAD transcriptional output (Tang, 2019). As described previously, these small molecule inhibitors bind within a pocket and prevents TEAD autopalmitylation necessary for YAP-TEAD binding and transcriptional activity (Chan, 2016; Noland, 2016). The lack of specific and selective inhibition of YAP was the primary limitation prior to the discovery of this class of compounds, as verteporfin was considered nonspecific and potentially toxic at concentrations necessary for anti-YAP activity (Liu-Chittenden, 2012; Liu, 2019). Based on the extensive literature reporting that TEAD is required for YAP oncogenic activity, we entered into a collaboration with Vivace Therapeutics to perform the first

combination studies with three proprietary compounds (Vassilev, 2001; Zhao, 2007; Zhang, 2008; Liu-Chittenden, 2012, Shi, 2017; Holden, 2018). In this dissertation, I am unable to provide mechanistic details on the specificity of each of the compounds studied due to a confidentiality agreement, but these details will be forthcoming in future publications.

We have shown that, as predicted, each of the three Vivace compounds (VT101, VT102, and VT103) showed no cytotoxicity in RAS-MAPK aberrant or MYCN amplified (and RAS-MAPK wildtype) neuroblastoma cell line models. This was expected as the isogenic *YAP1* knockout cell lines discussed in Chapter 2 displayed varying levels of subtle (but reproducible) growth delay, particularly the pooled sg*YAP1* population which displayed minimal growth delay. Additionally, TEAD palmitoylation inhibitors are only targeting one role of many performed by YAP within the cell. Discrepancies between the effects of these inhibitors compared to *YAP1* knockout could be partially due to alternate YAP functions or transcriptional partners which may affect cellular growth (Holden, 2018), or the relative potency of these compounds compared to precise depletion by gene editing.

Due to their recent discovery, there are no data describing combinations studies with TEAD palmitoylation inhibitors *in vitro* or *in vivo*. Here, we show that the combination of VT101 and trametinib is synergistic across three RAS-MAPK hyperactivated cell lines, while VT102 and trametinib was primarily antagonistic. With respect to VT101 and trametinib, these results are extremely encouraging

and serve as a further validation of the data presented in Chapter 2. Importantly, Vivace Therapeutics will be providing compounds for in vivo testing of this combination as soon as their medicinal chemistry modification to these tool compounds create molecules with improved pharmacologic properties. Furthermore, the striking discordance between the effect of VT101 and VT102 in combination with trametinib is intriguing and will provide mechanistic insights once the company releases the compound structures and TEAD1-4 specificity (or promiscuity) can be revealed. We posit that this difference is due to the differing specificity for each of the four TEAD family members, which would potentially implicate a specific TEAD transcription factor in YAP-driven *de novo* trametinib resistance in relapsed neuroblastoma.

III. Alternate MEK inhibitor drug combinations

We generated two unique and valuable datasets in our high throughput combination drug screen that we plan to make freely available to the academic community. First, our dataset ranking trametinib drug combinations will serve as an incubator for novel hypotheses for further preclinical validation. In parallel, the high-throughput screen generated single-agent data which describes the effect of each library compound alone on cell viability. This single-agent dataset could reveal novel potent inhibitors of neuroblastoma cell lines and serve as a reference guide for future drug development projects. One limitation of this study is that the screen was only performed as one replicate, so each data point representing

single-agent and combinatorial responses is N=1. This is not ideal because of the potential biological and technical variation that could bias our results, but the size and scale of the screen enabled us to profile an enormous collection of drugs. We think that future screens should include additional replicates will improve the reproducibility of the screen and streamline candidate drug selection. Nevertheless, the high-throughput screen analysis we performed will serve as a useful resource for trametinib combination drug design, as well as for understanding the activity of a vast library of across five cell lines.

We have presented two separate *in vitro* validations of two categories of drugs: HMG-CoA Reductase inhibitors, or statins, and epigenetic inhibitors. We find that the combination of two different statins, atorvastatin calcium and lovastatin, show synergy with trametinib in a panel of RAS-MAPK mutated neuroblastoma cell lines. In our validations of trametinib and epigenetic inhibitors, including inhibitors of HDAC6, EZH2, and DOT1L, the results were inconsistent, and no synergy was definitively identified. A survey of the literature lends credence to these observations that suggest the combination of a MEK1/2 inhibitor and a statin may be more viable as a therapeutic regimen to improve MEK1/2 inhibitor efficacy (Hindler, 2006; Cerezo-Guisado, 2007; Iizuka-Ohashi, 2018). Statins have been shown to be well-tolerated and inexpensive and have even been shown to play a role in cancer prevention in adults in a dose-dependent manner (Gronich and Rennert, 2013; Taylor, 2008; Kuoppala, 2008; Sleijfer, 2005; Karp, 2008). On the other hand, high dose statins have been reported to cause higher incidences

of hepatocellular, thyroid, and pulmonary cancers (MacDonald, 1988; Robison, 1994). Our results suggest that the most synergistic combinations of MEK1/2 and statins occur with high statin concentrations. Great care would be required to protect patient safety while also ensuring that statin levels in the blood are sufficiently high to elicit an anti-tumor effect. While this is a potentially interesting result, we do not consider it readily translatable and trametinib-statin combinations are not being pursued for clinical development.

The medical and pediatric oncology fields have struggled to find truly synergistic combinations for cancers with mutations in the MAPK pathway. Trametinib and other MEK1/2 inhibitors are being tested in the setting of mutated receptor tyrosine kinases like EGFR or ALK with specific inhibitors of these hyperactivated proteins. Empiric combinations with autophagy inhibitors and immune checkpoint inhibitors are also being pursued. However, MAPK pathway mutations are mutually exclusive of ALK mutations in neuroblastoma, and there is little evidence for activity of drugs like chloroquine and the myriad of new immune checkpoint inhibitors. This is one of the most difficult problems in oncology drug development, and our screen's limited translational success to date is likely not too surprising, but we were hoping to find an autonomic neuronal-based oncogenic vulnerability unique to this disease that we uncovered. Making these data publicly available will increase the chance that unique discoveries from the screen will impact patients in the not too distant future.

IV. Future Directions

This study utilized a dual approach to study the signaling vulnerabilities adopted in response to MEK1/2 inhibition in RAS hyperactivated neuroblastomas and to design combination drug therapies for further preclinical validation. The work presented in this dissertation has only begun to understand the complex signaling dynamics under the pressure of MEK1/2 inhibition. Further investigations are warranted to develop a clinically effective combination for treating relapsed neuroblastoma. First, the observation of trametinib-induced nuclear translocation of YAP protein is intriguing and may provide insight into the biology of relapsed neuroblastoma, especially MAPK-activated cases subjected to MEK1/2 inhibitors. To accomplish this, it would be useful to perform immunoprecipitation-mass spectrometry (IP-MS) to capture and identify proteins interacting with YAP in the presence and absence of trametinib treatment. If this experiment reveals novel protein-protein interactions, then additional studies would be warranted to understand this mechanism of YAP regulation. To test the hypothesis that actin stress fiber formation may play a role in YAP nuclear accumulation, immunocytochemistry of NLF and SKNAS cells stained for actin and YAP would provide snapshots of this potential interaction. Co-treatment of trametinib with an inhibitor of actin polymerization, such as cytochalasin D, could reveal whether blocking the assembly of actin stress fiber formation affects YAP nuclear localization. Furthermore, additional investigation could be done to elucidate the mechanism responsible for the cooperativity between MEK1/2 inhibition and YAP

knockdown. One approach to studying this could focus on the role of E2F and MYC(N) in the combination of trametinib and *YAP1* loss using ChIP-seq of TEAD1-4, YAP, E2F1, and MYC and MYCN. This experiment would illuminate the transcriptional dynamics and determine whether YAP-TEAD function in concert with E2F or MYCN, or rather compensate for the loss of E2F or MYCN in response to trametinib. Although this dissertation primarily focuses on downstream effectors of the Hippo pathway, it may be important to modulate the expression of upstream Hippo pathway kinases MST1/2 and LATS1/2 in NLF and SKNAS cells to fully discern the role of the core Hippo pathway components.

The results presented in Chapter 3 lay the groundwork for further preclinical and clinical development of a combination of trametinib and a TEAD palmitoylation inhibitor. We currently think this is the most likely combination to be translated to a clinical trial in the next 1-2 years, and the collaboration with Vivace is active and highly collaborative. To ensure on-target activity of the TEAD palmitoylation inhibitors, NLF and SKNAS *YAP1* knockout cell lines could be used with the hypothesis that the loss of YAP expression would ablate the effects of the inhibitors on cell viability. If these validations continue to show synergy between TEAD palmitoylation inhibitors and trametinib, it will be necessary to test the combination in a full *in vivo* study in NLF, SKNFI, and SKNAS xenograft models, as well as carefully selected PDX models from our growing armamentarium of these precious reagents (<https://www.biorxiv.org/content/10.1101/566455v1>). It will be important to assess the efficacy of the combination, but also determine any toxicity related

to *in vivo* inhibition of YAP-TEAD activity. We plan to test Vivace's next generation of compounds which are expected to be more specific for individual TEAD proteins and be optimized for *in vivo* testing in Q4 of 2019. As this collaboration matures, we expect to demonstrate improved efficacy in preclinical studies and deliver a final combination therapy for inclusion in a clinical trial at the Children's Hospital of Philadelphia.

Based on our preliminary results from the high-throughput trametinib combination drug screen, the observation of synergy between trametinib and statins is an interesting result but unlikely to be clinically meaningful and will not be pursued further. Rather, our efforts will focus on evaluating other top trametinib combinations. Ultimately, including additional replicates of the full screen or of smaller subsets, such as cancer-specific compounds, would improve the ability of our analysis to detect true positives and eliminate false-positive combinations. We plan to select a subset of top performing candidates for combination and perform a validation screen. In this screen, cells would be treated with each candidate compound over a 6-dose concentration range in combination with trametinib to produce dose-response curves, from which IC_{50} values could be extrapolated (Guo, 2017). In parallel, we will fully analyze the single-agent response data collected in the screen for potential new insights into neuroblastoma therapeutic vulnerabilities.

In sum, this body of work represents the first foray into the design of trametinib drug combinations for RAS-MAPK pathway activated neuroblastomas.

Insights gleaned from Chapters 2, 3, and 4 have significant implications in the Hippo-YAP, RAS-MAPK, and neuroblastoma fields of research. We have confirmed the role of YAP in intrinsic resistance to trametinib and validated a novel TEAD-YAP inhibitor as a synergist therapeutic combination with MEK1/2 inhibition. We also present a vast dataset profiling the activity of over 3,000 trametinib drug combinations, with early preclinical validations indicating synergy between trametinib and HMG-CoA Reductase inhibitors. In doing so, we have laid the groundwork for continued exploration of both combination therapy approaches to address the critical unmet need of new therapeutic options for relapsed neuroblastoma.

APPENDIX: Additional Published Manuscript

I. Genetic Susceptibility to Neuroblastoma

This section has been published: Tolbert, V.P.* , Coggins, G.E.* , Maris, J.M. (2017). Genetic Susceptibility to Neuroblastoma. *Curr Opin Genet Dev*: 81-90.

Abstract

Until recently, the genetic basis of neuroblastoma, a heterogeneous neoplasm arising from the developing sympathetic nervous system, remained undefined. The discovery of gain-of-function mutations in the ALK receptor tyrosine kinase gene as the major cause of familial neuroblastoma led to the discovery of identical somatic mutations and rapid advancement of ALK as a tractable therapeutic target. Inactivating mutations in a master regulator of neural crest development, PHOX2B, have also been identified in a subset of familial neuroblastomas. Other high penetrance susceptibility alleles likely exist, but together these heritable mutations account for less than 10% of neuroblastoma cases. A genome-wide association study of a large neuroblastoma cohort identified common and rare polymorphisms highly associated with the disease. Ongoing resequencing efforts aim to further define the genetic landscape of neuroblastoma.

INTRODUCTION

Neuroblastoma is the most common solid extracranial malignancy of childhood, accounting for about 7% of all cancers in children under the age of 15

(Howlader N, 2011). It is the most common cancer in the first year of life, with a median age of diagnosis of 17 months (Howlader N, 2011; London WB, 2005). It is a cancer of the developing sympathetic nervous system, arising in the adrenal medulla or paraspinal ganglia (Hoehner JC, 1996). Approximately 65% of these tumors present in the abdomen, along with the neck, pelvis and chest (Maris JM, 2007). Clinical course can vary widely, with infants often having spontaneous regression of the tumor without chemotherapy (Carlsen NL, 1990; Cole WH, 1956; Yamamoto K, 1998; Hero B, 2008), while older children generally have a poor prognosis despite highly intensive chemotherapy, radiation therapy, and immunotherapy (Maris JM, 2007). Demonstrating the phenotypic heterogeneity of neuroblastoma, low-risk patients have a greater than 95% survival probability whereas high-risk patients have a 40–50% probability of long-term survival (Oberthuer A, 2015; Maris JM, 2010). It has been known for some time that *MYCN* amplification in tumors portends a poor prognosis (Schwab M, 1983; Brodeur GM, 1984; Seeger RC, 1985), and thus is used as a biomarker for treatment stratification. Recently, there has been significant effort made to better classify subgroups of patients based on age, and tumor spread, genomics and differentiation (Brodeur GM, 1993; Cohn SL, 2009; Cecchetto G, 2005; Monclair T, 2009; Deyell RJ, 2011). The International Neuroblastoma Risk Group (INRG) classification has led to 16 statistically distinct risk groups based on clinical and molecular features which has made prognosis more accurate for patients and helps guide physicians on treatment regimens (Cohn SL, 2009).

Significant progress has been made recently in the understanding of the heritability of neuroblastoma through linkage scans of families with the disease and genome-wide association studies (GWAS) of sporadic cases ([Table 1](#)). The primary advantages of GWAS over previous methods are that no assumptions about candidate genes are necessary, variations can be localized precisely, and no testing in families or family members is required (Hirschhorn JN, 2005). From a clinical standpoint, it is clear that improvement must continue to be made in defining novel therapeutic approaches to neuroblastoma as it continues to account for 12% of childhood cancer mortality (Maris JM, 2010), with advancement especially crucial in high-risk patients (Tonini GP, 2012). One starting point to develop optimal treatments is to understand the underlying genetic alterations that initiate tumorigenesis. We review here the current understanding of the genetic susceptibility of neuroblastoma.

Genomic Locus	Phenotype Association	Top SNP	P-Value (combined)	MAF cases	Odds Ratio (OR)	Proposed Mechanism
6p22	High-risk	rs6939340	9.33×10^{-15}	56%	1.37	Loss of function
2q35	High-risk	rs6435862	5.20×10^{-18}	40%	1.68	Gain of function
11p15	High-risk	rs110419	5.20×10^{-16}	55%	1.34	Gain of function
6q16	High-risk	rs17065417	1.20×10^{-8}	8%	1.38	Gain of function
6q16	High-risk	rs4336470	2.70×10^{-7}	30%	1.26	Loss of function
1q23	Low-risk	rs1027702	2.07×10^{-6}	31%	2.01	unknown
5q11	Low-risk	rs2619046	2.94×10^{-6}	32%	1.47	unknown
5q11	Low-risk	rs10055201	6.54×10^{-7}	29%	1.49	unknown
11p11	Low-risk	rs11037575	4.20×10^{-7}	39%	1.67	unknown
8p21		rs11994014	0.005	20%	0.88	Loss of function
17p13		rs35850753	3.34×10^{-14}	3.6%	2.7	Loss of function
1q21		CNV	2.97×10^{-17}	15%	2.49	unknown

Table 1: Summary of neuroblastoma susceptibility loci. A majority of this cohort of genomic loci are significantly associated with distinct neuroblastoma phenotypes, while some remain to be characterized. P values and Odds Ratios (ORs) are combined values between discovery and replication studies from the original publication. Predicted mechanisms on protein function are indicated as loss of function, gain of function, or currently unknown. MAF = minor allele frequency.

Familial Neuroblastoma

About 1–2% of neuroblastoma is inherited in an autosomal dominant fashion within families (Knudson AG, 1972; Kushner BH, 1986; Dodge HJ, 1945; Chompret A, 1998). As with many cancer predisposition syndromes, patients often have multiple primary tumor sites and an earlier age of onset. The disease is typically highly penetrant, but there is variability and unaffected obligate carriers are often observed (Knudson AG, 1972; Kushner BH, 1986; Mosse YP, 2008). Neuroblastoma families often show significant clinical variability in severity of disease, with low- and high-risk cases observed in the same pedigrees (Hardy PC, 1972; Gerson JM, 1974; Wong KY, 1971; Bergstrom JF, 1974; Brodeur GM, 2003). While rare, these families provide a unique opportunity to learn about genetic drivers of neuroblastoma.

The first gene found to predispose to neuroblastoma was identified in families affected with neuroblastoma along with Hirschsprung disease and/or congenital central hypoventilation syndrome (also known as “Ondine’s Curse”). These disorders of neural crest-derived cells are known as neurocristopathies and are occasionally seen coincident with neuroblastoma (Bolande RP, 1997; Bower RJ, 1980; Michna BA, 1988; Roshkow JE, 1988; Stovroff M, 1995). Amiel and colleagues identified loss of function mutations in the paired-like homeobox 2B (*PHOX2B*) gene in the majority of patients with congenital central hypoventilation syndrome after sequencing this candidate gene (Amiel J, 2003, Weese-Mayer DE, 2003). This gene was of interest because the *PHOX2B* transcription factor is essential during development of the autonomic nervous system. Germline mutations in *PHOX2B* were subsequently found in a small proportion (~10%) of pedigrees with familial neuroblastoma, making this the first *bona fide* neuroblastoma predisposition gene (Trochet D, 2004; Mosse YP, 2004). As expected, the families with *PHOX2B* mutations also had variable penetrance of each of the component neurocristopathies, with non-polyalanine repeat expansion mutations (NPARM) typically lead to the most severe phenotype (Heide S, 2016; Nagashimada M, 2012).

In order to identify additional hereditary predisposition genes in the familial neuroblastoma cases, a genome-wide linkage scan at 6,000 single nucleotide polymorphisms (SNPs) was undertaken in 20 neuroblastoma families (Mosse YP, 2008). A linkage signal was found and narrowed down to chromosome bands

2p23–p24, which contained 104 genes including *MYCN*. This known neuroblastoma oncogene was resequenced in all probands, but no mutation was found. The anaplastic lymphoma kinase (*ALK*) is also in this region and had been previously identified as a potential oncogene in this malignancy (Osajima-Hakomori Y, 2005; George RE, 2007) as well as in other cancers through active translocations and point mutations (Griffin CA, 1999; Jazii FR, 2006; Morris SW, 1994; Rikova K, 2007; Soda M, 2007; Inamura K, 2008; Wang YW, 2011; Murugan AK, 2011). When *ALK* was resequenced, three distinct mutations were found in this gene in eight discrete families (Mosse YP, 2008). Subsequent studies have confirmed that about 80% of families with neuroblastoma harbor mutations in *ALK*. Mutations in *ALK* were also found to be somatically acquired in about 10% of all cases of neuroblastoma (Mosse YP, 2008; Janoueix-Lerosey I, 2008; George RE, 2008; Chen Y, 2008). *ALK* is a receptor tyrosine kinase, and all of these were activating mutations in the tyrosine kinase domain that caused constitutive phosphorylation and were predicted to be oncogenic drivers (Mosse YP, 2008). While Knudson and Strong's prediction of a "two-hit" model has held true for most hereditary cancers (Knudson AG, 1972), these susceptibility genes are usually tumor suppressor genes. In contrast, *ALK* was the first oncogene mutation shown to cause a familial pediatric cancer. The Mosse lab has subsequently biochemically characterized each of the germline and somatic mutations, and there is a correlation between penetrance and mutation type (Bresler SC, 2014; Bresler SC, 2011). For example, the R1275Q mutation leads to near complete penetrance

in families and was shown to be one of the most activating mutations tolerated in the germline, whereas the G1128A is more weakly activating and is correlated with an approximate 25% likelihood of developing neuroblastoma. Interestingly, the two most highly activating hotspot mutations acquired somatically (F1174* and F1245*) were each observed in the germline once, but in the setting of neuroblastoma with severe neurocognitive defects and brain stem abnormalities, further emphasizing the genotype-phenotype relationship as well as the critical role plays in normal neurodevelopment (de Pontual L, 2011). Genetic testing for both *ALK* and *PHOX2B* are currently available for identifying genetic susceptibility and informing decisions about screening other family members (<http://www.ncbi.nlm.nih.gov/sites/GeneTests/>).

ALK was quickly identified as a potential pharmacologic target in neuroblastoma when knockdown of *ALK* resulted in growth inhibition in all neuroblastoma cell lines with *ALK* mutations and some with wild-type *ALK* (Mosse YP, 2008). Further testing with an *ALK* small molecule inhibitor, crizotinib, showed profound sensitivity *in vitro* and *in vivo* to the drug in a panel of neuroblastoma cell lines and xenografts, respectively, with certain mutations and *ALK* amplification (Bresler SC, 2011; Schonherr C, 2011; Heuckmann JM, 2011; Carpenter EL, 2012). Based on these data, only 18 months after *ALK* was discovered as a neuroblastoma oncogene, the Children's Oncology Group initiated a Phase I/II clinical trial testing crizotinib in patients with relapsed pediatric solid tumors and anaplastic large cell lymphoma (ALCL) (www.clinicaltrials.gov, Identifier:

NCT00939770). Toxicity has remained low, and seven patients with ALCL and two patients with neuroblastoma have had complete responses as the trial continues (Mosse YP, 2013). This is a hallmark example of how identifying genetic susceptibility can be quickly advanced for clinical benefit.

However, there are some families that do not show mutations in *ALK* or *PHOX2B*, thus the search for additional familial neuroblastoma gene continues. Whole exome analysis of one family with two affected cousins and two healthy members showed a mutation in *GALNT14* predicted to be functionally damaging, but continued efforts are necessary to further define this familial variant (De Mariano M, 2015). In parallel, germline mutations in *TP53*, *SDHB*, *PTPN11*, *APC*, and *NF1* have been reported to occur rarely in neuroblastoma patients ([Figure 1](#)) (Birch JM, 2001; Hasle H, 2009; Mutesa L, 2008; Chantrain CF, 2007; Schimke RN, 2010; Cascon A, 2008; Vandepoele K, 2008; Zhang J, 2015). Neuroblastoma has also been reported to arise in complex congenital malformation syndromes, such as the subtelomeric 1p36.3 or 11q23 deletions (Isidor B, 2008; Mosse Y, 2003). The heritability of neuroblastoma remains only partially understood, yet continued investigation is expected to reveal new insights into familial neuroblastoma predisposition, including gene-gene and gene-environment interactions.

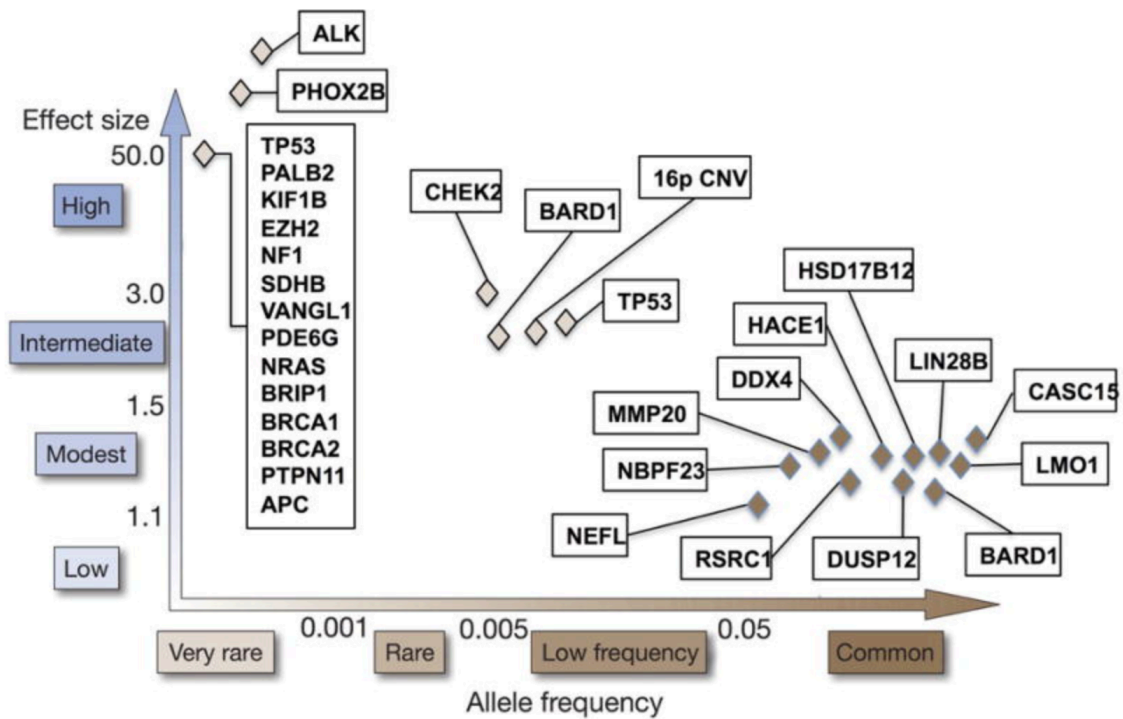


Figure 1: Graphical representation of genetic predisposition to neuroblastoma. Known familial and sporadic predisposition genes have been compiled into one summary figure across multiple studies. The familial mutations are shown in the top left of the graph representing a very rare allele frequency and high effect size. GWAS-discovered variations are in the bottom right corner representing a higher allele frequency with a lower effect size. Continued sequencing efforts are likely to uncover additional rare susceptibility variants along this spectrum, of which dozens are predicted to be discovered to explain the heritability of neuroblastoma.

Genetic susceptibility to familial neuroblastoma

In familial neuroblastoma, there are rare mutations that lead to a high probability of disease. For the 99% of cases that occur sporadically, a common variant hypothesis proposes that common germline variations influence the probability of disease occurrence, each with a low relative risk, but presumably acting in concert. A large GWAS consisting of 720 neuroblastoma cases and 2,128 controls was undertaken in neuroblastoma as an unbiased method for discovering these polymorphisms ([Figure 2](#)) (Diskin SJ, 2012). This original GWAS has been expanded and replicated as additional patient samples have been accrued, leading to the identification of DNA alleles significantly associated with high-risk and low-risk neuroblastoma predisposition, including *CASC15*, *BARD1*, *LMO1*, *LIN28B*, *HACE1*, *DUSP12*, *DDX4*, *IL31RA*, *HSD17B12*, *NEFL*, *TP53*, AND *NBPF23* ([Table 1](#)) (Maris JM, 2008; Pandey GK, 2014; Bosse KR, 2012; Wang K, 2011; Oldridge DA, 2015; Diskin SJ, 2012; Capasso M, 2014; Nguyen le B, 2011; Diskin SJ, 2009; Gamazon ER, 2013). The discovery of these susceptibility loci demonstrates the utility of interrogating GWAS signals for clues into the underlying biology driving neuroblastoma genesis.

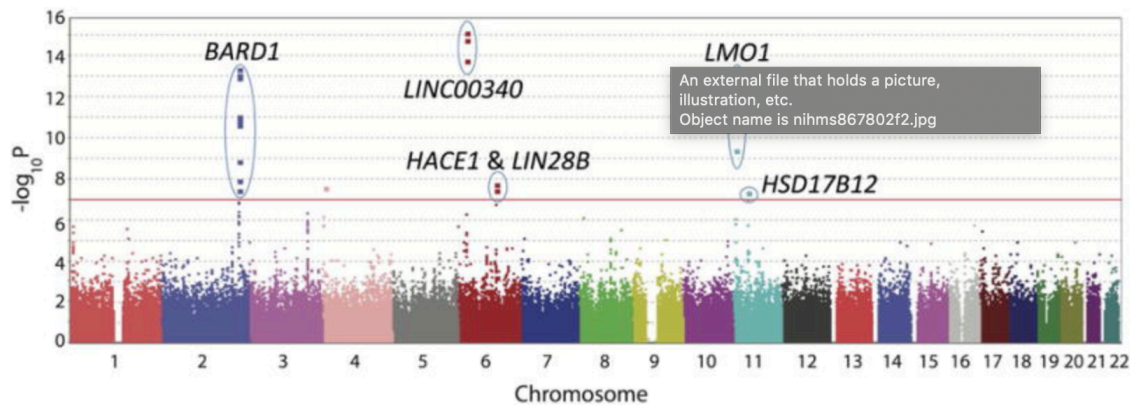


Figure 2. Manhattan plot of high-risk neuroblastoma GWAS results across multiple studies. Level of significance ($-\log_{10}$ transformed p values) for each SNP along the genome in chromosomal order is plotted, and the corresponding genes are labeled. Red line: genome-wide significance threshold based on Bonferroni adjustment. Adapted from Diskin, et al. 2012.

Results from the initial GWAS identified three SNPs at chromosome 6p22 within a newly identified long noncoding RNA (lncRNA) annotated as *CASC15* (Maris JM, 2008). Homozygosity for the risk alleles was significantly associated with metastatic disease, amplification of *MYCN* oncogene in the tumors, and patient relapse. Recently, decreased expression of the truncated isoform *CASC15-S* was associated with more advanced disease (Russell MR, 2015). Another lncRNA, *NBAT-1* (*CASC14*), was shown to be located at the 6p22 susceptibility locus as well, and functional studies have shown that loss of *NBAT-1* promotes proliferation and invasion (Pandey GK, 2014). Subsequently, a GWAS

restricted to high-risk neuroblastoma identified the BRCA-associated ring domain-1 gene (*BARD1*) at chromosome 2q35 was identified as a susceptibility locus (Capasso M, 2009). Six SNPs were discovered in three different N-terminal introns of this gene. *BARD1*, along with its binding partner, breast cancer 1, early onset (*BRCA1*), had been previously implicated in breast and other cancers, but genetic variants in *BARD1* had not been shown to lead to cancer susceptibility, even in breast cancer (Wu LC, 1996; Irminger-Finger I, 2006; Hosking FJ, 2011). Continuing efforts in *BARD1* have found that an isoform, BARD1 β , which lacks the RING domain necessary for BRCA1 binding, is preferentially expressed in neuroblastoma cell lines that are homozygous for the risk alleles (Bosse KR, 2012). Consistent with oncogenic behavior, knockdown of this isoform inhibits cell growth, while overexpression leads to increased proliferation. Additionally, BARD1 β was found to stabilize the Aurora family of kinases in neuroblastoma cell lines, suggesting a possible mechanism of action and potential therapeutic strategy as Aurora kinase inhibitors are in clinical development for cancer (Bosse KR, 2012; Ryser S, 2009).

This GWAS was expanded (2,251 neuroblastoma cases and 6,097 controls) and the gene *LMO1* was shown to be significantly associated with high-risk neuroblastoma, which had previously been implicated in human cancer, but not neuroblastoma. Four SNPs that were significantly associated with neuroblastoma at chromosome 11p15.4 were within the LIM domain only 1 (*LMO1*) gene (Wang K, 2011). This gene, along with *LMO2*, *LMO3* and *LMO4*, encodes a

cysteine-rich transcriptional cofactor that is preferentially expressed in the nervous system (Su AI, 2004). This family of genes has been found to be critically involved in leukemia (reviewed in Curtis DJ, 2010) and breast cancers (Sum EY, 2002; Visvader JE, 2011; Montanez-Wiscovich ME, 2009), while *LMO3* has been shown to be oncogenic in neuroblastoma through its interaction with a neuronal-restricted transcription factor (Aoyama M, 2005). These common variations in *LMO1* were found to be associated with high-risk disease and decreased survival (Wang K, 2011). Neuroblastoma tumors with *LMO1* risk alleles were found to have increased expression of *LMO1*, and depletion of *LMO1* in cell lines decreased growth while forced over-expression increased growth (Wang K, 2011). This is consistent with a gain-of-function role in tumor progression. Recent investigation showed that the causal SNP resides in a super enhancer element within the first intron, with the G>A transversion ablating a canonical GATA transcription factor binding site (Oldridge DA, 2015). Investigators showed that the A allele was “protective”, as there was no GATA binding, and not cis-mediated *LMO1* transcription, providing one of the first clear mechanistic insights into a genetic association.

By further expanding this GWAS to 2,817 neuroblastoma cases and 7,473 controls, two new association signals emerged at 6q16 in two different genes, *HACE1* and *LIN28B* (Diskin SJ, 2012). *HACE1* encodes an E3 ubiquitin ligase and has been identified as a tumor suppressor gene silenced in Wilms’ tumors, colorectal cancer, and gastric carcinoma (Anglesio MS, 2004; Hibi K, 2008; Sakata M, 2009). It has also been shown to suppress cell growth in human

cancer cells, including a neuroblastoma cell line, by inhibiting cell cycle progression during stress (Zhang L, 2007). *LIN28B*, a known oncogene, encodes an RNA-binding protein that is developmentally regulated and blocks the expression of the let-7 family of microRNAs (Piskounova E, 2011). High expression of *LIN28B* and correlated low levels of let-7 have been observed in many human cancers (Iliopoulos D, 2009; Vixwanathan SR, 2009). *LIN28B* and let-7 are involved in stem cell differentiation, as overexpressing the former or inhibiting the latter leads to the reprogramming of human and mouse fibroblasts into pluripotent stem cells (Melton C, 2010; Yu J, 2007). In the GWAS, *LIN28B* was expressed at significantly higher levels in neuroblastoma cell lines homozygous for the risk allele, and this correlated with lower levels of let-7 and growth inhibition following knockdown of *LIN28B* (Diskin SJ, 2012). In tumor samples, *HACE1* expression was significantly lower and *LIN28B* significantly higher in high-risk neuroblastomas and were correlated similarly with worse overall survival. Mechanistic studies have shown that *LIN28B* promotes increased expression of the oncogenic protein RAN, which both converge on Aurora Kinase A (Schnepp RW, 2015). Increased activity was shown to drive tumorigenesis, providing further evidence that targeting Aurora kinases may provide a benefit to neuroblastoma patients (Carol H, 2011; Mosse YP, 2012).

In an integrated proteomic-GWAS approach, Capasso identified three SNPs significantly associated with neuroblastoma in the *NEFL* gene, encoding the light chain neurofilament protein in which mutations are known in disorders of the

peripheral nervous system (Capasso M, 2014). Overexpression of *NEFL* in cells with a protective allele caused cells to adopt a more differentiated phenotype and to have reduced proliferative capacity. The authors suggested that decreased expression of *NEFL* alters the differentiation state of sympathetic neurons and may predispose neuroblastoma (Capasso M, 2014).

After enriching the GWAS for patients with low-risk neuroblastoma, SNPs in four genes, *DUSP12*, *DDX4*, *IL31RA* and *HSD17B12*, were discovered to be significantly associated with this phenotypic subset (Nguyen le B, 2011). These genes are different than those found in high-risk neuroblastoma, suggesting these subtypes are likely genetically distinct and emphasizing the importance of robust phenotypic information in GWAS efforts. These data further support the notion that widely divergent neuroblastoma phenotypes are genetically predetermined.

A genome wide SNP scan for copy number variation (CNV) identified a novel CNV at 1q21.1 that is associated with neuroblastoma, and they were able to confirm deletions in this region by quantitative PCR and FISH (Diskin SJ, 2009). A new neuroblastoma breakpoint family gene, *NBPF23*, was identified at this location by a transcript that was similar to other genes in the family. This transcript is most commonly expressed in fetal brain and sympathetic nervous system tissues, and in neuroblastoma, its expression was correlated with this CNV. *NBPF1* was identified originally at the translocation breakpoint in the germline of a child with neuroblastoma (Vandepoele K, 2008), and research continues to elucidate the role of this family of genes in disease development.

The prevalence of GWAS-associated genes has been further interrogated among different ethnic groups. A follow up study to the previously described *BARD1* GWAS was carried out in African American children with neuroblastoma looking at SNPs in the gene regions identified by the GWAS in Caucasians (Latorre V, 2012). Two of the six SNPs found in *BARD1* were also significantly associated with neuroblastoma in the African-American cohort, validating the original GWAS. Due to different patterns of linkage disequilibrium in the two ethnicities, this effort narrowed the potential location of the causal variant. Another study in patients of African descent identified an allele in a new gene, sperm associated antigen 16 (*SPAG16*), associated with high-risk neuroblastoma in patients of both African and European ancestry showing the potential of discovering new associations by studying specific ethnic groups (Gamazon ER, 2013).

In the Oldridge manuscript noted above defining a mechanistic basis for the LMO1 association, the protective T-allele was noted to be common in people of European ancestry, but is largely absent in African and African-American populations, which retain the G-allele (Capasso M, 2014). This may provide a partial explanation for the more aggressive forms of neuroblastoma observed in African-American patients. Altogether, these results indicate that ethnic background may play a role in genetic predisposition and that therapeutic approaches may require requisite tailoring.

Collectively, these GWAS-discovered genes account for only a small portion of neuroblastoma heritability, which remains poorly understood. It is likely that further expansion of GWAS efforts will continue to uncover more susceptibility genes that will confer risk in an additive manner. No epistasis was found when the most significant SNPs from 2q35, 6p22, 11p15.4 and 1q21.1 CNV were studied together (Wang K, 2011); however, specific clusters of combinations of these SNPs were significantly associated with neuroblastoma (Capasso M, 2014). Mechanistic insights are being discovered, but the underlying basis for most statistical associations remain unknown. Neuroblastoma GWASs were expected to discover genes that affect development of the sympathetic nervous system, showing that common variants can lead to missteps in development and therefore malignancies. Investigators are pursuing ongoing studies to model GWAS variants and heritability in zebrafish and induced pluripotent stem cell models to understand the biological consequences in neuroblastoma and investigate potential therapeutic interventions.

Rare Variants

There are currently two main groups of germline DNA variations that predispose to neuroblastoma: very rare genetic mutations leading to Mendelian inheritance of familial neuroblastoma with a high penetrance, and common variations that only increase risk of disease in small increments. These discoveries thus far have only explained a small proportion of the heritability of neuroblastoma.

While further expansion of the GWAS will continue to uncover more common variants and genes important in the development of neuroblastoma, we suggest that these discoveries lie on a spectrum with the middle ground only beginning to be realized ([Figure 1](#)). These are rare germline variations or mutations with a lower penetrance than familial disease but with a larger effect on predisposition than the common SNPs. Owing to their rarity and the relatively small number of patients with neuroblastoma, it has been difficult to identify these rare variants. Recently, two rare germline variants in *TP53* were found to be robustly associated with neuroblastoma using the 1000 Genomes Project (The 1000 Genomes Project Consortium, 2010) and an advanced imputation process elucidating associations with SNPs not directly assayed on the limited arrays (Diskin SJ, 2014). Likewise, germline sequencing has identified putative damaging mutations in *ALK*, *CHEK2*, *PINK1*, *BARD1* and *APC1* in small percentages of patients with neuroblastoma (Zhang J, 2015; Pugh TJ, 2013). As sequencing technology improves and costs decrease, discoveries of additional rare variants are on the horizon to define and characterize further the heritability of neuroblastoma. The influence of germline mosaicism and epistatic interaction of de novo or inherited mutations with GWAS-defined polymorphisms remains undefined.

Summary and Future Directions

Significant progress has been made in the last six years in describing the genetic landscape of neuroblastoma and continuing studies will aim to further

identify Mendelian susceptibility genes. This is already influencing clinical care as genetic testing is available, and there are noninvasive screening methods to surveil for disease in young children. Current recommendations suggest that children with a known damaging germline mutation in *ALK* or *PHOX2B* based on familial pedigrees should undergo surveillance with every 3-month ultrasonography and urinary catecholamines until a minimum of age 5, if not beyond (Laug WE, 1978). The main impact of GWAS studies to date is in identifying genes critical to neuroblastoma progression and maintenance, thus uncovering potential oncogenic vulnerabilities. With the discovery of *ALK* as an example, it is important that translational approaches related to these genes be prioritized, as additional targeted therapies for patients with neuroblastoma are essential to improving survival. Future work to extend the discovery of germline polymorphisms to those that influence response to therapy and impact co-morbidities such as hearing loss also has the potential to improve patient survival and quality of life. The ultimate goal of genomic studies in neuroblastoma is to inform precision medicine with genetic evaluations to tailor clinical treatments and extend survival (Schnepp RW, 2015; De Mariano M, 2015). As additional patient samples are accrued over time, future GWAS endeavors will be required to continue the discovery of additional susceptibility alleles. Extensive further investigation, both computationally and in designing better models for these rare genetically defined subsets, will be required to translate these genomic discoveries into actionable targets for diagnosis and treatment.

Acknowledgements

This work was supported by the Institutional Clinical and Translational Science Award, grant number TL1 RR024133, and John Maris' grant R01 CA124709: The Genetic Basis of Neuroblastoma Tumorigenesis.

Grant support: This work was supported by the Institutional Clinical and Translational Science Award, grant number TL1 RR024133, and John Maris' grant R01 CA124709: The Genetic Basis of Neuroblastoma Tumorigenesis.

References

1. Howlader N, Noone A, Krapcho M, Neyman N, Aminou R, Waldron W, Altekruse S, Kosary C, Ruhl J, Tatalovich Z, et al. SEER Cancer Statistics Review 1975–2008 based on November 2010 SEER data submission. National Cancer Institute; Bethesda MD: 2011.
2. London WB, Castleberry RP, Matthay KK, Look AT, Seeger RC, Shimada H, Thorner P, Brodeur G, Maris JM, Reynolds CP, et al. Evidence for an age cutoff greater than 365 days for neuroblastoma risk group stratification in the Children's Oncology Group. *Journal of clinical oncology: official journal of the American Society of Clinical Oncology*. 2005;23:6459–6465.
3. Hoehner JC, Gestblom C, Hedborg F, Sandstedt B, Olsen L, Pahlman S. A developmental model of neuroblastoma: differentiating stroma-poor tumors' progress along an extra-adrenal chromaffin lineage. *Lab Invest*. 1996;75:659–675.
4. Maris JM, Hogarty MD, Bagatell R, Cohn SL. Neuroblastoma. *Lancet*. 2007;369:2106–2120.
5. Carlsen NL. The new International Neuroblastoma Staging System: some critical notes. *Journal of clinical oncology: official journal of the American Society of Clinical Oncology*. 1990;8:935–936.
6. Cole WH, Everson TC. Spontaneous regression of cancer: preliminary report. *Ann Surg*. 1956;144:366–383.

7. Yamamoto K, Hanada R, Kikuchi A, Ichikawa M, Aihara T, Oguma E, Moritani T, Shimanuki Y, Tanimura M, Hayashi Y. Spontaneous regression of localized neuroblastoma detected by mass screening. *Journal of clinical oncology: official journal of the American Society of Clinical Oncology*. 1998;16:1265–1269.
8. Hero B, Simon T, Spitz R, Ernestus K, Gnekow AK, Scheel-Walter HG, Schwabe D, Schilling FH, Benz-Bohm G, Berthold F. Localized infant neuroblastomas often show spontaneous regression: results of the prospective trials NB95-S and NB97. *Journal of clinical oncology: official journal of the American Society of Clinical Oncology*. 2008;26:1504–1510.
9. Oberthuer A, Juraeva D, Hero B, Volland R, Sterz C, Schmidt R, Faldum A, Kahlert Y, Engesser A, Asgharzadeh S, et al. Revised risk estimation and treatment stratification of low- and intermediate-risk neuroblastoma patients by integrating clinical and molecular prognostic markers. *Clin Cancer Res*. 2015;21:1904–1915. *Event free survival and overall survival of low- and intermediate-risk neuroblastoma patients were stratified and utilized to propose revised courses of treatment based on risk group.
10. Maris JM. Recent advances in neuroblastoma. *The New England Journal of Medicine*. 2010;362:2202–2211.
11. Schwab M, Alitalo K, Klempnauer KH, Varmus HE, Bishop JM, Gilbert F, Brodeur G, Goldstein M, Trent J. Amplified DNA with limited homology to

myc cellular oncogene is shared by human neuroblastoma cell lines and a neuroblastoma tumour. *Nature*. 1983;305:245–248.

12. Brodeur GM, Seeger RC, Schwab M, Varmus HE, Bishop JM. Amplification of N-myc in untreated human neuroblastomas correlates with advanced disease stage. *Science*. 1984;224:1121–1124.
13. Seeger RC, Brodeur GM, Sather H, Dalton A, Siegel SE, Wong KY, Hammond D. Association of multiple copies of the N-myc oncogene with rapid progression of neuroblastomas. *New England Journal of Medicine*. 1985;313:1111–1116.
14. Brodeur GM, Pritchard J, Berthold F, Carlsen NL, Castel V, Castelberry RP, De Bernardi B, Evans AE, Favrot M, Hedborg F, et al. Revisions of the international criteria for neuroblastoma diagnosis staging and response to treatment. *Journal of clinical oncology: official journal of the American Society of Clinical Oncology*. 1993;11:1466–1477.
15. Cohn SL, Pearson AD, London WB, Monclair T, Ambros PF, Brodeur GM, Faldum A, Hero B, Iehara T, Machin D, et al. The International Neuroblastoma Risk Group (INRG) classification system: an INRG Task Force report. *Journal of clinical oncology: official journal of the American Society of Clinical Oncology*. 2009;27:289–297.
16. Cecchetto G, Mosseri V, De Bernardi B, Helardot P, Monclair T, Costa E, Horcher E, Neuenschwander S, Toma P, Rizzo A, et al. Surgical risk factors in primary surgery for localized neuroblastoma: the LNESG1 study of the

- European International Society of Pediatric Oncology Neuroblastoma Group. Journal of clinical oncology: official journal of the American Society of Clinical Oncology. 2005;23:8483–8489.
17. Monclair T, Brodeur GM, Ambros PF, Brisse HJ, Cecchetto G, Holmes K, Kaneko M, London WB, Matthay KK, Nuchtern JG, et al. The International Neuroblastoma Risk Group (INRG) staging system: an INRG Task Force report. Journal of clinical oncology: official journal of the American Society of Clinical Oncology. 2009;27:298–303.
 18. Deyell RJ, Attiyeh EF. Advances in the understanding of constitutional and somatic genomic alterations in neuroblastoma. Cancer Genet. 2011;204:113–121.
 19. Hirschhorn JN, Daly MJ. Genome-wide association studies for common diseases and complex traits. Nat Rev Genet. 2005;6:95–108.
 20. Tonini GP, Nakagawara A, Berthold F. Towards a turning point of neuroblastoma therapy. Cancer Lett. 2012;326:128–134.
 21. Knudson AG, Jr, Strong LC. Mutation and cancer: neuroblastoma and pheochromocytoma. Am J Hum Genet. 1972;24:514–532.
 22. Kushner BH, Gilbert F, Helson L. Familial neuroblastoma. Case reports *literature review* and etiologic considerations. Cancer. 1986;57:1887–1893.
 23. Dodge HJ. BM: Neuroblastoma of the adrenal medulla in siblings. Rocky Mt Med. 1945;42:35–38.

24. Chompret A, dVF, Brugieres L, Abel A, Raquin MA, Hartmann O, et al. Excess of cancers in relatives of patients with neuroblastoma. *Med Pediatr Oncol.* 1998;31:211.
25. Mosse YP, Laudenslager M, Longo L, Cole KA, Wood A, Attiyeh EF, Laquaglia MJ, Sennett R, Lynch JE, Perri P, et al. Identification of ALK as a major familial neuroblastoma predisposition gene. *Nature.* 2008;455:930–935.
26. Hardy PC, Nesbit ME., Jr Familial neuroblastoma: report of a kindred with a high incidence of infantile tumors. *The Journal of pediatrics.* 1972;80:74–77.
27. Gerson JM, Chatten J, Eisman S. Letter: Familial neuroblastoma: a follow-up. *N Engl J Med.* 1974(290):1487.
28. Wong KY, Hanenson IB, Lampkin BC. Familial neuroblastoma. *Am J Dis Child.* 1971;121:415–416.
29. Bergstrom JF, Long JM. Familial occurrence of ganglioneuromas. *Tex Med.* 1974;70:62–65.
30. Brodeur GM. Neuroblastoma: biological insights into a clinical enigma. *Nature reviews Cancer.* 2003;3:203–216.
31. Bolande RP. Neurocristopathy: its growth and development in 20 years. *Pediatr Pathol Lab Med.* 1997;17:1–25.
32. Bower RJ, Adkins JC. Ondine's curse and neurocristopathy. *Clinical pediatrics.* 1980;19:665–668.

33. Michna BA, McWilliams NB, Krummel TM, Hartenberg MA, Salzberg AM. Multifocal ganglioneuroblastoma coexistent with total colonic aganglionosis. *J Pediatr Surg.* 1988;23:57–59.
34. Roshkow JE, Haller JO, Berdon WE, Sane SM. Hirschsprung's disease, Ondine's curse, and neuroblastoma—manifestations of neurocristopathy. *Pediatr Radiol.* 1988;19:45–49.
35. Stovroff M, Dykes F, Teague WG. The complete spectrum of neurocristopathy in an infant with congenital hypoventilation, Hirschsprung's disease, and neuroblastoma. *J Pediatr Surg.* 1995;30:1218–1221.
36. Amiel J, Laudier B, Attie-Bitach T, Trang H, de Pontual L, Gener B, Trochet D, Etchevers H, Ray P, Simonneau M, et al. Polyalanine expansion and frameshift mutations of the paired-like homeobox gene PHOX2B in congenital central hypoventilation syndrome. *Nature genetics.* 2003;33:459–461.
37. Weese-Mayer DE, Berry-Kravis EM, Zhou L, Maher BS, Silvestri JM, Curran ME, Marazita ML. Idiopathic congenital central hypoventilation syndrome: analysis of genes pertinent to early autonomic nervous system embryologic development and identification of mutations in PHOX2b. *Am J Med Genet A.* 2003;123A:267–278.
38. Trochet D, Bourdeaut F, Janoueix-Lerosey I, Deville A, de Pontual L, Schleiermacher G, Coze C, Philip N, Frebourg T, Munnich A, et al. Germline

- mutations of the paired-like homeobox 2B (PHOX2B) gene in neuroblastoma. *Am J Hum Genet.* 2004;74:761–764.
39. Mosse YP, Laudenslager M, Khazi D, Carlisle AJ, Winter CL, Rappaport E, Maris JM. Germline PHOX2B mutation in hereditary neuroblastoma. *Am J Hum Genet.* 2004;75:727–730.
 40. Heide S, Masliah-Planchon J, Isidor B, Guimier A, Bodet D, Coze C, Deville A, Thebault E, Pasquier CJ, Cassagnau E, et al. Oncologic Phenotype of Peripheral Neuroblastic Tumors Associated With PHOX2B Non-Polyalanine Repeat Expansion Mutations. *Pediatr Blood Cancer.* 2016;63:71–77. *This study identified four patients with poorly differentiated neuroblastomas with PHOX2B NPARM, indicating that this predisposition can be associated with more aggressive cancer phenotypes.
 41. Nagashimada M, Ohta H, Li C, Nakao K, Uesaka T, Brunet JF, Amiel J, Trochet D, Wakayama T, Enomoto H. Autonomic neurocristopathy-associated mutations in PHOX2B dysregulate Sox10 expression. *J Clin Invest.* 2012;122:3145–3158.
 42. Osajima-Hakomori Y, Miyake I, Ohira M, Nakagawara A, Nakagawa A, Sakai R. Biological role of anaplastic lymphoma kinase in neuroblastoma. *Am J Pathol.* 2005;167:213–222.
 43. George RE, Attiyeh EF, Li S, Moreau LA, Neuberg D, Li C, Fox EA, Meyerson M, Diller L, Fortina P, et al. Genome-wide analysis of

- neuroblastomas using high-density single nucleotide polymorphism arrays. *PLoS One*. 2007;2:e255.
44. Griffin CA, Hawkins AL, Dvorak C, Henkle C, Ellingham T, Perlman EJ. Recurrent involvement of 2p23 in inflammatory myofibroblastic tumors. *Cancer Res*. 1999;59:2776–2780.
 45. Jazii FR, Najafi Z, Malekzadeh R, Conrads TP, Ziaee AA, Abnet C, Yazdznbod M, Karkhane AA, Salekdeh GH. Identification of squamous cell carcinoma associated proteins by proteomics and loss of beta tropomyosin expression in esophageal cancer. *World J Gastroenterol*. 2006;12:7104–7112.
 46. Morris SW, Kirstein MN, Valentine MB, Dittmer KG, Shapiro DN, Saltman DL, Look AT. Fusion of a kinase gene, ALK, to a nucleolar protein gene, NPM, in non-Hodgkin's lymphoma. *Science*. 1994;263:1281–1284.
 47. Rikova K, Guo A, Zeng Q, Possemato A, Yu J, Haack H, Nardone J, Lee K, Reeves C, Li Y, et al. Global survey of phosphotyrosine signaling identifies oncogenic kinases in lung cancer. *Cell*. 2007;131:1190–1203.
 48. Soda M, Choi YL, Enomoto M, Takada S, Yamashita Y, Ishikawa S, Fujiwara S, Watanabe H, Kurashina K, Hatanaka H, et al. Identification of the transforming EML4-ALK fusion gene in non-small-cell lung cancer. *Nature*. 2007;448:561–566.
 49. Inamura K, Takeuchi K, Togashi Y, Nomura K, Ninomiya H, Okui M, Satoh Y, Okumura S, Nakagawa K, Soda M, et al. EML4-ALK fusion is linked to

- histological characteristics in a subset of lung cancers. *J Thorac Oncol.* 2008;3:13–17.
50. Wang YW, Tu PH, Lin KT, Lin SC, Ko JY, Jou YS. Identification of oncogenic point mutations and hyperphosphorylation of anaplastic lymphoma kinase in lung cancer. *Neoplasia.* 2011;13:704–715.
 51. Murugan AK, Xing M. Anaplastic thyroid cancers harbor novel oncogenic mutations of the ALK gene. *Cancer Res.* 2011;71:4403–4411.
 52. Janoueix-Lerosey I, Lequin D, Brugieres L, Ribeiro A, de Pontual L, Combaret V, Raynal V, Puisieux A, Schleiermacher G, Pierron G, et al. Somatic and germline activating mutations of the ALK kinase receptor in neuroblastoma. *Nature.* 2008;455:967–970.
 53. George RE, Sanda T, Hanna M, Frohling S, Luther W, 2nd, Zhang J, Ahn Y, Zhou W, London WB, McGrady P, et al. Activating mutations in ALK provide a therapeutic target in neuroblastoma. *Nature.* 2008;455:975–978.
 54. Chen Y, Takita J, Choi YL, Kato M, Ohira M, Sanada M, Wang L, Soda M, Kikuchi A, Igarashi T, et al. Oncogenic mutations of ALK kinase in neuroblastoma. *Nature.* 2008;455:971–974.
 55. Bresler SC, Weiser DA, Huwe PJ, Park JH, Krytska K, Ryles H, Laudenslager M, Rappaport EF, Wood AC, McGrady PW, et al. ALK mutations confer differential oncogenic activation and sensitivity to ALK inhibition therapy in neuroblastoma. *Cancer Cell.* 2014;26:682–694. *Analyses of ALK mutations in over 1,500 neuroblastoma tumor

samples characterized oncogenic and passenger mutations using biochemical assays and computational prediction studies. Crizotinib sensitivity varied among the ALK mutant variants suggesting differential clinical outcomes based on ALK genomic status.

56. Bresler SC, Wood AC, Haglund EA, Courtright J, Belcastro LT, Plegaria JS, Cole K, Toporovskaya Y, Zhao H, Carpenter EL, et al. Differential inhibitor sensitivity of anaplastic lymphoma kinase variants found in neuroblastoma. *Sci Transl Med*. 2011;3:108ra114.
57. de Pontual L, Kettaneh D, Gordon CT, Oufadem M, Boddaert N, Lees M, Balu L, Lachassinne E, Petros A, Mollet J, et al. Germline gain-of-function mutations of ALK disrupt central nervous system development. *Hum Mutat*. 2011;32:272–276.
58. Schonherr C, Ruuth K, Yamazaki Y, Eriksson T, Christensen J, Palmer RH, Hallberg B. Activating ALK mutations found in neuroblastoma are inhibited by Crizotinib and NVP-TAE684. *Biochem J*. 2011;440:405–413.
59. Heuckmann JM, Holzel M, Sos ML, Heynck S, Balke-Want H, Koker M, Peifer M, Weiss J, Lovly CM, Grutter C, et al. ALK mutations conferring differential resistance to structurally diverse ALK inhibitors. *Clin Cancer Res*. 2011;17:7394–7401.
60. Carpenter EL, Mosse YP. Targeting ALK in neuroblastoma—preclinical and clinical advancements. *Nat Rev Clin Oncol*. 2012;9:391–399.

61. Mosse YP, Lim MS, Voss SD, Wilner K, Ruffner K, Laliberte J, Rolland D, Balis FM, Maris JM, Weigel BJ, et al. Safety and activity of crizotinib for paediatric patients with refractory solid tumours or anaplastic large-cell lymphoma: a Children's Oncology Group phase 1 consortium study. *Lancet Oncol.* 2013;14:472–480.
62. Birch JM, Alston RD, McNally RJ, Evans DG, Kelsey AM, Harris M, Eden OB, Varley JM. Relative frequency and morphology of cancers in carriers of germline TP53 mutations. *Oncogene.* 2001;20:4621–4628.
63. Hasle H. Malignant diseases in Noonan syndrome and related disorders. *Horm Res.* 2009;72(Suppl 2):8–14.
64. Mutesa L, Pierquin G, Janin N, Segers K, Thomee C, Provenzi M, Bours V. Germline PTPN11 missense mutation in a case of Noonan syndrome associated with mediastinal and retroperitoneal neuroblastic tumors. *Cancer Genet Cytogenet.* 2008;182:40–42.
65. Chantrain CF, Jijon P, De Raedt T, Vermylen C, Poirel HA, Legius E, Brichard B. Therapy-related acute myeloid leukemia in a child with Noonan syndrome and clonal duplication of the germline PTPN11 mutation. *Pediatr Blood Cancer.* 2007;48:101–104.
66. Schimke RN, Collins DL, Stolle CA. Paraganglioma, neuroblastoma, and a SDHB mutation: Resolution of a 30-year-old mystery. *Am J Med Genet A.* 2010;152A:1531–1535.

67. Cascon A, Landa I, Lopez-Jimenez E, Diez-Hernandez A, Buchta M, Montero-Conde C, Leskela S, Leandro-Garcia LJ, Leton R, Rodriguez-Antona C, et al. Molecular characterisation of a common SDHB deletion in paraganglioma patients. *J Med Genet.* 2008;45:233–238.
68. Vandepoele K, Andries V, Van Roy N, Staes K, Vandesompele J, Laureys G, De Smet E, Berx G, Speleman F, van Roy F. A constitutional translocation t(1;17)(p36.2;q11.2) in a neuroblastoma patient disrupts the human NBPF1 and ACCN1 genes. *PLoS One.* 2008;3:e2207.
69. Zhang J, Walsh MF, Wu G, Edmonson MN, Gruber TA, Easton J, Hedges D, Ma X, Zhou X, Yergeau DA, et al. Germline Mutations in Predisposition Genes in Pediatric Cancer. *N Engl J Med.* 2015;373:2336–2346. *This next-generation sequencing effort identified a new association of germline APC and SDHB mutations in neuroblastoma.
70. Isidor B, Le Cunff M, Boceno M, Boisseau P, Thomas C, Rival JM, David A, Le Caignec C. Complex constitutional subtelomeric 1p36.3 deletion/duplication in a mentally retarded child with neonatal neuroblastoma. *Eur J Med Genet.* 2008;51:679–684.
71. Mosse Y, Greshock J, King A, Khazi D, Weber BL, Maris JM. Identification and high-resolution mapping of a constitutional 11q deletion in an infant with multifocal neuroblastoma. *Lancet Oncol.* 2003;4:769–771.
72. Maris JM, Mosse YP, Bradfield JP, Hou C, Monni S, Scott RH, Asgharzadeh S, Attiyeh EF, Diskin SJ, Laudenslager M, et al. Chromosome 6p22 locus

associated with clinically aggressive neuroblastoma. *N Engl J Med.* 2008;358:2585–2593.

73. Russell MR, Penikis A, Oldridge DA, Alvarez-Dominguez JR, McDaniel L, Diamond M, Padovan O, Raman P, Li Y, Wei JS, et al. CASC15-S Is a Tumor Suppressor lncRNA at the 6p22 Neuroblastoma Susceptibility Locus. *Cancer Res.* 2015;75:3155–3166. *This study identified CASC15 as the tumor suppressor lncRNA located at a known susceptibility locus on chromosome 6p22 and showed that reduced expression of the shortened form, CASC15-S, increased cellular migration and was associated with poor patient outcome.
74. Pandey GK. The Risk-Associated Long Noncoding RNA NBAT-1 Controls Neuroblastoma Progression by Regulating Cell Proliferation and Neuronal Differentiation. *Cancer Cell.* 2014 *Differential expression of NBAT-1, a lncRNA located at the 6p22 susceptibility locus, was identified as a predictive biomarker of patient outcome in neuroblastoma. Decrease or loss of NBAT-1 conferred increased proliferative and invasive properties in vitro via epigenetic silencing.
75. Capasso M, Devoto M, Hou C, Asgharzadeh S, Glessner JT, Attiyeh EF, Mosse YP, Kim C, Diskin SJ, Cole KA, et al. Common variations in BARD1 influence susceptibility to high-risk neuroblastoma. *Nat Genet.* 2009;41:718–723.

76. Wu LC, Wang ZW, Tsan JT, Spillman MA, Phung A, Xu XL, Yang MC, Hwang LY, Bowcock AM, Baer R. Identification of a RING protein that can interact in vivo with the BRCA1 gene product. *Nat Genet.* 1996;14:430–440.
77. Irminger-Finger I, Jefford CE. Is there more to BARD1 than BRCA1? *Nat Rev Cancer.* 2006;6:382–391.
78. Hosking FJ, Dobbins SE, Houlston RS. Genome-wide association studies for detecting cancer susceptibility. *Br Med Bull.* 2011;97:27–46.
79. Bosse KR, Diskin SJ, Cole KA, Wood AC, Schnepf RW, Norris G, Nguyen le B, Jagannathan J, Laquaglia M, Winter C, et al. Common variation at BARD1 results in the expression of an oncogenic isoform that influences neuroblastoma susceptibility and oncogenicity. *Cancer Res.* 2012;72:2068–2078.
80. Ryser S, Dizin E, Jefford CE, Delaval B, Gagos S, Christodoulidou A, Krause KH, Birnbaum D, Irminger-Finger I. Distinct roles of BARD1 isoforms in mitosis: full-length BARD1 mediates Aurora B degradation, cancer-associated BARD1beta scaffolds Aurora B and BRCA2. *Cancer Res.* 2009;69:1125–1134.
81. Wang K, Diskin SJ, Zhang H, Attiyeh EF, Winter C, Hou C, Schnepf RW, Diamond M, Bosse K, Mayes PA, et al. Integrative genomics identifies LMO1 as a neuroblastoma oncogene. *Nature.* 2011;469:216–220.

82. Su AI, Wiltshire T, Batalov S, Lapp H, Ching KA, Block D, Zhang J, Soden R, Hayakawa M, Kreiman G, et al. A gene atlas of the mouse and human protein-encoding transcriptomes. *Proc Natl Acad Sci U S A*. 2004;101:6062–6067.
83. Curtis DJ, McCormack MP. The molecular basis of Lmo2-induced T-cell acute lymphoblastic leukemia. *Clin Cancer Res*. 2010;16:5618–5623.
84. Sum EY, Peng B, Yu X, Chen J, Byrne J, Lindeman GJ, Visvader JE. The LIM domain protein LMO4 interacts with the cofactor CtIP and the tumor suppressor BRCA1 and inhibits BRCA1 activity. *J Biol Chem*. 2002;277:7849–7856.
85. Visvader JE, Venter D, Hahm K, Santamaria M, Sum EY, O'Reilly L, White D, Williams R, Armes J, Lindeman GJ. The LIM domain gene LMO4 inhibits differentiation of mammary epithelial cells in vitro and is overexpressed in breast cancer. *Proc Natl Acad Sci U S A*. 2001;98:14452–14457.
86. Montanez-Wiscovich ME, Seachrist DD, Landis MD, Visvader J, Andersen B, Keri RA. LMO4 is an essential mediator of ErbB2/HER2/Neu-induced breast cancer cell cycle progression. *Oncogene*. 2009;28:3608–3618.
87. Aoyama M, Ozaki T, Inuzuka H, Tomotsune D, Hirato J, Okamoto Y, Tokita H, Ohira M, Nakagawara A. LMO3 interacts with neuronal transcription factor, HEN2, and acts as an oncogene in neuroblastoma. *Cancer Res*. 2005;65:4587–4597.

88. Oldridge DA, Wood AC, Weichert-Leahey N, Crimmins I, Sussman R, Winter C, McDaniel LD, Diamond M, Hart LS, Zhu S, et al. Genetic predisposition to neuroblastoma mediated by a LMO1 super-enhancer polymorphism. *Nature*. 2015;528:418–421. **This study identified the G-allele of the GATA binding site for transcription factor GATA3 as a SNP highly associated with neuroblastoma and found more commonly in African and African-American populations. The more recently evolved T-allele (TATA), shown to prevent GATA3 binding in association with decreased LMO1 expression, was found more commonly in European populations.
89. Diskin SJ, Capasso M, Schnepf RW, Cole KA, Attiyeh EF, Hou C, Diamond M, Carpenter EL, Winter C, Lee H, et al. Common variation at 6q16 within HACE1 and LIN28B influences susceptibility to neuroblastoma. *Nat Genet*. 2012;44:1126–1130.
90. Anglesio MS, Evdokimova V, Melnyk N, Zhang L, Fernandez CV, Grundy PE, Leach S, Marra MA, Brooks-Wilson AR, Penninger J, et al. Differential expression of a novel ankyrin containing E3 ubiquitin-protein ligase, Hace1, in sporadic Wilms' tumor versus normal kidney. *Hum Mol Genet*. 2004;13:2061–2074.
91. Hibi K, Sakata M, Sakuraba K, Shirahata A, Goto T, Mizukami H, Saito M, Ishibashi K, Kigawa G, Nemoto H, et al. Aberrant methylation of the HACE1 gene is frequently detected in advanced colorectal cancer. *Anticancer Res*. 2008;28:1581–1584.

92. Sakata M, Kitamura YH, Sakuraba K, Goto T, Mizukami H, Saito M, Ishibashi K, Kigawa G, Nemoto H, Sanada Y, et al. Methylation of HACE1 in gastric carcinoma. *Anticancer Res.* 2009;29:2231–2233.
93. Zhang L, Anglesio MS, O’Sullivan M, Zhang F, Yang G, Sarao R, Mai PN, Cronin S, Hara H, Melnyk N, et al. The E3 ligase HACE1 is a critical chromosome 6q21 tumor suppressor involved in multiple cancers. *Nat Med.* 2007;13:1060–1069.
94. Piskounova E, Polytarchou C, Thornton JE, LaPierre RJ, Pothoulakis C, Hagan JP, Iliopoulos D, Gregory RI. Lin28A and Lin28B inhibit let-7 microRNA biogenesis by distinct mechanisms. *Cell.* 2011;147:1066–1079.
95. Iliopoulos D, Hirsch HA, Struhl K. An epigenetic switch involving NF-kappaB, Lin28, Let-7 MicroRNA, and IL6 links inflammation to cell transformation. *Cell.* 2009;139:693–706.
96. Viswanathan SR, Powers JT, Einhorn W, Hoshida Y, Ng TL, Toffanin S, O’Sullivan M, Lu J, Phillips LA, Lockhart VL, et al. Lin28 promotes transformation and is associated with advanced human malignancies. *Nat Genet.* 2009;41:843–848.
97. Melton C, Judson RL, Blelloch R. Opposing microRNA families regulate self-renewal in mouse embryonic stem cells. *Nature.* 2010;463:621–626.
98. Yu J, Vodyanik MA, Smuga-Otto K, Antosiewicz-Bourget J, Frane JL, Tian S, Nie J, Jonsdottir GA, Ruotti V, Stewart R, et al. Induced pluripotent stem

- cell lines derived from human somatic cells. *Science*. 2007;318:1917–1920.
99. Schnepf RW, Khurana P, Attiyeh EF, Raman P, Chodosh SE, Oldridge DA, Gagliardi ME, Conkrite KL, Asgharzadeh S, Seeger RC, et al. A LIN28B-RAN-AURKA Signaling Network Promotes Neuroblastoma Tumorigenesis. *Cancer Cell*. 2015;28:599–609. **This study identified RAN as a target of the neuroblastoma oncogenic driver LIN28B and characterized the downstream effects of both proteins on increased Aurora Kinase A activity to further drive oncogenesis.
100. Carol H, Boehm I, Reynolds CP, Kang MH, Maris JM, Morton CL, Gorlick R, Kolb EA, Keir ST, Wu J, et al. Efficacy and pharmacokinetic/pharmacodynamic evaluation of the Aurora kinase A inhibitor MLN8237 against preclinical models of pediatric cancer. *Cancer chemotherapy and pharmacology*. 2011;68:1291–1304.
101. Mosse YP, Lipsitz E, Fox E, Teachey DT, Maris JM, Weigel B, Adamson PC, Ingle MA, Ahern CH, Blaney SM. Pediatric Phase I Trial and Pharmacokinetic Study of MLN8237, an Investigational Oral Selective Small-Molecule Inhibitor of Aurora Kinase A: A Children's Oncology Group Phase I Consortium Study. *Clinical Cancer Research*. 2012;18:6058–6064.
102. Capasso M, Diskin S, Cimmino F, Acierno G, Totaro F, Petrosino G, Pezone L, Diamond M, McDaniel L, Hakonarson H, et al. Common genetic variants in NEFL influence gene expression and neuroblastoma risk. *Cancer*

- Res. 2014;74:6913–6924. *GWAS efforts identified three SNPs in the neurofilament gene NEFL shown to associated with neuroblastoma. High levels of NEFL were shown to promote differentiation and limit proliferation and are association with improved overall survival in neuroblastoma.
103. Nguyen le B, Diskin SJ, Capasso M, Wang K, Diamond MA, Glessner J, Kim C, Attiyeh EF, Mosse YP, Cole K, et al. Phenotype restricted genome-wide association study using a gene-centric approach identifies three low-risk neuroblastoma susceptibility Loci. *PLoS Genet.* 2011;7:e1002026.
104. Diskin SJ, Hou C, Glessner JT, Attiyeh EF, Laudenslager M, Bosse K, Cole K, Mosse YP, Wood A, Lynch JE, et al. Copy number variation at 1q21.1 associated with neuroblastoma. *Nature.* 2009;459:987–991.
105. Capasso M, Calabrese FM, Iolascon A, Mellerup E. Combinations of genetic data in a study of neuroblastoma risk genotypes. *Cancer Genet.* 2014;207:94–97. *In this study, combinations of genotypes were investigated for susceptibility between neuroblastoma patients and controls, finding 24 combinations with a significant association to neuroblastoma.
106. Latorre V, Diskin SJ, Diamond MA, Zhang H, Hakonarson H, Maris JM, Devoto M. Replication of neuroblastoma SNP association at the BARD1 locus in African-Americans. *Cancer epidemiology, biomarkers & prevention: a publication of the American Association for Cancer Research, cosponsored by the American Society of Preventive Oncology.* 2012;21:658–663.

107. Gamazon ER, Pinto N, Konkashbaev A, Im HK, Diskin SJ, London WB, Maris JM, Dolan ME, Cox NJ, Cohn SL. Trans-population analysis of genetic mechanisms of ethnic disparities in neuroblastoma survival. *Journal of the National Cancer Institute*. 2013;105:302–309.
108. The 1000 Genomes Project Consortium. A map of human genome variation from population-scale sequencing. *Nature*. 2010;467:1061–1073.
109. Diskin SJ, Capasso M, Diamond M, Oldridge DA, Conkrite K, Bosse KR, Russell MR, Iolascon A, Hakonarson H, Devoto M, et al. Rare variants in TP53 and susceptibility to neuroblastoma. *Journal of the National Cancer Institute*. 2014;106:dju047. *Two rare germline variants in TP53 were discovered to be associated with neuroblastoma, despite the rarity of TP53 mutations in the majority of cases.
110. Pugh TJ, Morozova O, Attiyeh EF, Asgharzadeh S, Wei JS, Auclair D, Carter SL, Cibulskis K, Hanna M, Kiezun A, et al. The genetic landscape of high-risk neuroblastoma. *Nat Genet*. 2013;45:279–284.
111. Laug WE, Siegel SE, Shaw KN, Landing B, Baptista J, Gutenstein M. Initial urinary catecholamine metabolite concentrations and prognosis in neuroblastoma. *Pediatrics*. 1978;62:77–83.
112. Schnepf RW, Bosse KR, Maris JM. Improving patient outcomes with cancer genomics: unique opportunities and challenges in pediatric oncology. *JAMA*. 2015;314:881–883.

113. De Mariano M, Gallesio R, Chierici M, Furlanello C, Conte M, Garaventa A, Croce M, Ferrini S, Tonini GP, Longo L. Identification of GALNT14 as a novel neuroblastoma predisposition gene. *Oncotarget*. 2015;6:26335–26346.

REFERENCES

- Adler JJ, Johnson DE, Heller BL, Bringman LR, Ranahan WP, Conwell MD, *et al*. Serum deprivation inhibits the transcriptional co-activator YAP and cell growth via phosphorylation of the 130-kDa isoform of Angiotensin II type 1 receptor by the

LATS1/2 protein kinases. *Proc Natl Acad Sci U S A* **2013**;110:17368-73.

Al-Lazikani B, Banerji U, Workman P. Combinatorial drug therapy for cancer in the post-genomic era. *Nat Biotechnol* **2012**;30:679-692.

Attiyeh, EF, London, WB, Mossé, YP, Wang, Q, *et al.* Chromosome 1p and 11q deletions and outcomes in neuroblastoma. *N Engl J Med* **2005**;353:2243-53.

Barretina J, Caponigro G, Stransky N, Venkatesan K, Margolin AA, Kim S, *et al.* The cancer cell Line encyclopedia enables predictive modelling of anti-cancer drug sensitivity. *Nature* **2012**; 483: 603-307.

Basso AD, Kirschmeier P, and Bishop WR. Lipid posttranslational modifications. Farnesyl transferase inhibitors. *J Lipid Res* **2006**;47:15-31.

Berndt N, Hamilton AD, and Sefti SM. Targeting protein prenylation for cancer therapy. *Nat Rev Cancer* **2011**;11:775-791.

Bianchi AB, Mitsunaga SI, Cheng JQ, Klein WM, Jhanwar SC, Seizinger B, *et al.* High frequency of inactivating mutations in the neurofibromatosis type 2 gene (NF2) in primary malignant mesotheliomas. *Proc. Natl. Acad. Sci.* **1995**;92:10854–10858.

Brodeur GM, Seeger RC, Schwab M, Varmus HE, Bishop JM. Amplification of N-myc in untreated human neuroblastomas correlates with advanced disease stage. *Science.* **1984**;224:1121–1124.

Campeau E, Ruhl VE, Rodier F, Smith CL, Rahmberg BL, Fuss JO, *et al.* A versatile viral system for expression and depletion of proteins in

- mammalian cells. PLoS One **2009**;4:e6529.
- Carpenter EL, Mosse YP. Targeting ALK in neuroblastoma—preclinical and clinical advancements. Nat Rev Clin Oncol. **2012**;9:391–399.
- Cerezo-Guisado MI, García-Román N, García-Marín LJ, Alvarez-Barrientos A, Bragado MJ, Lorenzo MJ. Lovastatin inhibits the extracellular-signal-regulated kinase pathway in immortalized rat brain neuroblasts. Biochem J. **2007**;401(1):175–183. doi:10.1042/BJ2006073
- Chan, P, Han, X, Zheng, B, DeRan, M, Yu, J, Jarugumilli, GK, *et al.* Autopalmitoylation of TEAD proteins regulates transcriptional output of the Hippo pathway. Nat Chem Biol **2016**;12:282-9.
- Chan SW, Lim CJ, Chen L, Chong YF, Huang C, Song H, *et al.* The Hippo pathway in biological control and cancer development. J Cell Physiol **2011**;226:928-39.
- Chen J, Bardes EE, Aronow BJ, Jegga AG. ToppGene Suite for gene list enrichment analysis and candidate gene prioritization. Nucleic Acids Res **2009**;37:W305-11.
- Chen L, Chan SW, Zhang X, Walsh M, Lim CJ, Hong W, *et al.* Structural basis of YAP recognition by TEAD4 in the Hippo pathway. Genes Dev **2010**;24:290-300
- Chen Q, Zhang N, Xie R, Wang W, Cai J, Choi KS, *et al.* Homeostatic control of Hippo signaling activity revealed by an endogenous activating mutation in YAP. Genes Dev **2015**;29:1285-97

- Cheung NV, Zhang J, Lu C, Parker M, Bahrami A, Tickoo SK, *et al.* Association of age at diagnosis and genetic mutations in patients with neuroblastoma. *JAMA* **2012**;307(10):1062-1071.
- Chou TC. Theoretical basis, experimental design, and computerized simulation of synergism and antagonism in drug combination studies. *Pharmacol Rev* **2006**;58:621-681.
- Chou TC. Drug combination studies and their synergy quantification using the Chou-Talalay method. *Cancer Res* **2010**;70:440-446.
- Cohn SL, Pearson AD, London WB, Monclair T, Ambros PF, Brodeur GM, *et al.* The International Neuroblastoma Risk Group (INRG) classification system: an INRG Task Force report. *J Clin Oncol* **2009**;27:289-97.
- Cottini F, Hideshima T, Xu C, Sattler M, Dori M, Agnelli L, *et al.* Rescue of Hippo coactivator YAP1 triggers DNA damage-induced apoptosis in hematological cancers. *Nat Med* **2014**;20:599-606.
- Delloye-Bourgeois C, Castellani V. Hijacking of Embryonic Programs by Neural Crest-Derived Neuroblastoma: From Physiological Migration to Metastatic Dissemination. *Front Mol Neurosci*. **2019**;12:52.
- Dobin A, Davis CA, Schlesinger F, Drenkow J, Zaleski C, Jha S, *et al.* STAR: ultrafast universal RNA-seq aligner. *Bioinformatics* **2013**;29:15-21.
- Dong J, Feldmann G, Huang J, Wu S, Zhang N, Comerford SA, *et al.* Elucidation of a universal size-control mechanism in *Drosophila* and mammals. *Cell* **2007**;130:1120-33.

- Durrant DE, Morrison DK. Targeting the Raf kinases in human cancer: the Raf dimer dilemma. *Br J Cancer*. **2018**;118(1):3–8.
- Eleveld TF, Oldridge DA, Bernard V, Koster J, Colmet Daage L, Diskin SJ, *et al*. Relapsed neuroblastomas show frequent RAS-MAPK pathway mutations. *Nat Genet* **2015**;47:864-71.
- Fernandez-L, A, Northcott, PA, Dalton, J, Fraga, C, Ellison, D, Angers, S, *et al*. YAP1 is amplified and up-regulated in hedgehog-associated medulloblastomas and mediates Sonic hedgehog-driven neural precursor proliferation. *Gen Dev* **2009**;23:2729-2741.
- Foucquier J, Guedj M. Analysis of drug combinations: current methodological landscape. *Pharmacol Res Perspect* **2015**;3:e00149.
- Gammill LS, Roffers-Agarwal J. Division of labor during trunk neural crest development. *Dev Biol* **2010**;344:555-565.
- Garnett MJ, Edelman EJ, Heidorn SJ, Greenman CD, Dastur A, Lau KW, *et al*. Systematic identification of genomic markers of drug sensitivity in cancer cells. *Nature* **2012**; 483: 570-575.
- Gronich, N, Rennert, G. Beyond aspirin-cancer prevention with statins, metformin and bisphosphonates. *Nat Rev Clin Oncol*. **2013**; 10(11):625-42.
- Guo J, Grovola MR, Xie H, *et al*. Comprehensive pharmacological profiling of neurofibromatosis cell lines. *Am J Cancer Res*. **2017**;7(4):923–934.
- Greshock J, Bachman KE, Degenhardt YY, Jing J, Wen YH, Eastman S, McNeil E, Moy C, We-grzyn R, Auger K, Hardwicke MA and Wooster R.

- Molecular target class is predictive of in vi- tro response profile. *Cancer Research* **2010**; 70: 3677-86.
- Han, K, Jeng, EE, Hess, GT, Morgens, DW, Li, A, Bassik, MC. Synergistic drug combinations for cancer identified in a CRISPR screen for pairwise genetic interactions. *Nat Biotechnol* **2017**;35:463-474.
- Hardwick SA, Chen WY, Wong T, Deveson IW, Blackburn J, Andersen SB, *et al.* Spliced synthetic genes as internal controls in RNA sequencing experiments. *Nat Methods* **2016**;13:792-8.
- Harenza JL, Diamond MA, Adams RN, Song MM, Davidson HL, Hart LS, *et al.* Transcriptomic profiling of 39 commonly-used neuroblastoma cell lines. *Sci Data* **2017**;4:170033.
- Hart LS, Rader J, Raman P, Batra V, Russell MR, Tsang M, *et al.* Preclinical Therapeutic Synergy of MEK1/2 and CDK4/6 Inhibition in Neuroblastoma. *Clin Cancer Res* **2017**;23:1785-96.
- Harvey, KF, Zhang, X, Thomas, DM. The hippo pathway and human cancer. *Nat Rev Can* **2013**;13:246-257.
- Heuckmann JM, Holzel M, Sos ML, Heynck S, Balke-Want H, Koker M, Peifer M, Weiss J, Lovly CM, Grutter C, *et al.* ALK mutations conferring differential resistance to structurally diverse ALK inhibitors. *Clin Cancer Res.* **2011**;17:7394–7401.
- Hindler, K, Cleeland, CS, Rivera, E, Collard, CD. The role of statins in cancer therapy. *Oncologist.* **2006**;11(3):306-315.

- Hindley CJ, Condurat, AL, Menon, V, Thomas, R, Azmitia, LM, Davis, JA, Pruszek, J. The Hippo pathway member YAP enhances human neural crest cell fate and migration. *Sci Rep* **2016**;6:23208.
- Hoehner JC, Gestblom C, Hedborg F, Sandstedt B, Olsen L, Pahlman S. A developmental model of neuroblastoma: differentiating stroma-poor tumors' progress along an extra-adrenal chromaffin lineage. *Lab Invest* **1996**;75:659-75.
- Holden JK, Cunningham CN. Targeting the Hippo Pathway and Cancer through the TEAD Family of Transcription Factors. *Cancers (Basel)*. **2018**;10(3):81.
- Hong X, Nguyen HT, Chen Q, Zhang R, Hagman Z, Voorhoeve PM, *et al.* Opposing activities of the RAS and Hippo pathways converge on regulation of YAP protein turnover. *EMBO J* **2014**;33:2447-57.
- Howlander N, Noone A, Krapcho M, Neyman N, Aminou R, Waldron W, Altekruse S, Kosary C, Ruhl J, Tatalovich Z, *et al.* SEER Cancer Statistics Review 1975–2008 based on November 2010 SEER data submission. National Cancer Institute; Bethesda, MD: **2011**.
- Huang J, Wu S, Barrera J, Matthews K, Pan D. The Hippo signaling pathway coordinately regulates cell proliferation and apoptosis by inactivating Yorkie, the *Drosophila* Homolog of YAP. *Cell* **2005**;122:421-34.
- Iizuka-Ohashi M, Watanabe M, Sukeno M, *et al.* Blockage of the mevalonate pathway overcomes the apoptotic resistance to MEK inhibitors with

- suppressing the activation of Akt in cancer cells. *Oncotarget*.
2018;9(28):19597–19612.
- Kapoor A, Yao W, Ying H, Hua S, Liewen A, Wang Q, *et al*. Yap1 activation enables bypass of oncogenic Kras addiction in pancreatic cancer. *Cell* **2014**;158:185-97.
- Karp, I, Behloul, H, Leloir, J, Pilote, L. Statins and cancer risk. *Am J Med*.
2008;121:302-309.
- Kim MH, Kim J, Hong H, Lee SH, Lee JK, Jung E, *et al*. Actin remodeling confers BRAF inhibitor resistance to melanoma cells through YAP/TAZ activation. *EMBO J* **2016**;35:462-78.
- Kim J, Jo H, Hong H, Kim MH, Kim JM, Lee JK, *et al*. Actin remodelling factors control ciliogenesis by regulating YAP/TAZ activity and vesicle trafficking. *Nat Com* **2015**;6:6781.
- Kuoppala J, Lamminpää A, Pukkala E. Statins and cancer: A systematic review and meta-analysis. *Eur J Cancer*. **2008**;44:2122-2132.
- Lawrence MS, Stojanov P, Mermel CH, Robinson JT, Garraway LA, Golub TR, *et al*. Discovery and saturation analysis of cancer genes across 21 tumour types. *Nature* **2014**;505:495-501.
- Lei QY, Zhang H, Zhao B, Zha ZY, Bai F, Pei XH, *et al*. TAZ promotes cell proliferation and epithelial-mesenchymal transition and is inhibited by the Hippo pathway. *Mol Cell Biol* **2008**;28:2426-36.

- Li B, Dewey CN. RSEM: accurate transcript quantification from RNA-Seq data with or without a reference genome. *BMC Bioinformatics* **2011**;12:323.
- Li W, Cooper J, Zhou L, Yang C, Erdjument-Bromage H, Zagzag D, Snuderl M, *et al.* Merlin/NF2 loss-driven tumorigenesis linked to CRL4(DCAF1)-mediated inhibition of the hippo pathway kinases Lats1 and 2 in the nucleus. *Cancer Cell* **2014**;26: 48–60.
- Lin L, Sabnis AJ, Chan E, Olivas V, Cade L, Pazarentzos E, *et al.* The Hippo effector YAP promotes resistance to RAF- and MEK-targeted cancer therapies. *Nat Genet* **2015**;47:250-6.
- Lito P, Rosen N, Solit DB. Tumor adaptation and resistance to RAF inhibitors. *Nat Med* **2013**;19:1401-9.
- Lito P, Saborowski A, Yue J, Solomon M, Joseph E, Gadala S, *et al.* Disruption of CRAF-mediated MEK activation is required for effective MEK inhibition in KRAS mutant tumors. *Cancer Cell* **2014**;25:697-710.
- Liu F, Yang X, Geng M, Huang M. Targeting ERK, an Achilles' Heel of the MAPK pathway, in cancer therapy. *Acta Pharm Sin B.* **2018**;8(4):552–562.
- Liu, JA, Cheung, M. Neural crest stem cells and their potential therapeutic applications. *Dev Biol* **2016**;419:199-216.
- Lui JW, Xiao S, Ogomori K, Hammarstedt JE, Little EC, Lang D. The Efficiency of Verteporfin as a Therapeutic Option in Pre-Clinical Models of Melanoma. *J Cancer.* **2019**;10(1):1–10.

- Liu-Chittenden Y, Huang B, Shim JS, Chen Q, Lee SJ, Anders RA, *et al.* Genetic and pharmacological disruption of the TEAD-YAP complex suppresses the oncogenic activity of YAP. *Genes Dev* **2012**;26:1300-5.
- Lugowska I, Kosela-Paterczyk H, Kozak K, Rutkowski P. Trametinib: a MEK inhibitor for management of metastatic melanoma. *Onco Targets Ther* **2015**;8:2251-9.
- Ma Y.-W., Liu Y.-Z., Pan J.-X. Verteporfin induces apoptosis and eliminates cancer stem-like cells in uveal melanoma in the absence of light activation. *Am. J. Cancer Res.* **2016**;6:2816–2830.
- MacDonald JS, Gerson RJ, Kornbrust DJ *et al.* Preclinical evaluation of lovastatin. *Am J Cardiol.* **1988**;62:16J–27J.
- Manchado, E, Weissmueller, S, Morris, JP, Chen, CC, Wullenkord, R, Lujambio, A, *et al.* *Nature* **2016**;534:647-651.
- Maris JM. Recent advances in neuroblastoma. *N Engl J Med* **2010**;362:2202-11.
- Maris JM, Hogarty MD, Bagatell R, Cohn SL. Neuroblastoma. *Lancet* **2007**;369:2106-20.
- Maris JM, Matthay KK. Molecular biology of neuroblastoma. *J Clin Oncol* **1999**;17:2264-79.
- Mlakar, V, Mlakar, SJ, Lopez, G, Maris, JM, Ansari, M, Gumy-Pause, F. 11q deletion in neuroblastoma: a review of biological and clinica implications. *Mol Cancer* **2017**; 16:114.

- Molenaar JJ, Koster J, Zwijnenburg DA, van Sluis P, Valentijn LJ, van der Ploeg, I, *et al.* Sequencing of neuroblastoma identifies chromothripsis and defects in neuritogenesis genes. *Nature* **2012**;483:589-593.
- Mosse YP, Laudenslager M, Khazi D, *et al.* Germline PHOX2B Mutation in Hereditary Neuroblastoma. *Am J Hum Genet.* **2004**;75:727–30.
- Mosse YP, Laudenslager M, Longo L, Cole KA, Wood A, Attiyeh EF, *et al.* Identification of ALK as a major familial neuroblastoma predisposition gene. *Nature* **2008**;455:930-5.
- Noland, CL, Gierke, S, Schnier, PD, Murray, J, Sandoval, WN, Sagolla, M, Dey, A, Hannoush, RN, Fairbrother, WJ, Cunningham, CN. Palmitoylation of TEAD Transcription Factors Is Required for Their Stability and Function in Hippo Pathway Signaling. *Structure.* **2016**;24(1):179-186.
- Oberthuer A, Juraeva D, Hero B, Volland R, Sterz C, Schmidt R, Faldum A, Kahlert Y, Engesser A, Asgharzadeh S, *et al.* Revised risk estimation and treatment stratification of low- and intermediate-risk neuroblastoma patients by integrating clinical and molecular prognostic markers. *Clin Cancer Res.* **2015**;21:1904–1915.
- Orr, BA, Bai, H, Odia, Y, Jain, D, Anders, RA, Eberhart, CG. Yes-associated protein 1 is widely expressed in human brain tumors and promotes glioblastoma growth. *J Neuro Exp Neuro* **2011**;70(7):568-577.

- Overholtzer M, Zhang J, Smolen GA, Muir B, Li W, Sgroi DC, *et al.* Transforming properties of YAP, a candidate oncogene on the chromosome 11q22 amplicon. *Proc Natl Acad Sci U S A* **2006**;103:12405-10.
- Padovan-Merhar OM, Raman P, Ostrovnaya I, Kalletta K, Rubnitz KR, Sanford EM, *et al.* Enrichment of Targetable Mutations in the Relapsed Neuroblastoma Genome. *PLoS Genet* **2016**;12:e1006501.
- Pan D. The Hippo signaling pathway in development and cancer. *Dev Cell* **2010**;19:491-505
- Park JR, Bagatell R, London WB, Maris JM, Cohn SL, Mattay KK, *et al.* Children's Oncology Group's 2013 blueprint for research: neuroblastoma. *Pediatr Blood Cancer* **2013**;60:985-93.
- Park JR, Eggert A, Caron H. Neuroblastoma: biology, prognosis, and treatment. *Hematol Oncol Clin North Am* **2010**;24:65-86.
- Poulikakos PI, Zhang C, Bollag G, Shokat KM, and Rosen N. RAF inhibitors transactivate RAF dimers and ERK signalling in cells with wild-type BRAF. *Nature* **2010**;464:427-430.
- Rader J, Russell MR, Hart LS, Nakazawa MS, Belcastro LT, Martinez D, *et al.* Dual CDK4/CDK6 inhibition induces cell-cycle arrest and senescence in neuroblastoma. *Clin Cancer Res* **2013**;19:6173-82.
- Rajbhandari, P, Lopez, G, Capdevila, C, Salvatori, B, Yu, J, Rodriguez-Barrueco, R, *et al.* Cross-cohort analysis identifies a TEAD4-MYCN positive

- feedback loop as the core regulatory element of high-risk neuroblastoma. *Cancer Discovery* **2018**;8:582-99.
- Rayego-Mateos S, Rodrigues-Diez R, Morgado-Pascual JL, Rodrigues Diez RR, Mas S, Lavoiz C, *et al.* Connective tissue growth factor is a new ligand of epidermal growth factor receptor. *J Mol Cell Biol* **2013**;5:323-35.
- Robison RL, Suter W, Cox RH. Carcinogenicity and mutagenicity studies with fluvastatin, a new, entirely synthetic HMG-CoA reductase inhibitor. *Fundam Appl Toxicol.* **1994**;23:9–20.
- Ryan MB and Corcoran RB. Therapeutic strategies to target RAS-mutant cancers. *Nat Rev Clin Oncol* **2018**;15:709-720.
- Santarpia L, Lippman SM, El-Naggar AK. Targeting the MAPK-RAS-RAF signaling pathway in cancer therapy. *Expert Opin Ther Targets.* **2012**;16(1):103–119.
- Sausen M, Leary RJ, Jones S, Wu J, Reynolds, CP, Liu X, *et al.* Integrated genomic analyses identify ARID1A and ARID1B alterations in the childhood cancer neuroblastoma. *Nat Genet* **2013**;45(1):12-17.
- Schleiermacher G, Javanmardi N, Bernard V, Leroy Q, Cappo J, Rio Frio T, *et al.* Emergence of new ALK mutations at relapse of neuroblastoma. *J Clin Oncol* **2014**;32:2727-3.
- Schonherr C, Ruuth K, Yamazaki Y, Eriksson T, Christensen J, Palmer RH, Hallberg B. Activating ALK mutations found in neuroblastoma are inhibited by Crizotinib and NVP-TAE684. *Biochem J.* **2011**;440:405–413.

- Schramm A, Koster J, Assenov Y, Althoff K, Peifer M, Mahlow E, *et al.* Mutational dynamics between primary and relapse neuroblastomas. *Nat Genet* **2015**;47:872-7.
- Schwab M, Alitalo K, Klemptner KH, Varmus HE, Bishop JM, Gilbert F, Brodeur G, Goldstein M, Trent J. Amplified DNA with limited homology to myc cellular oncogene is shared by human neuroblastoma cell lines and a neuroblastoma tumour. *Nature*. **1983**;305:245–248.
- Seeger RC, Brodeur GM, Sather H, Dalton A, Siegel SE, Wong KY, Hammond D. Association of multiple copies of the N-myc oncogene with rapid progression of neuroblastomas. *New England Journal of Medicine*. 1985;313:1111–1116.
- Sekido Y, Pass HI, Bader S, Mew DJ, Christman MF, Gazdar AF, and Minna JD. Neurofibromatosis type 2 (NF2) gene is somatically mutated in mesothelioma but not in lung cancer. *Cancer Res*. **1995**;55:1227–1231
- Seo, J, Kim, J. Regulation of Hippo signaling by actin remodeling. *BMB Rep*. **2018**;51(3):151–156.
- Seong BK, Fathers KE, Hallett R, Yung CK, Stein LD, Mouaaz S, *et al.* A Metastatic Mouse Model Identifies Genes That Regulate Neuroblastoma Metastasis. *Cancer Res* **2017**;77:696-706.
- Shao DD, Xue W, Krall EB, Bhutkar A, Piccioni F, Wang X, *et al.* KRAS and YAP1 converge to regulate EMT and tumor survival. *Cell* **2014**;158:171-84.

- Shi, Z, He, F, Chen, M, Hua, L, Wang, W, Jiao, S, Zhou, Z. DNA-binding mechanism of the Hippo pathway transcription factor TEAD4. *Oncogene*. **2017**;36(30):4362-4369.
- Sleijfer, S, van der Gaast, A, Planting, AS, Stoter, G, Verweij, J. The potential of statins as part of anti-cancer treatment. *Eur J Cancer*. **2005**;41:516-522.
- Slemmons KK, Crose LE, Rudzinski E, Bentley RC, Linardic CM. Role of the YAP Oncoprotein in Priming RAS-Driven Rhabdomyosarcoma. *PLoS One* **2015**;10:e0140781.
- Steinhardt AA, Gayyed MF, Klein AP, Dong J, Maitra A, Pan D, *et al*. Expression of Yes-associated protein in common solid tumors. *Hum Pathol* **2008**;39:1582-9.
- Strieder V, Lutz W. E2F proteins regulate MYCN expression in neuroblastomas. *J Biol Chem* **2003**;278:2983-9.
- Sun, X, Vilar, S, Tatonetti, NP. High-throughput methods for combinatorial drug discovery. *Sci Transl Med*. **2013**;5(205):205rv1.
- Tang, TT, Konradi, AW, Feng, Y, Peng, X, Qiao, S, Post, L. Targeting the Hippo-YAP pathway with novel small-molecule inhibitors of the YAP-TEAD transcription activity. *Cancer Res (Abstract)* 13 Supplement 2963.
- Taylor ML, Wells BJ, Smolak MJ. Statins and cancer: a meta-analysis of case-control studies. *Eur J Cancer Prev*. **2008**;17:259-268.

- Tidyman WE, Rauen KA. The RASopathies: developmental syndromes of RAS/MAPK pathway dysregulation. *Curr Opin Genet Dev.* **2009**;19(3):230–236.
- Umapathy G, Guan J, Gustafsson DE, Javanmardi N, Cervantes-Madrid D, Djos A, *et al.* MEK inhibitor trametinib does not prevent the growth of anaplastic lymphoma kinase (ALK)-addicted neuroblastomas. *Sci Signal* **2017**;10(507).
- Vassilev A, Kaneko KJ, Shu H, Zhao Y, DePamphilis ML. TEAD/TEF transcription factors utilize the activation domain of YAP65, a Src/Yes-associated protein localized in the cytoplasm. *Genes Dev.* **2001**;15(10):1229–1241.
- Wang C., Zhu X., Feng W., Yu Y., Jeong K., Guo W., Lu Y., Mills G.B. Verteporfin inhibits YAP function through up-regulating 14-3-3 σ sequestering YAP in the cytoplasm. *Am. J. Cancer Res.* **2015**;6:27–37.
- Wang S, Lu Y, Yin MX, Wang C, Wu W, Li J, Wu W, Ge L, Hu L, Zhao Y *et al.* Importin alpha1 mediates Yorkie nuclear import via an N-terminal Non-canonical nuclear localization signal. *J Biol Chem.* **2016b**;291:7926–7937.
- Wang Y, Xu X, Maglic D, Dill MT, Mojumdar K, Ng PK, *et al.* Comprehensive molecular characterization of the hippo signaling pathway in cancer. *Cell Reports* **2018**;25:1304-1317.

- Wei, JS, Song, YK, Durinck, S, Chen, QR, Cheuk, AT, Tsang, P, *et al.* The MYCN oncogene is a direct target of miR-34a. *Oncogene* **2008**;27:5204-13.
- Wei X, Shimizu T, Lai ZC. Mob as tumor suppressor is activated by Hippo kinase for growth inhibition in *Drosophila*. *EMBO J* **2007**;26:1772-81.
- Weinstein JN, Myers TG, O'Connor PM, Friend SH, Fornace AJ Jr, Kohn KW, *et al.* An information-intensive approach to the molecular pharmacology of cancer. *Science* **1997**; 275: 343-349.
- Williams SP, Barthorpe AS, Lightfoot H, Garnett MJ, McDermott U. High-throughput RNAi screen for essential genes and drug synergistic combinations in colorectal cancer [published correction appears in *Sci Data*. *Sci Data*. **2018**;4:170139.
- Williams VC, Lucas J, Babcock MA, Gutmann DH, Korf B, Maria BL. Neurofibromatosis type 1 revisited. *Pediatrics* **2009**;123(1):124-33.
- Wong T, Deveson IW, Hardwick SA, Mercer TR. ANAQUIN: a software toolkit for the analysis of spike-in controls for next generation sequencing. *Bioinformatics* **2017**;33:1723-4.
- Wright, CJ, McCormack, PL. Trametinib: first global approval. *Drugs*. **2013**;73(11):1245-54.
- Wu S, Huang J, Dong J, Pan D. Hippo encodes a Ste-20 family protein kinase that restricts cell proliferation and promotes apoptosis in conjunction with salvador and warts. *Cell* **2003**;114:445-56.

- Yaeger R and Corcoran RB. Targeting alterations in the RAF-MEK pathway. *Cancer Discovery* **2019**;9(3):329-341.
- Yang, C, Tan, J, Zhu, J, Wang, S, Wei, G. YAP promotes tumorigenesis and cisplatin resistance in neuroblastoma. *Oncotarget*. **2017**;8(23):37154-163.
- Yao Z, Torres NM, Tao A, Gao Y, Luo L, Li Q, *et al*. BRAF Mutants Evade ERK-Dependent Feedback by Different Mechanisms that Determine Their Sensitivity to Pharmacologic Inhibition. *Cancer Cell* **2015**;28:370-83.
- Yu FX, Zhao B, Panupinthu N, Jewell JL, Lian I, Wang LH, *et al*. Regulation of the Hippo-YAP pathway by G-protein-coupled receptor signaling. *Cell* **2012**;150:780-91.
- Zanconato, F, Cordenonsi, M, Piccolo, S. YAP/TAZ at the roots of cancer. *Cancer Cell* **2016**;29(6):783-803.
- Zhang H, Pasolli HA, Fuchs E. Yes-associated protein (YAP) transcriptional coactivator functions in balancing growth and differentiation in skin. *Proc Natl Acad Sci U S A*. **2011**;108(6):2270–2275.
- Zhang, XD *et al*. The use of strictly standardized mean difference for hit selection in primary RNA interference high-throughput screening experiments. *J. Biomol. Screen*. **2007**;12, 497–509.
- Zhao B, Wei X, Li W, Udan RS, Yang Q, Kim J, *et al*. Inactivation of YAP oncoprotein by the Hippo pathway is involved in cell contact inhibition and tissue growth control. *Genes Dev* **2007**;21:2747-61.

Zhao Y, Adjei AA. The clinical development of MEK inhibitors. *Nat Rev Clin Oncol* **2014**;11:385-400.